Quantum Mechanical Study on the Chemical Reactions Including Light-particle Transfers

Hiroto TACHIKAWA

1994

CONTENTS

CHAPTER I.

INTRODUCTION

1. Background and Purpose of This Study

Chemical reactions are in principle described as the motion of nuclei or atoms on the potential energy surface (PES) derived from the electronic state of reaction system. One of the simplest ways for describing the reaction dynamics is to apply the statistic approximation (classical approximation) in which the energy of the reaction system is assumed to be distributed statistically among the particles composing the reaction system. The transition state theory, a theory for calculating the rate constant based on the statistic approximation, has been successfully applied to many reaction systems.[1]

In the last decade, a number of experiments have shown that the statistic approximation is not necessarily a good approximation for the description of chemical reaction. Recently-developed experimental techniques, such as crossed-beam method,[2] flowing afterglow method[3] and laser-induced fluorescence (LIF) method,[4] have provided considerable amount of information on vibrational and rotational state distributions of reaction products for charge-, proton- and hydrogen atom transfer reactions. The most important result is the discovery of non-statistic features in the chemical reaction in which the statistic approximation gives poor results on the vibrational and rotational energy distributions of the product molecules. Importance of total available energy, kinematics effects, and the shape of the potential energy surface in reaction dynamics has been pointed out by several authors. Investigations on state-selected and vibrational mode-specific reactions have been revealed new reaction channels which have not been considered in the classical reaction theory.[5] For example, electron spin resonance (ESR) and fourier-transform infrared (FT-IR) spectroscopic studies on the hydrogen atom transfer reactions in condensed phase have shown the importance of non-classical effect in hydrogen atom transfer reaction, *i.e.* the quantum mechanical tunneling effect.[6-8]

Theoretical models for non-classical behavior in chemical reaction have been developed in these last 10 years.[9] *Quasi*-classical trajectory calculation has been widely used to elucidate the reaction dynamics. However, the trajectory calculation generally employs experimental data for PES parameters because there are few theoretical studies based on the *ab-initio* molecular orbital (MO) model. The rate calculations including tunneling effect have also been performed using semi-empirical potential energy curve. The semi-empirical parameter, however, frequently gives quite different PES from the *ab-initio* PES. The shape of PES is known as a dominant

factor in determing the reaction dynamics. The dynamic calculation based on the ab-initio MO model is required to compare directly with experiment.

In the present thesis work, three light-particle transfer reactions:

1) charge transfer reaction
2) proton transfer reaction
3) hydrogen transfer reaction

have been investigated theoretically by using the quantum mechanical and dynamical methods based on the *ab-initio* MO model to elucidate the non-classical behavior in the chemical reaction.

These reactions are typical examples where dynamical and quantum effects cause the deviation of kinetic features from that expected from classical theory. The light-particle transfer reactions are the fundamental and simple processes in chemical reaction systems and are involved in many chemical reaction systems.

2. Experimental observations.

A. Charge Transfer Reactions

Charge transfer (CT) reaction is the simplest chemical reaction, because it involves no bond-forming and bond-breaking processes. The CT reaction in a triatomic system,

$$A^+ + BC \rightarrow A + BC^+(v,j) \qquad (I)$$

is a prototype chemical reaction that involves the non-adiabatic transitions among several adiabatic potential energy surfaces (PESs). Almost all ion-molecule systems are characterized by two close-lying PESs corresponding to the two charge transfer states, $A^+ + BC$ and $A + BC^+$, at large intermolecular distance.

Recent experiments have provide considerable information on the vibrational- and rotational-state distributions and the translational energy distributions of the product $BC^+(v,j)$ formed by reaction I.[5,10-14]

There are two models that explain the internal energy distributions of the product $BC^+(v,j)$. One is simple Franck-Condon (FC) model and another is the energy resonance (ER) model. The FC model pressumes the charge transfer occurring through a long range electron jump. In this situation, the BC molecule is not perturbed by the A^+ ion to any significant extent and $BC^+(v,j)$ product state distribution is governed by the Franck-Condon factors for vertical ionization,

$$BC\,(v'=0) \rightarrow BC^+\,(v) + e^- \qquad (II)$$

The energy resonance model presumes close matching of the A^+ recombination energy with the sum of the BC ionization potential and BC^+ internal energy is required for efficient charge transfer. Theoretical studies of energy resonance indicate that rotational excitation of BC^+ is minimal. These two models have been used to explain the vibrational distributions observed experimentally.

However, the charge transfer reaction,

$$N^+(^3P) + CO(X^1\Sigma^+) \rightarrow N(^4S) + CO^+(X^2\Sigma^+) \qquad \text{(III)}$$

is one of the exceptional reactions. Lin *et al.*[11] and Hamilton *et al.*[12] studied the vibrational distributions of the product CO^+. by using the flowing afterglow and the laser induced fluorescence (LIF) techniques and found that 1) the vibrational modes of CO^+ are distributed in v=0,1 and 2, and 2) population of the rotational quantum number of CO^+ shows a Boltzmann distribution with 410K in the CO^+(v=0) whereas a non-Boltzmann distribution with a highly rotationally excited state in CO^+(v=1). These experimental results are not explained adequately neither by the FC model nor by the ER model. A new theoretical model would be necessary for understanding the charge transfer mechanism. In the present study, *ab-initio* MO and classical trajectory calculations have been performed to elucidate the reaction mechanism, and a new reaction model is proposed.

B. Proton transfer reactions

Proton transfer reaction is the simplest reaction among those involving the bond-forming and bond-breaking processes. Several experimental studies have been carried out for the gas phase proton transfer reactions.

Although there are number of types of proton transfer reaction, the main target in this thesis work is the proton transfer in the ion-molecule reaction system. Especially, we focus our attention on the proton transfer reaction in heavy-light-heavy system,

$$A^- + H\text{-}B \rightarrow A\text{-}H(v) + B^-, \qquad \text{(I)}$$

where, A and B are heavy atoms. It is generally believed that the vibrational distributions of product A-H(v) is independent of the collision energy of reactants, while the relative translational energy between A-H and B^- is increased with increasing collision energy.[16]

In 1992, Knutsen *et al.* have investigated a proton transfer reaction

$$O^- + HF \rightarrow OH(v) + F^- \qquad \text{(II)}$$

by means of a flow-drift tube method and determined relative vibrational state populations in the product OH as a function of reactant center-of-mass collision energy.[17] The fractional population of v=1,

$$P(v=1) = \frac{OH(v=1)}{OH(v=0)+OH(v=1)} \qquad \text{(III)}$$

increases to 0.25 and 0.33 atcollision energies of 9.6 and 15.4 kJ/mol, respectively. This result strongly indicates that reaction II contradicts with previous view of the proton transfer reaction.

In the present study, *ab-initio* MO and quasi-classical trajectory calculations are performed to elucidate the mechanism for this reaction, and a new reaction model is proposed.

C. Hydrogen atom transfer reactions in gas phase

The reaction between ammonia cation radical and neutral ammonia,

$$NH_3^+ + NH_3 \rightarrow NH_4^+ + NH_2 \qquad \text{(I).}$$

found by Derwish *et al.*[18] in 1963, provides an interesting example of H-atom transfer in gas phase. Adam *et al.*[19] investigated reaction I by means of isotope labeling technique (ND_3^+) and found that these reactions are composed of three reaction channels,

$$ND_3^+ + NH_3 \rightarrow ND_2 + NH_3D^+ \qquad \text{(channel I)}$$

$$ND_3^+ + NH_3 \rightarrow ND_3H^+ + NH_2 \qquad \text{(channel II).}$$

$$ND_3^+ + NH_3 \rightarrow ND_3 + NH_3^+ \qquad \text{(channel III)}$$

Channel I is a proton transfer (actually D^+ transfer) reaction from ND_3^+ to NH_3, and Channel II is a hydrogen atom transfer reaction from NH_3 to ND_3^+. Channel III is a charge transfer reaction. Relative reactive cross sections were determined to be 0.85 for channel I and 0.15 for channel II, respectively. The hydrogen transfer is less favored than the proton transfer. Therefore, each reaction channel is the state-selected chemical reactions.

In 1987, Conaway *et al.*[20] determined the reaction cross sections for channels I and II as a function of vibrational energy of ν_2 umbrella mode of NH_3^+ (E_{vib}). The reactive cross section for channel I decreased with increasing E_{vib}, whereas that for channel II increased gradually

with increasing E_{vib}. This vibrational energy directly corresponds to quantum number of v_2 umbrella mode of NH_3^+.

In 1990, Tomoda *et al.*[21] measured the reactive cross sections for channels I, II and III, as a function of total energy (= E_{vib} + Center-of-mass collision energy). The reactive cross section for channels II and III increases with increasing total energy, and that for channel III is slightly larger than that for channel II.

There are no theoretical work on branching among these channels. In the present thesis work, *ab-initio* MO, and classical trajectory calculations have been performed to elucidate the reaction mechanism. Attention is focused on vibrational state-specificity of channel II.

D. Hydrogen transfer reactions in condensed phase.

The gas phase reactions are essentially considered to be a collision process between particles, so that the reactive cross section is mainly affected by the collision energy and by the lifetime of intermediate. Chemical reactions in condensed phase at low-temperature are influenced by the quantum mechanical tunnel effect.[8,22] Especially, a hydrogen atom transfer would be dominated by the tunnel effect.

Tunneling effect was first demonstrated experimentally for the hydrogen-abstraction reaction from methanol by methyl radical.[23] The hydrogen abstraction has been found from both the methyl group and the hydroxyl group in the gas phase reaction at high temperature.

$$\cdot CH_3 + CH_3OH \rightarrow \cdot CH_2OH + CH_4 \qquad (I)$$

$$\cdot CH_3 + CH_3OH \rightarrow CH_3O\cdot + CH_4 \qquad (II)$$

Extrapolation of the Arrhenius relation at high temperature predicts that channel II becomes prevailing at low temperature.[24] However, the hydrogen abstraction is believed to proceed from the methyl group (channel I) at low temperature in condensed phase. The radical transformation of $\cdot CH_3$ to $\cdot CH_2OH$ was actually observed in solid methanol by the ESR method.[24] Primary concern of the present investigation is to study theoretically the reaction rate of channels I and II at low temperature based on *ab-initio* MO and tunneling treatments and to reveal the reason why channel I prevails in solid state.

E. Solvation effects in hydrogen atom transfer reactions

In the field of theoretical chemistry, one of the current topics is how to describe the reaction in condensed phase. In this thesis, we treat the microscopic electronic interaction between a

chemical reaction system and solvent molecules, and calculate a reaction rate of hydrogen transfer reaction.

As a model reaction system, an intramolecular hydrogen transfer reaction in condensed phase

$$CH_3O\cdot \rightarrow \cdot CH_2OH \qquad (I)$$

is chosen. In 1987, Iwasaki and Toriyama observed this reaction in methanol polycristalline phase and pointed out importance of the quantum mechanical tunnel effect.[25] A new model to describe the solvation effect on the chemical reaction has been proposed in this work.

3. Outline of the present thesis

In this thesis work, charge, proton and hydrogen atom transfer reactions have been investigated theoretically. These are key reactions for understanding of the chemical reaction. In addition, the structures and electronic states of some intermediates, which play an important role in chemical reactions, have been determined by means of *ab-initio* MO calculations.

In the following chapter, the method of the calculations is described.
In chapter III, the charge transfer reaction

$$N^+(^3P) + CO(X^1\Sigma^+) \rightarrow N(^4S) + CO^+(X^2\Sigma^+)$$

is studied by *ab-initio* CI method and dynamics calculation. Potential energy surfaces (PESs) for ground- and first excited states are calculated theoretically. Using ab-initio fitted PESs, classical trajectories and vibrational distributions are determined. Based on the molecular orbital theory, electronic states of the ground- and excited state intermediates $[NCO]^{+*}$ is discussed.

In chapter IV, dynamics of a proton transfer reaction, $O^- + HF \rightarrow OH(v,J) + F^-$, in gas phase is investigated by using *ab-initio* MO and quasi-classical trajectory calculations. In chapter V, a hydrogen transfer reaction in gas phase, $NH_3^+ + NH_3 \rightarrow NH_4^+ + NH_2$, is studied. Mechanism of the vibrational state specificity in this reaction is discussed base on the theoretical results. The following theree chapters concern with reactions observed in solid methanol. In chapter VI, hydrogen transfer reactions at low temperature in condensed phase are investigated based on the quantum mechanical tunneling model. In chapter VII, both solvation and tunnel effects in chemical reaction are treated theoretically. In chapter VIII, an intermolecular hydrogen transfer reaction in frozen methanol is studied by using the continuum model and the RRKM theory including tunnel effects.

References

1. (a) Almond, M. J., "Short-lived Molecules", Ellis Horwood, New York, 1990.
   (b) Setser, D. W. " Reactive Intermediates in the Gas Phase" Academic Press, New York, 1979.
2. (a) Scoles, G. Ed., *Atomic and Molecular Beam Methods*, Vol. 1, Oxford University Press , 1988.
   (b) Tiernan, T. O.; Lifshitz, C., *Advan. Chem. Phys.*, **1981**, *45*, 81.
2. Urena, A.G., *Advances in Chemical Physics*, Vol. 66, John Wiley & Sons, 1987.
3. (a) Hamilton, C. E.; Duncan, M. A.; Zwier, T.S.; Weisshaar, J. C., Ellison, G. B., Bierbaum, V. M., Leone, S. R., *Chem. Phys. Lett.*, **1983**, *94*, 4.
   (b) Bierbaum, V. M.; Ellison, G. B.; Leone, S. R., "Ions and Light, Gas Phase Ion Chemistry", Vol.3, M.T. Bowers ed, Academic Press, New York, 1983.
4. (a) Sonnenfroh, D. M.; Leone, S. R., *J. Chem. Phys.*, **1989**, *90*, 1677.
   (b) Danon, J.; Marx, R., *Chem. Phys.*, **1982**, *68*, 255.
   (c) Matsumi, Y.; Tonokura, K.; Kawasaki, M.; Kim, H.L. *J. Phys.Chem.* **1992**, *96*, 10622.
   (d) Matsumi, Y.; Tonokura, K.; Kawasaki, M.; Tsuji, K., Obi, K. *J. Chem. Phys.* **1993**, *98*, 8330.
5. Ng, C.Y., in *State-Selected and State-to-State Ion-Molecule Reaction Dynamics*: Part I, Experiment, edited by C.Y. Ng and M.Baer, vol.82 in Advances in Chemical Physics (Wiley, New York, 1992), p.401.
6. (a) Campion, A.; Williams, F., *J. Am. Chem. Soc.*, **1972**, *94*, 7633.
   (b) Hudson, R. L.; Shiotani, M.; Williams, F. *Chem. Phys. Lett.*, **1977**, *48*, 193.
   (c) Tsuruta, H.; Miyazaki, T.; Fueki, K.; Azuma, N., *J. Phys. Chem.* **1983**, *87*, 5422.
   (d) Miyazaki,T.; Hiraku, T.; Fueki,K.; Tsuchihashi,Y., *J. Phys. Chem.* **1991**, *95*, 26.
7. (a) Andrews, L.; Moskovist, M., Eds, "Chemistry and Physics of Matrix-Isolated Species", Elsevier, 1989. (b) Jacox, M. E. *J. Phys. Chem.*, **1987**, *91*, 6595.
8. Jortner, J.; Pullman, B. Eds, "Tunneling", D.Reidel Publishing, 1986.
9. Ng, C.Y., in *State-Selected and State-to-State Ion-Molecule Reaction Dynamics*: Part II, Theory, edited by C.Y. Ng and M.Baer, vol.82 in Advances in Chemical Physics (Wiley, New York, 1992).
10. Kato, S.; Leone, S. R.; Can. J. Chem. **1994** (in press).
11. Lin, G. H.; Maier; J.; Leone, S.R. *J. Chem. Phys.*, **1986**, *84*, 2180.
12. Hamilton, C. E.; Bierbaum V. M.; Leone, S. R., *J. Chem. Phys.*, **1985**, *83*, 601.
13. Hamilton, C. E.; Bierbaum V. M.; Leone, S. R., *J. Chem. Phys.*, **1985**, *83*, 2284.

14. Kato, T.; *J. Chem. Phys.*, **1984**, *80*, 6105.
15. Henchman, M. J. "Ion-Molecule Reactions", J.L. Franklin, Ed, Plenum Press, New York, 1972.
16. (a) Weisshaar, J.C.; Zwier, T.S.; Leone, S.R., *J. Chem. Phys.*, **1981**, *75*, 4873.
(b) Langford, A.O.; Bierbaum, V.M.; Leone, S.R., *J. Chem. Phys.*, **1985**, *83*, 3913.
17. Knutsen, K.; Bierbaum, V. M.; Leone, S.R., *J. Chem. Phys.*, **1992**, *96*, 298.
18. Derwish, G.A.W.; Galli, A.; Giardini-Guidoni.; Volpi, G.G., *J. Chem. Phys.*, **1963**, *39*, 1599.
19. Adam, N.G.; Smith, D.; Paulson, J.F. *J. Chem. Phys.*, **1980**, *72*, 288.
20. Conaway, W.E.; Ebata, T.; Zare, R. N., *J. Chem. Phys*, **1987**, *87*, 3453.
21. Tomoda,S.; Suzuki, S.; Koyano, I., *J. Chem. Phys*, **1988**, *89*, 7268.
22. Bell, R.P., "The Tunnel Effect in Chemistry", Chapman and Hall, 1980.
23. Tsang, W., *J. Phys. Chem. Ref. Data.* **1987**, *16*, 471.
24. (a) Doba, T.; Ingold, K. U.; Siebrand, W.; Wildman, T. A., *Faraday Discuss. Chem. Soc.* **1984**, *78*, 175.
(b) Doba, T.; Ingold, K. U.; Siebrand, W.; Wildman, T. A., *J. Phys. Chem.*, **1984**, *88*, 3165.
25. (a) Iwasaki, M.; Toriyama, K., *J. Am. Chem. Soc.*, **1987**, *100*, 1964.
(b) Iwasaki, M.; Toriyama, K., *J. Chem. Phys.*, **1987**, *86*, 5970.

CHAPTER II.

GENERAL METHODS OF THE THEORETICAL CALCULATION

1. *Ab-initio* molecular orbital calculation.

In this section, the theoretical background for *ab-initio* molecular orbital calculations will be presented. Since most of the basic theories of the molecular orbital theory can be found in textbooks and recent reviews,[1-4] we briefly outline the basic concept of molecular orbital theory.

A. Schrödinger equation.

Electronic structure and physical properties of any molecule in any of its stationary states can be determined in principle by solving time-independent Schrödinger equation. For a system of N electrons, moving in the potential field due to nuclei, the time-independent Schrödinger equation takes the form

$$H\,\Psi(x_1, x_2, \ldots x_N) = E\Psi(x_1, x_2, \ldots x_N) \qquad (2.1)$$

where H is the Hamiltonian operator given by

$$H = \sum_i h(i) + \frac{1}{2}\sum_{ij}{}' g(i,j) \qquad (2.2a)$$

Here

$$h(i) = -\frac{\hbar^2}{2m}\nabla^2(i) + V(i) \qquad (2.2b)$$

is the one-electron Hamiltonian operator for the *i-th* electron, while

$$g(i,j) = \frac{e^2}{r_{ij}} \qquad (2.2c)$$

is the electronic interaction term between *i-th* and *j-th* electrons. The operator h(*i*) consists of two parts: the first is the kinetic energy operator which in Cartesian coordinate becomes

$$-\frac{\hbar^2}{2m}\nabla^2(i) = -\frac{\hbar^2}{2m}\left(\frac{\partial^2}{\partial x_i^2} + \frac{\partial^2}{\partial y_i^2} + \frac{\partial^2}{\partial z_i^2}\right) \qquad (2.3),$$

and the second is simply the potential energy of *i-th* electron in the field of the nuclei. We assume that the nuclei in the molecule are fixed in space so that the potential energy of *i-th* electron is given by

$$V(i) = -\sum \frac{Z_n e^2}{r_{ni}} \qquad (r_{ni}=|r_i - R_n|) \qquad (2.4)$$

where R_n and eZ_n are the position vector and charge of *n-th* nuclei, and r_{ni} is the magnitude of the position vector of *i-th* electron relative to *n-th* nuclei.

The electronic energy E is the energy of the N electrons moving in the field due to the nuclei. It contains the coordinates of the nuclei as parameters and is sometimes indicated explicitly as a function of these coordinate, $E=E(R_n)$. For a system with fixed nuclei the total energy of the molecule E_{tot} is just the sum of the electronic energy and the nuclear repulsion energy:

$$E_{tot} = E + \frac{1}{2}\sum_{n\ n'} \frac{Z_n Z_{n'}}{R_{n\,n'}} \qquad (2.5)$$

E_{tot} must be negative for molecular binding and it must also be less than the sum of the energies of the separated atoms if the molecule is stable against dissociation into atom.

B. *Hartree-Fock* method

Almost all *ab-initio* calculations of molecules are performed by means of the Hartree-Fock (HF) method, where total wave function for a closed-shell molecule is expressed by one slater determinant,

$$\Phi_0 = \frac{1}{\sqrt{(2n)!}}\left|\varphi_1(1)\alpha\ (1)\varphi_1(2)\beta\ (2)\ldots\ \varphi_n(2n)\beta\ (2n)\right| = A\left\{\varphi_1\varphi_1'\varphi_2\varphi_2'\ldots\varphi_n\varphi_n'\right\} \qquad (2.6)$$

A is antisymmetrizer, and φ_1 and φ_1' mean that the *1st* electron occupies φ_1 orbital with α spin and the *2nd* electron occupies φ_1 orbital for β spin, respectively. The *3rd* electron occupies φ_2 for α spin. The Hamiltonian and energy (E_0) of this system are given by

$$H = \sum_{i=1}^{2n} h(i) + \sum_{i<j}^{2n} \frac{e^2}{r_{ij}}$$

$$h(i) = -\frac{\hbar^2}{2m}\Delta_i - \sum \frac{Ze^2}{r_{ij}}$$

$$E_0 = 2\sum_{i=1}^{n} H_i + \sum_{i,j=1}^{n} (2J_{ij} - K_{ij}) \qquad (2.7a)$$

where J_{ij} and K_{ij} are, respectively, coulomb and exchange integrals expressed by

$$J_{ij} = \int \varphi_i^*(1)\varphi_i(1)\frac{1}{r_{12}}\varphi_j^*(2)\varphi_j(2)\, d\tau \qquad (2.7b)$$

$$K_{ij} = \int \varphi_i^*(1)\varphi_j(1)\frac{1}{r_{12}}\varphi_j^*(2)\varphi_i(2)\, d\tau \qquad (2.7c)$$

H_i is one-electron integral given by

$$H_i = \int \varphi_i^*(1)h(1)\varphi_i(1)\, d\tau \qquad (2.7d)$$

By using the variational approximation to the energy, the Hartree-Fock equation is obtained as

$$F\varphi_i = \sum_j \varepsilon_{ji}\, \varphi_j \qquad (2.8)$$
$$\varepsilon_{ji} = \varepsilon_{ij}^*$$

where F is the *Fock operator* , ε_{ji} is eigenvalue (*i-th* orbital energy). The Fock operator is expressed by

$$F = h + \sum_j (2J_j - K_j) \qquad (2.9a)$$

where the coulomb operator J_i and the exchange operator K_i are difined by

$$J_j\, \varphi_i(1) = \int \frac{\varphi_j(2)\varphi_j(2)}{r_{12}}\, d\tau\, \varphi_i(1) \qquad (2.9b)$$

$$K_j\, \varphi_i(1) = \int \frac{\varphi_j(2)\varphi_i(2)}{r_{12}}\, d\tau\, \varphi_j(1) \qquad (2.9c)$$

The HF molecular orbital satisfies the equation

$$F\varphi_i = \varepsilon_i\varphi_i \qquad (2.10)$$

and the orbital energy is given by

$$\varepsilon_i = \int \varphi_i^*\, F\, \varphi_i\, d\tau = F_i$$

$$= H_i + \sum_{j=1}^{n} (2J_{ij} - K_{ij}) \qquad (2.11)$$

If one introduces the linear combination of atomic orbitals (LCAO) MO approximation,

$$\varphi_i = \sum c_{ir}\chi_r$$

Eq.(2.10) is expressed by

$$\begin{aligned}
&(F_{11} - \varepsilon_i)C_{i1} + (F_{12} - S_{12}\varepsilon_i)C_{i2} + \ldots + (F_{1m} - S_{1m}\varepsilon_i)C_{im} = 0 \\
&(F_{21} - S_{21}\varepsilon_i)C_{i1} + (F_{22} - \varepsilon_i)C_{i2} + \ldots + (F_{2m} - S_{2m}\varepsilon_i)C_{im} = 0 \\
&\qquad\qquad \ldots\ldots\ldots\ldots\ldots\ldots \\
&(F_{m1} - S_{m1}\varepsilon_i)C_{i1} + (F_{12} - S_{m2}\varepsilon_i)C_{i2} + \ldots + (F_{mm} - S_{mm}\varepsilon_i)C_{im} = 0
\end{aligned} \qquad (2.12a)$$

Here the overlap integral S_{rs} is difined by

$$S_{rs} = \int \varphi_r(1)\varphi_s(1)\, d\tau \qquad (2.12b)$$

and F_{rs} is given by

$$\begin{aligned}
F_{rs} &= \int \varphi_r(1)\left(-\frac{\hbar^2}{2m}\nabla^2(i) + V(i)\right)\varphi_s(1)\, d\tau \\
&+ \sum_{j=1}^{n} \{ \int \chi_r(1)\chi_s(1)\frac{1}{r_{12}}\varphi_j(2)\varphi_j(2)\, d\tau \\
&- \int \chi_r(1)\varphi_j(1)\frac{1}{r_{12}}\chi_s(2)\varphi_j(2)\, d\tau \ \}
\end{aligned} \qquad (2.12c)$$

where χ_r is *r-th* atomic orbital of molecule. By solving this equation, HF energies and canonical orbitals can be obtained.

2. Dynamics calculations

The detailed theoretical description of a chemical reaction is essentially a dynamical problem in which the motion (dynamics) of the electrons and nuclei involved must be analyzed. Since 1958, trajectory calculations have been utilized in theoretical studies of bi-molecular reactions.[5,6] The significance of these calculations is that they permit examination of the

detailed dynamics of individual reactive collision. In this section, a quasi-classical procedure for the examination of the collision dynamics of atom-diatomic molecule reactions is outlined.

A. Potential energy surface

The first step of the dynamics calculation is the evaluation of the potential energy surface for three atomic system, A+ BC, as a function of distances R_1=R(A-B), R_2=R(B-C), R_3=R(C-A). In the present work, all potential energy surfaces are calculated by means of the *ab-initio* MO method. The ab-initio PESs are fitted by the London-Eyring-Polanyi-Sato (LEPS) surface function $V(R_1,R_2,R_3)$,

$$V = \frac{Q_{AB}}{1+S_{AB}} + \frac{Q_{BC}}{1+S_{BC}} + \frac{Q_{AC}}{1+S_{AC}}$$

$$- \frac{\alpha}{\sqrt{2}}\left[\left(\frac{J_{AB}}{1+S_{AB}} - \frac{J_{BC}}{1+S_{BC}}\right)^2 + \left(\frac{J_{BC}}{1+S_{BC}} - \frac{J_{AC}}{1+S_{AC}}\right)^2 + \left(\frac{J_{AC}}{1+S_{AC}} - \frac{J_{AB}}{1+S_{AB}}\right)^2\right]^{\frac{1}{2}} \qquad (2.13)$$

in which

$$J_i = \frac{1+S_i}{2} D_i\left[e^{-2b_i(r_i-r_i^0)} - 2e^{-b_i(r_i-r_i^0)}\right] - \frac{1-S_i}{2} D_i\left[e^{-2b_i(r_i-r_i^0)} + 2e^{-b_i(r_i-r_i^0)}\right] \qquad (2.14)$$

and Q_i is the sum rather than difference of these two terms. The subscript i has the values AB, BC, and AC, and D_i, β_i and r_i^0 are *Morse constants* for the corresponding isolated molecules. The S_i and α are adjustable parameters. This *ab-initio* fitted PESs are used for the dynamics calculations.

B. Trajectory calculation

For the point masses m_A, m_B, and m_C with Cartesian coordinates (q_1,q_2,q_3), (q_4,q_5,q_6), (q_7,q_8,q_9) and conjugated momenta (p_1,p_2,p_3), (p_4,p_5,p_6) and (p_7,p_8,p_9), respectively, the Hamiltonian function H' for a potential $V(q_1,q_2,\ldots,q_9)$ has the form

$$H' = \frac{1}{2m_A}\sum_{i=1}^{3} p_i^2 + \frac{1}{2m_B}\sum_{i=4}^{6} p_i^2 + \frac{1}{2m_C}\sum_{i=7}^{9} p_i^2 + V(q_1,q_2,\ldots,q_9). \qquad (2.15)$$

To simplify Eq.(2.15), we introduce the generalized coordinates $Q_j(j=1,2,..,9)$ defined by the relations

$$Q_j = q_{j+6} - q_{j+3},$$

$$Q_{j+3} = q_j - (m_B q_{j+3} + m_C q_{j+6}) / (m_B + m_C),$$
$$Q_{j+6} = (1/M)\,(m_A q_j + m_B q_{j+3} + m_C q_{j+6}), \qquad (j = 1,2,3) \qquad (2.16)$$

where $M=m_A+m_B+m_C$. From Eq.(2.16), it is clear that (Q_1,Q_2,Q_3) represent the Cartesian coordinates of particle C with respect to B as origin, (Q_4,Q_5,Q_6) are the Cartesian coordinate of particle A with respect to the center of mass of the pair (B,C) as origin, and (Q_7,Q_8,Q_9) are the Cartesian coordinates of the center of mass of the entire three-particle system. The equations of the inverse transformation required for obtaining the transformed Hamiltonian are

$$q_i = [(m_B + m_C) / M] Q_{i+3} + Q_{i+6}$$
$$q_{i+3} = -[m_C / (m_B + m_C)] Q_i - (m_A/M) Q_{i+3} + Q_{i+6}$$
$$q_{i+6} = -[m_B / (m_B + m_C)] Q_i - (m_A/M) Q_{i+3} + Q_{i+6} \qquad (i = 1,2,3). \qquad (2.17)$$

If $P_j(j=1,2,...,9)$ represents the momenta conjugate to the coordinates $(Q_j(j=1,2,...,9)$, we have

$$p_i = \sum_j P_j \left(\frac{\partial Q_j}{\partial q_i}\right) \qquad (2.18)$$

since we are performing a point contact transformation, i.e., $Q_i=Q_i(q_i)$. With Eqs.(2.16) and (2.18), we find

$$p_i = m_A q_i = P_{i+3} + (m_A/M) P_{i+6}$$
$$p_{i+3} = m_B q_{i+3} = -P_i - [m_B/(m_B + m_C)] P_{i+3} + (m_B/M) P_{i+6}$$
$$p_{i+6} = m_C q_{i+6} = P_i - [m_C/(m_B + m_C)] P_{i+3} + (m_C/M) P_{i+6}$$
$$(i = 1,2,3) \qquad (2.19)$$

If $H'(q_i,p_i)$ and $H(Q_j, P_j)$ are the Hamiltonian functions in the old and new variables, respectively, we have

$$H(Q_j, P_j) = H' [\, q_i(Q_j), p_i(P_i)], \qquad (2.20)$$

Consequently, the Hamiltonian function Eq.(2.15) becomes

$$H = \frac{1}{2\mu_{BC}} \sum_{j=1}^{3} P_j^2 + \frac{1}{2\mu_{A,BC}} \sum_{j=4}^{6} P_j^2 + \frac{1}{2M} \sum_{j=7}^{9} P_j^2 + V(Q_1, \ldots, Q_6) \qquad (2.21)$$

where

$$\frac{1}{\mu_{BC}} = \frac{1}{m_B} + \frac{1}{m_C} \quad \text{and} \quad \frac{1}{\mu_{A,BC}} = \frac{1}{m_A} + \frac{1}{m_C + m_B},$$

and V is the potential energy function expressed in terms of the $Q_j(j=1,2,...,6)$, which explicitly exhibits its independence of the coordinates of the center of mass.

Hamilton's equations for the three-body system described by the general dynamical coordinates Qj, Pj are

$$\frac{dQ_j}{dt} = Q_j = \frac{\partial H}{\partial P_j}, \quad \frac{dP_j}{dt} = P_j = -\frac{\partial H}{\partial Q_j} = -\frac{\partial V}{\partial Q_j} \tag{2.22}$$

Although the derivatives of the potential energy with respect to the Q_j are required in Eq.(2.22), the form of V used here is an explicit function of R_1, R_2, and R_3 (the A-B, B-C, and A-C internuclear distance). Introducing the relations between the R_1, R_2, R_3 and the $Q_j (j=1,2,...,6)$,

$$R_1 = [(q_4 - q_1)^2 + (q_5 - q_2)^2 + (q_6 - q_3)^2]^{1/2}$$

$$= \left[\left(\frac{m_C}{m_B + m_C} Q_1 + Q_4\right)^2 + \left(\frac{m_C}{m_B + m_C} Q_2 + Q_5\right)^2 + \left(\frac{m_C}{m_B + m_C} Q_3 + Q_6\right)^2\right]^{1/2},$$

$$R_2 = [(q_7 - q_4)^2 + (q_8 - q_5)^2 + (q_9 - q_6)^2]^{\frac{1}{2}}$$
$$= (Q_1^2 + Q_2^2 + Q_3^2)^{1/2},$$

$$R_3 = [(q_7 - q_1)^2 + (q_8 - q_2)^2 + (q_9 - q_3)^2]^{\frac{1}{2}}$$

$$= \left[\left(\frac{m_B}{m_B + m_C} Q_1 - Q_4\right)^2 + \left(\frac{m_B}{m_B + m_C} Q_2 - Q_5\right)^2 + \left(\frac{m_B}{m_B + m_C} Q_3 - Q_6\right)^2\right]^{1/2} \tag{2.23}$$

and making use of the "chain rule",

$$\frac{\partial V}{\partial Q_j} = \sum_j \frac{\partial V}{\partial R_k} \frac{\partial R_k}{\partial Q_j}, \tag{2.24}$$

we obtain Hamilton's equations of motion from Eqs. (2.21) and (2.22) in the form

$$Q_j = (1/\mu_{BC})\, P_j \qquad (j = 1,2,3),$$
$$Q_j = (1/\mu_{A,BC})\, P_j \qquad (j = 4,5,6),$$
$$Q_j = (1/M)\, P_j \qquad (j = 7,8,9)$$

$$-P_j = \frac{1}{R_1} \frac{m_C}{m_B + m_C} \left(\frac{m_C}{m_B + m_C} Q_j + Q_{j+3}\right) \frac{\partial V}{\partial R_1} + \frac{Q_j}{R_2} \frac{\partial V}{\partial R_2}$$
$$+ \frac{1}{R_3} \frac{m_B}{m_B + m_C} \left(\frac{m_B}{m_B + m_C} Q_j - Q_{j+3}\right) \frac{\partial V}{\partial R_3}; \qquad (j = 1,2,3)$$

$$-P_j = \frac{1}{R_1} \left(\frac{m_C}{m_B + m_C} Q_j + Q_{j+3}\right) \frac{\partial V}{\partial R_1} - \frac{1}{R_3} \left(\frac{m_B}{m_B + m_C} Q_j - Q_{j+3}\right) \frac{\partial V}{\partial R_3}$$
$$(j = 4,5,6)$$

$$P_j = 0 \tag{2.25}$$

Since P_7, P_8 and P_9 are constants of the motion, the term containing them in the Hamiltonian may be subtracted out to give the net Hamiltonian

$$H = \frac{1}{2\mu_{BC}} \sum_{j=1}^{3} P_j^2 + \frac{1}{2\mu_{A,BC}} \sum_{j=4}^{6} P_j^2 + V(R_1, R_2, R_3) \qquad (2.26)$$

with 12 simultaneous differential equations to be integrated for the determination of the time variation of the Q_j and P_j. Although a further reduction in the number of dynamical equations can be achieved by use of the conservation of energy and of total angular momentum, this does not appear to be worthwhile since the remaining equations are considerably more complicated to solve. Furthermore, with the equations in their present form, the constancy of the energy and total angular momentum can serve as a partial check on the accuracy of the integration method that is used.

C. Numerical integration

Trajectories for the particles, A,B, and C, are determined by integrating numerically the four simultaneous differential equations, Eq (2.22). The procedure begins by selecting initial values for the coordinates Qj and the momenta Pj. These boundary conditions are valid at the starting time $t = t_0$. To proceed as a function of time a numerical procedure is employed to find the solution at times $t=t_0+h$, $t=t_0+2h$, etc. Two fourth order methods are usually used. A *Runge-Kutta* method is used to begin the trajectory and after three time steps of length h a predictor-corrector method is used. The forth order Runge-Kutta method is used in this thesis work because this method minimizes the truncation error.

D. Analysis of the Results of Trajectory Calculations

Integration of Hamilton's equation is continued until the separation between two atoms is so large that there is no interaction between them. At the end of the calculation it is necessary to analyze the trajectory to determine what the product molecule is, whether it is bound, quasi-bound or in a dissociative state, to determine the final relative kinetic energy, to partition the internal energy into vibrational and rotational energy and to obtain the scattering angle. Since the trajectories are calculated by classical mechanics, the internal energy of the product does not correspond to a particular vibration-rotation energy level.

The internal energy of the product molecule in each reactive collision is partitioned into vibrational and rotational contribution using the following sequence of equations:

$$J(J+1) = \frac{4\pi^2 A_J^2}{h^2} \qquad (2.27)$$

$$E_{rot} = J\,(J+1)\,B_e \tag{2.28}$$

$$E_{vib} = E_{int} - E_{rot} \tag{2.29}$$

$$B_v = B_e - (v+\frac{1}{2})\,\alpha_e \tag{2.30}$$

$$E_{rot} = J\,(J+1)\,B_v - [J\,(J+1)]^2\,D_e \tag{2.31}$$

$$E_{vib} = E_{int} - E_{rot} \tag{2.32}$$

where A_J is the product molecule rotational angular momentum, E_{rot} and E_{vib} are initial estimates of product rotational and vibrational energies, and the remaining symbols have their usual spectroscopic interpretations. It should be noted that J(J+1) and (v+1/2) are continuous quantities in this partitioning procedure. The rotational and vibrational energies given in Eqs. (2.31) and (2.32) reflect a sufficient degree of convergence so as not to require additional iterations.

The opacity function for chemical reaction (*i.e,.*, reaction probability vs impact parameter) is calculated by

$$P_r = \frac{N_r(v', J', E, b)}{N(v', J', E, b)} \tag{2.33}$$

where N_r (v',J',E,b) is the number of reactive collisions at collision energy E with the molecule initially in the (v', J') state occuring at impact parameters between b and $b+db$, and N (v', J', E, b) is the total number of collisions.

The energy dependence of the reaction cross section is expressed by

$$\sigma_r(v', J'\,E) = \pi b_{max}^2 \frac{N_r(v', J', E)}{N(v', J', E)} \tag{2.34}$$

where N_r(v',J',E) and N(v', J', E) represent the integals over impact parameter of N_r(v', J', E, b) for the reaction.

REFERENCES

1. McWeeny, R,; Sutcliffe, B.T., "Method of Molecular Quantum Mechanics", Academic Press, New York, 1969.
2. Tribute, A.; Mulliken, R.S., "Molecular Orbital In Chemistry, Physics, and Biology", Academic Press, New York, 1964.
3. Szabo, A.; Ostlund, N.S., "Modern Quantum Chemistry - Introduction to Advanced Electronic Structure Theory", Macmillan Publishing, 1982
4. Hinchliffe, A. "*Ab-initio* Determination of Molecular Properties", IOP Publishing, 1987.
5. Karplus, M.; Porter, R.N.; Sharma, R.D., *J. Chem. Phys.*, **1965**, *43*, 3259.
6. Child, M.S., "Molecular Collision Theory" , Academic Press, 1974.

CHAPTER III

DYNAMICS OF THE CHARGE TRANSFER REACTION $N^+ + CO \rightarrow N + CO^+$

1. Introduction

Charge transfer is one of the fundamental processes in chemical reactions. Reactions involving charge transfer have received much attention from experimental and theoretical points of view.[1] Recent experiments have provided direct information on the internal states of the product molecules formed by charge transfer reactions, e.g., vibrational-rotational distributions.[1(a-k),2]

Leone and co-workers measured by laser-induced fluorescence (LIF) method the product CO^+ produced by the charge transfer reaction

$$N^+(^3P) + CO(X^1\Sigma^+, v'=0) \rightarrow N(^4S) + CO^+(X^2\Sigma^+, v, J) \quad (I)$$

and determined the vibrational- and rotational-state distributions of the CO^+ cation.[3] The relative vibrational distribution of the CO^+ observed is $(0.40)_{v=0}:(0.57)_{v=1}:(0.03)_{v=2}$ under single collision conditions at 0.16 eV energy. The rotational distribution in the v=0 channel is characterized by a Boltzmann distribution with a temperature of T=410 K, and the distribution in v=1 has a highly excited and non-Boltzmann rotational distribution.

Simple models, such as the Franck-Condon and the energy resonance models, have been used commonly to explain the vibrational distributions of the products of charge transfer reactions.[1] The Franck-Condon prediction for reaction I gives predominantly v=0 production, whereas the energy resonance picture predicts preferential population of v=2. The experimental results on reaction I suggest that neither picture adequately describes this charge transfer process. This means that other reaction mechanisms are involved in the charge transfer process of reaction I.

Several mechanisms have been considered to describe qualitatively the experimental results. Lin *et al.*[3b] suggested a dual channel mechanism for reaction I: an adiabatic reaction channel via an NCO^+ intermediate and a diabatic channel in which the reaction proceeds directly. In this mechanism, the diabatic channel leads to the vibrational ground state CO^+ product with a Franck-Condon distribution. Similar two-channel mechanisms are suggested by Gerlich[4] and by Hamilton *et al.*[3a] The structure of the intermediate NCO^+ suggested by Hamilton *et al.* is slightly different from that proposed by Gerlich: a bent-form of NCO^+ can lead to a statistical distribution, namely, vibrational excitation of the CO^+ caused by a side-on collision. Thus the mechanism of reaction I is still in controversy.

From the theoretical view point, there are a few *ab-initio* studies for the potential energy curves (PECs) of reaction I[5] and the electronic states of the NCO^+ intermediate,[6] although there has been no theoretical investigations of the vibrational distribution of the product CO^+ cation. Wu[5] have carried out MR-SD-CI calculations on the PECs of reaction I. In the collinear approach, the PEC for the $N^+(^3P)$ + CO reaction was weakly repulsive, whereas the one for the $N(^4S)$ + CO^+ reaction was strongly bound by 3.55 eV with respect to the energy of the products (N + CO^+). The heat of the reaction was calculated to be 0.49 eV, which is in good agreement with experimental value (0.52 eV).[7] More detailed calculations of the NCO^+ intermediate have recently been performed at the MR-SD-CI level of theory.[6] The structure of the NCO^+ intermediate at ground state ($X^3\Sigma^-$) was predicted as linear with geometrical parameters, r(C-O)= 1.121 A and r(N-C)= 1.402 A.

In this chapter, in order to shed light on the reaction mechanism, we have performed an *ab-initio* MO calculation on the PESs of the reaction I and classical trajectory calculations on the *ab-initio* fitted PESs. We focus our attention on the vibrational distribution of the product CO^+ cation on the exit channel PESs. Primary aims of this study are (i) to provide theoretical information on the relevant PESs of the reaction I and (ii) to discuss the mechanism of the charge transfer process in reaction I on the basis of both the PES characteristics and the results obtained from the classical trajectory calculations. In the next section, the method of the calculations is described. In Sec.3, the results of the *ab-initio* MO calculations are presented. We examine the properties of the PES for reaction I and propose a reaction model based on the *ab-initio* MO results. In Sec. 4, the results of the classical trajectory calculations on the *abinitio* fitted PESs are shown. The conclusions are summarized in Sec.5. A new theoretical explanation of reaction I will be also described as a summary.

2. Method of calculation

A. Ab-initio potential energy surfaces.

The energy correlation diagram of the NCO^+ reaction system is shown in Figure III-1. The energy level of the initial state is composed of three degenerate states ($^3\Sigma^-$ and $^3\Pi$). Upon lowering symmetry from *Cv* to *Cs*, the $NCO^+(1^3\Pi)$ state splits into $1^3A'+2^3A''$ states. The $^3A'$ state assumes to be non-reactive due to orthogonality to final state. $3^3A''$ state is not bound and shows a strongly repulsive curve at longdistance.[3] Therefore, two channels (initial state → $1^3A''$ and $2^3A''$), strongly correlate to the charge transfer process. In the present study, we considered two low-lying adiabatic surfaces ($1^3A''$ and $2^3A''$ states).

The *ab-initio* self-consistent field (SCF) energies for the ground and excited states are

calculated for each state:

$1\sigma^2\ 2\sigma^2\ 3\sigma^2\ 4\sigma^2\ 5\sigma^2\ 6\sigma^2\ 1\pi^4\ 7\sigma^2\ 2\pi^2$ $(1^3\Sigma^-)$

and $1\sigma^2\ 2\sigma^2\ 3\sigma^2\ 4\sigma^2\ 5\sigma^2\ 6\sigma^2\ 1\pi^4\ 7\sigma^1\ 2\pi^2\ 8\sigma^1$ $(1^3\Pi)$

In the calculations of the excited state, MO coefficients and density matrix obtained at dissociation limit (r_{CN} = 8.0 A) were used for the first initial guess of SCF calculation. The initial guess was updated at each point. In the ground state calculation, the values of NCO^+ intermediate complex were used for the first initial guess.

In order to calculate electron correlation, the MP2, MP3 and D-CI methods[8,9] were used for each state with configuration state functions (CSFs) constructed from HF configurations ($1^3A''$ and $2^3A''$). The weights of the main configuration at the D-CI calculations were larger than 0.95 at all points. Two dimensional adiabatic PESs as functions of the C-O and C-N distances were obtained at the Hartree-Fock (HF) and post-HF levels (HF, MP2, MP3 and D-CI) with 4-31G basis sets.[8-10] Three sets of N-C-O angles, 180°, 135° and 90° were chosen to express the angle dependency for the ground state PES. In case of the excited state, the PESs for two sets of N-C-O angles (180° and 135°) were calculated. The *ab-initio* calculations of the PES were carried out at 120 points on each surface.

Geometries for the neutral CO, the CO^+ cation and the reaction intermediate NCO^+ were fully optimized using the energy gradient method[11] with 4-31G and 6-31G* basis sets.[12]

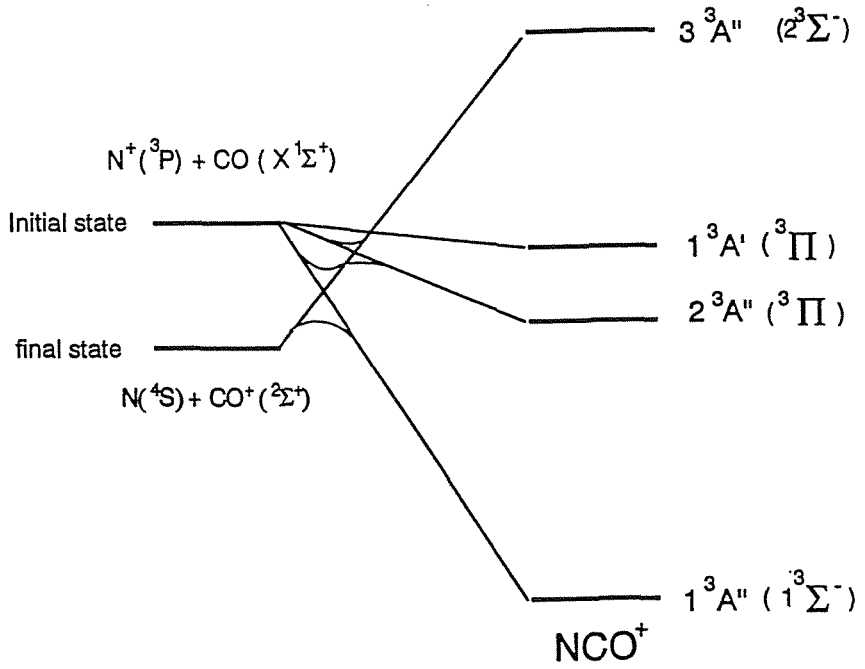

Figure III-1. Energy correlation diagram of N^+ + CO reaction.

B. Classical trajectory calculations.

The PESs obtained theoretically were fitted to an analytical equation with the least-squares method. To express the analytical function of the PES, we employed the extended-*LEPS* surface.[13] One thousand trajectory calculations on the LEPS surface were computed at each initial condition. Integration of the classical equations of motion was performed at the standard fourth-order Runge-Kutta and sixth-order AdamsMoulton combined algorithm[14] with the time increment of $1x10^{-16}$ s.

C. Lifetime of NCO^+ ($^3\Sigma^-$)

The NCO^+, formed by the collision of N^+ with CO, decomposes to N atom and CO^+ cation on the ground state PES. The lifetime (T) of NCO^+ on the ground state 2D-PES was calculated by using RRK theory.[15] According to the RRK theory, the lifetime as a function of energy E is expressed by

$$T = \frac{1}{\langle \nu \rangle}\left[\frac{E-V}{E}\right]^{-s} \qquad (1)$$

where $\langle \nu \rangle$ is an average of vibrational frequencies of modes related to the reaction, V is the dissociation energy of the reaction; $NCO^+ \rightarrow N + CO^+$, *s* is the number of degrees of freedom of vibrations. The $\langle \nu \rangle$ is calculated with the CO stretching mode and the C-N stretching mode obtained at the MP2/4-31G level.

3. Results

3.1 Ab-initio MO calculations

A. Global features of the reaction.

Geometry optimizations are performed to obtain the structures of reactant, product and an intermediate NCO^+. As shown in Table III-1, four independent calculations gave a similar geometry. We discuss the geometries derived from the MP2/6-31G* calculation. The C-O bond lengths of the neutral CO and the CO^+ cation are calculated to be 1.1503 A and 1.1026 A, respectively. This small difference in the bond lengths implies that little geometrical change in the C-O molecule occurs before and after the charge transfer. The C-O and C-N bond lengths of the NCO^+ intermediate are 1.1155 A and 1.3978 A in the $1^3\Sigma^-$ state, respectively. The skeleton of N-C-O^+ is most stable for a linear form.

Table III-1. Optimized geometries of CO, CO^+ and intermediate complex $[NCO]^+$ .Bond length and angles in angstrom and degrees, respectively.

	CO	CO^+	$[NCO]^+$		
method	r(C-O)	r(C-O)	r(C-O)	r(N-C)	θ
HF/4-31G	1.1277	1.1229	1.1299	1.3542	180.0
MP2/4-31G	1.1723	1.1070	1.1108	1.4716	180.0
HF/6-31G*	1.1138	1.0978	1.1048	1.3536	180.0
MP2/6-31G*	1.1503	1.1026	1.1155	1.3978	180.0

TABLE III-2. Total energies (in a.u), ionization energies (in eV), and heat of reactions (ΔH in kcal/mol) for the $N^+ + CO \rightarrow N + CO^+$ reaction system.

method[a]	$CO(X^1\Sigma^+)$	$CO^+(X^2\Sigma^+)$	$NCO^+(X^3\Sigma^-)$	$N(^4S)$	$N^+(^3P)$	IP(N-N+)	IP(CO-CO^+)	ΔH
HF/4-31G//HF/4-31G	-112.55236	-112.07722	-166.48576	-54.32748	-53.81059	14.06	12.93	1.13
HF/6-31G*//HF/6-31G*	-112.73788	-112.26052	-166.75386	-54.38544	-53.87220	13.97	12.99	0.98
MP2/4-31G//MP2/4-31G	-112.54792	-112.07669	-166.76194	-54.35544	-53.83487	14.16	12.82	1.34
MP2/6-31G*//MP2/6-31G*	-113.02121	-112.53025	-167.14271	-54.45765	-53.92819	14.41	13.36	1.05
DCI/4-31G//HF/4-31G	-112.74406	-112.24758	-166.72831	-54.36145	-53.84820	13.97	13.51	0.46
DCI/4-31G//MP2/4-31G	-112.74418	-112.24795	-166.72888				13.50	0.47
DCI+QC[b]//4-31G//MP2/4-31G	-112.75621	-112.25731	-166.74996	-54.36171	-53.84867	13.96	13.57	0.40
DCI/6-31G*//HF/6-31G*	-113.00406	-112.49765	-167.10756	-54.47229	-53.94822	13.96	13.78	0.48
DCI/6-31G*//MP2/6-31G*	-113.00443	-112.49767	-167.10777				13.79	0.47
DCI+QC[b]/6-31G**//MP2/6-31G**	-113.02371	-112.51229	-167.14316	-54.47385	-53.94960	14.26	13.92	0.34

[a]" // " means " optimized by ".

[b]Size-consistency correction.

As shown in Table III-2, the heats of reaction calculated at the HF and MP2 levels are much larger than that at the D-CI level. The D-CI/431G value (0.47 eV) is in reasonably agreement with experimental value (0.52 eV)[7] This agreement implies that one can discuss the reaction mechanism with the D-CI/4-31G level, and we calculate the PESs at the DCI/4-31G level of theory.

B. Potential energy surface for the entrance region ($2^3A''$ state PES)

Adiabatic PESs for the $2^3A''$ state are shown in Figure III-2. An excited state complex, which is weakly bound on the PES, is found at r(C-N)= 2.50 A and r(C-O)= 1.125 A. The complex has a linear structure. The binding energy is estimated to be 0.62 eV relative to $N^+(^3P)$ + $CO(^1S)$ at r(C-N) = 7.0 A, r(C-O) = 1.15 A and θ=180° at the D-CI/4-31G level. The excited state complex is formed by an avoided crossing between $1^3A''$ state and $2^3A''$ state.

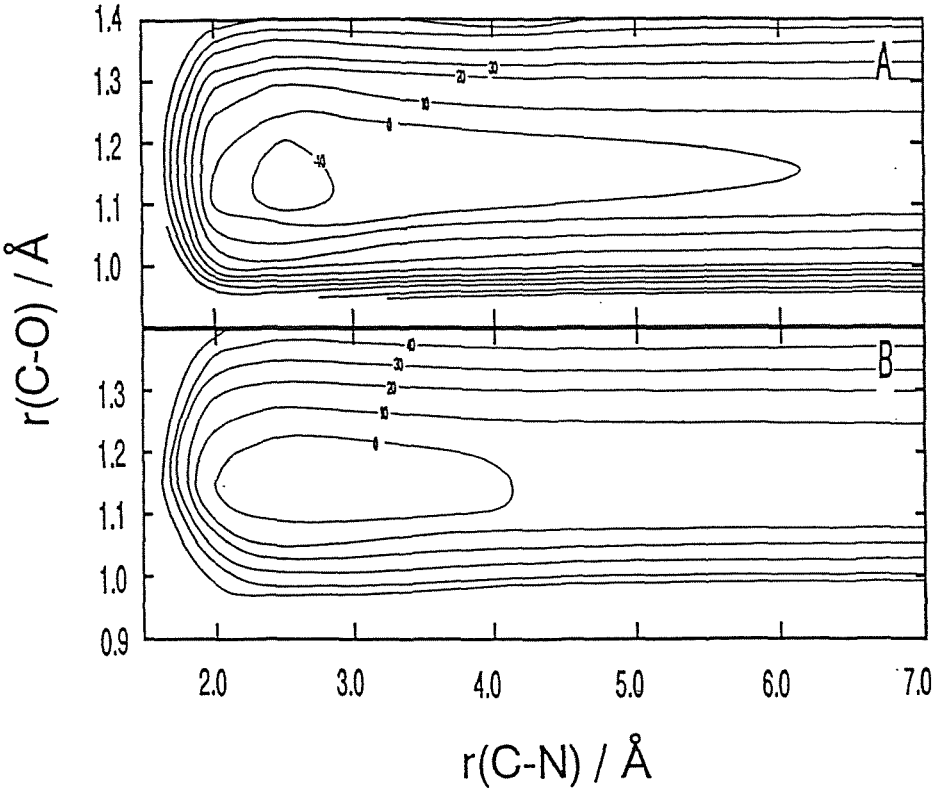

Figure III-2. Potential energy surfaces of the N^+ + CO charge transfer reaction for the excited state calculated at the D-CI/4-31G level. (A) θ =180.0°, (B) θ =135.0°. Contours are drawn for each 10 kcal/mol.

The shape of the PES exhibits that the excited state complex is loosely bound along the C-N direction, whereas it is tightly bound along the C-O direction. This feature of the PES implies that vibrational excitation of the C-O mode does not take place in the region of the excited state complex. In addition, the repulsive region of the PES (r(C-N) < 2.0 A) does not contribute to the excitation. The direction of the momentum vector of a trajectory may only be changed by this repulsive region.

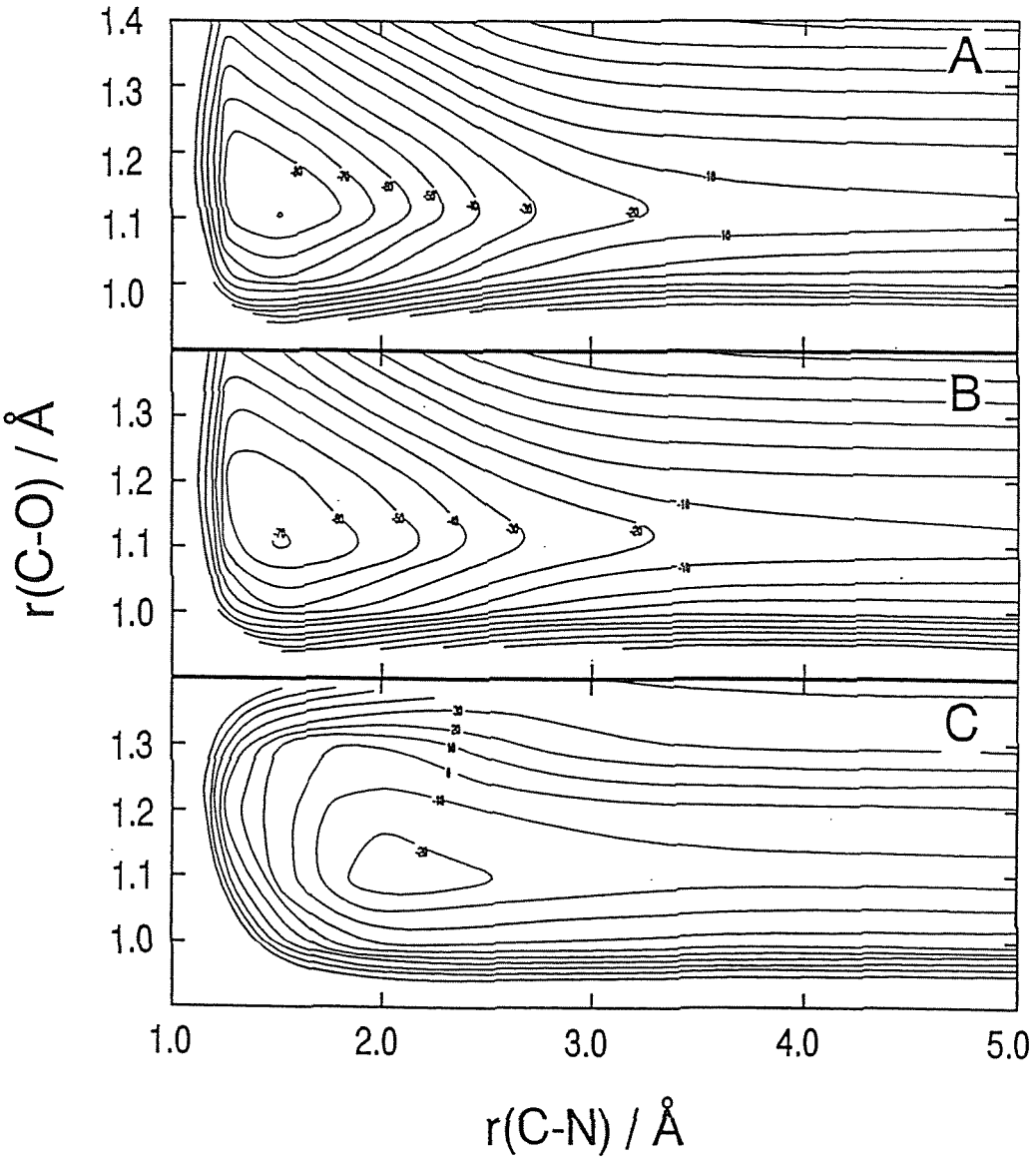

Figure III-3. Potential energy surfaces of the N^+ + CO reaction for the ground state calculated at the D-CI/4-31G level. (A) θ = 180.0°, (B) θ =135.0° and (C) θ =90.0°. Contours are drawn for each 10 kcal/mol.

C. Potential energy surface for the exit region ($1^3A''$ state PES).

The PESs of the $1^3A''(\Sigma^-)$ state for the $N^+ + CO$ reaction in the exit region are shown in Figure III-3. A strongly bound complex is formed at r(CN)= 1.5 A and r(C-O)= 1.1 A on the ground state PES. The potential basin of the NCO^+ complex is deepest for the collinear collision. The stabilization energy of the NCO^+ is calculated to be 3.326 eV with respect to the product state (r(C-N) = 5.0 A and r(C-O) = 1.10 A).

The shape of the ground state PES is much different from that of the excited state PES. The potential basin for the ground state is very deep and expanded in the C-O direction. Therefore, it can be expected that energy transfer from the translational mode to the C-O stretching mode takes place in this region by the collision. The PES shape clearly shows that vibrational excitation of CO^+ is occurring. This feature will be confirmed by the trajectory calculations in the next section.

D. Potential energy curves (PECs) for the complex formation reactions

In order to confirm further the existence of the excited and ground state complexes, we have calculated the PEC as a function of r(C-N) at the several levels of theory. As shown in Figure III-4, the PECs obtained by all levels of theory gave bound curves for the ground and excited states. Well depths calculated by the DCI/6-31G* method are 0.52 eV for the excited state complex and 4.10 eV for the ground state complex. These results indicate that both complexes can be formed in the reaction region. The PEC calculations with the 4-31G basis set gave similar results.

E. The reaction model

Based on the results derived from the *ab-initio* MO calculations, we propose here a simple model to describe the experimental results. In the present model, it is considered that the reaction leading to the product CO^+ is composed of two elementary reaction channels; one is a direct channel and the other is an intermediate complex channel. A schematic representation for these reaction channels is shown in Figure III-5. To introduce these channels, the PESs are divided into six regions (A, B, C, D, E and I) on the PESs. A reaction pathway for the direct channel is expressed by

$$A \rightarrow B \rightarrow C \rightarrow B \rightarrow D \rightarrow E \qquad \text{(path I)}$$

A reaction pathway for the intermediate complex channel proceeds via the intermediate

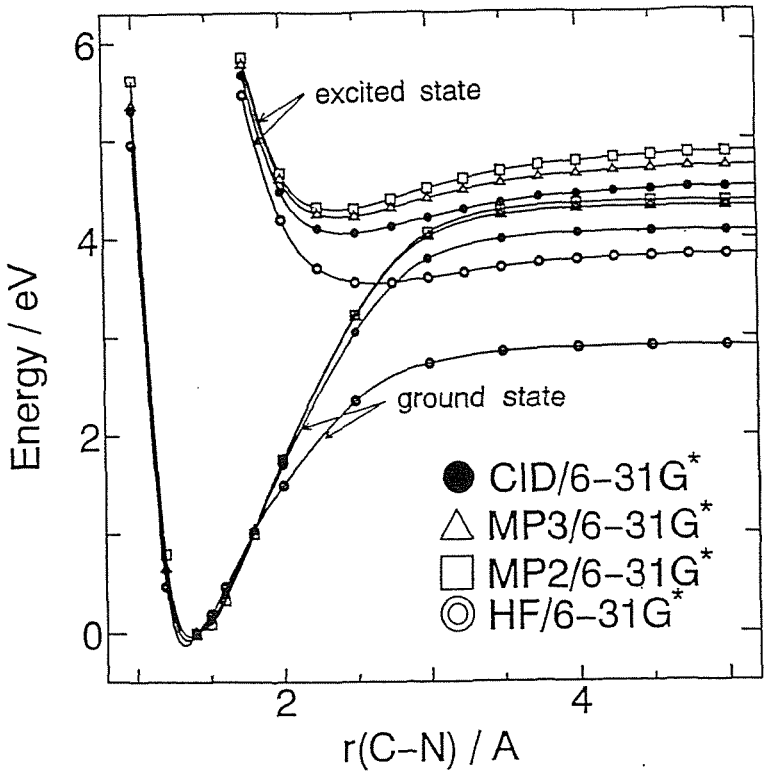

Figure III-4. Potential energy curves for the N^+ + CO reaction at the ground and excited states. The curves are drawn as a function of C-N distance. The C-O distance is fixed to the HF/6-31G* optimized value (1.1138 A).

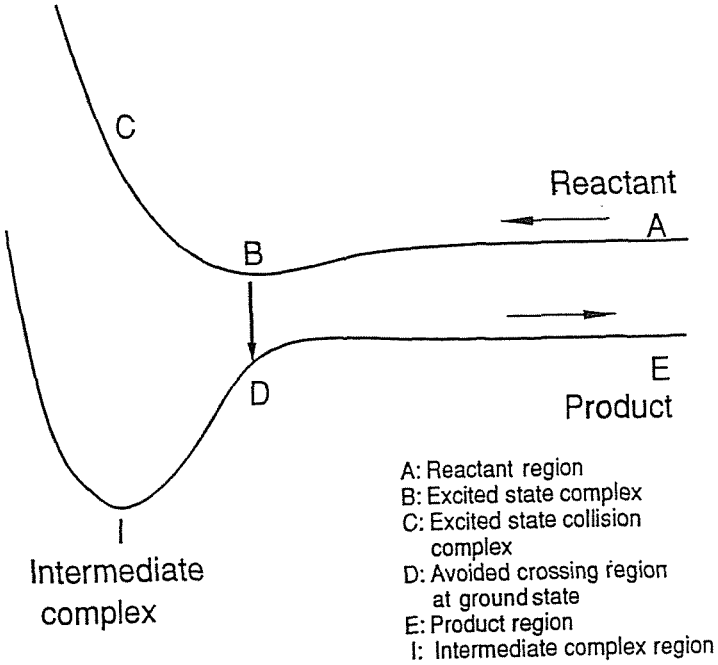

Figure III-5. Schematic illustration of the potential energy curves for the N^+ + CO charge transfer reaction system. The reaction starts at the A point and leads to the product (*E* point).

complex region, so that the reaction pathway is expressed by

$$A \rightarrow B \rightarrow D \rightarrow I \rightarrow D \rightarrow E \qquad \text{(path II)}$$

In both channels, the $2^3A'' \rightarrow 1^3A''$ electronic transition occurs through the excited state complex, i.e., $B \rightarrow D$.

3.2. Classical trajectory calculation on the PESs.

A. Collinear collision trajectory on the excited state PES.

Fitting parameters for the ground and the excited state PESs are listed in Table III-3. *Ab-initio* fitted PESs for the excited and ground states are given in Figures III-6 and III-8, respectively. The well depths, the shape of the PESs and the structures of the ground and excited state complexes are excellently reproduced by the fitted PESs.

According to the reaction model described in Section 3-E, the trajectories start from the entrance region, A, at r(C-N) = 7.0 A. The collision energy at the starting point is chosen to 0.16 eV, to match the experimental conditions. One thousand trajectory calculations are examined. A typical trajectory is sketched on the excited state PES as shown in Figure III-6. The C-O stretching mode of the neutral CO molecule is not changed before and after collision with N^+ and is still in the vibrational ground state. This result implies that non-reactive collisions of CO with N^+ does not enhance the C-O stretching mode.

The time dependence of the potential energy is given in Figure III-7(A) for a typical trajectory. A lifetime of the excited state complex is estimated to be about 0.1 ps from the trajectory calculations. Figure III-7(B) shows the interatomic distances plotted as a function of reaction time. The amplitude of the C-O stretching mode is not changed by the collision. These figures exhibit that the excited state complex has a lifetime in the *B*-region. Therefore, it is reasonable that a transition from the upper PES to the lower PES occurs in this region of the excited state complex.

For the transition point, we have chosen some points in the region of the excited state complex (r(C-N)= 2.40-2.80 A and r(C-O) = 1.09-1.20 A); a lowest energy point on the upper PES, a minimum energy-difference point between the upper and lower PESs, and some other points on the region. Since preliminary trajectory calculations starting from each transition point gave the similar results, we will discuss the results based on the trajectory from the lowest energy point on the upper PES.

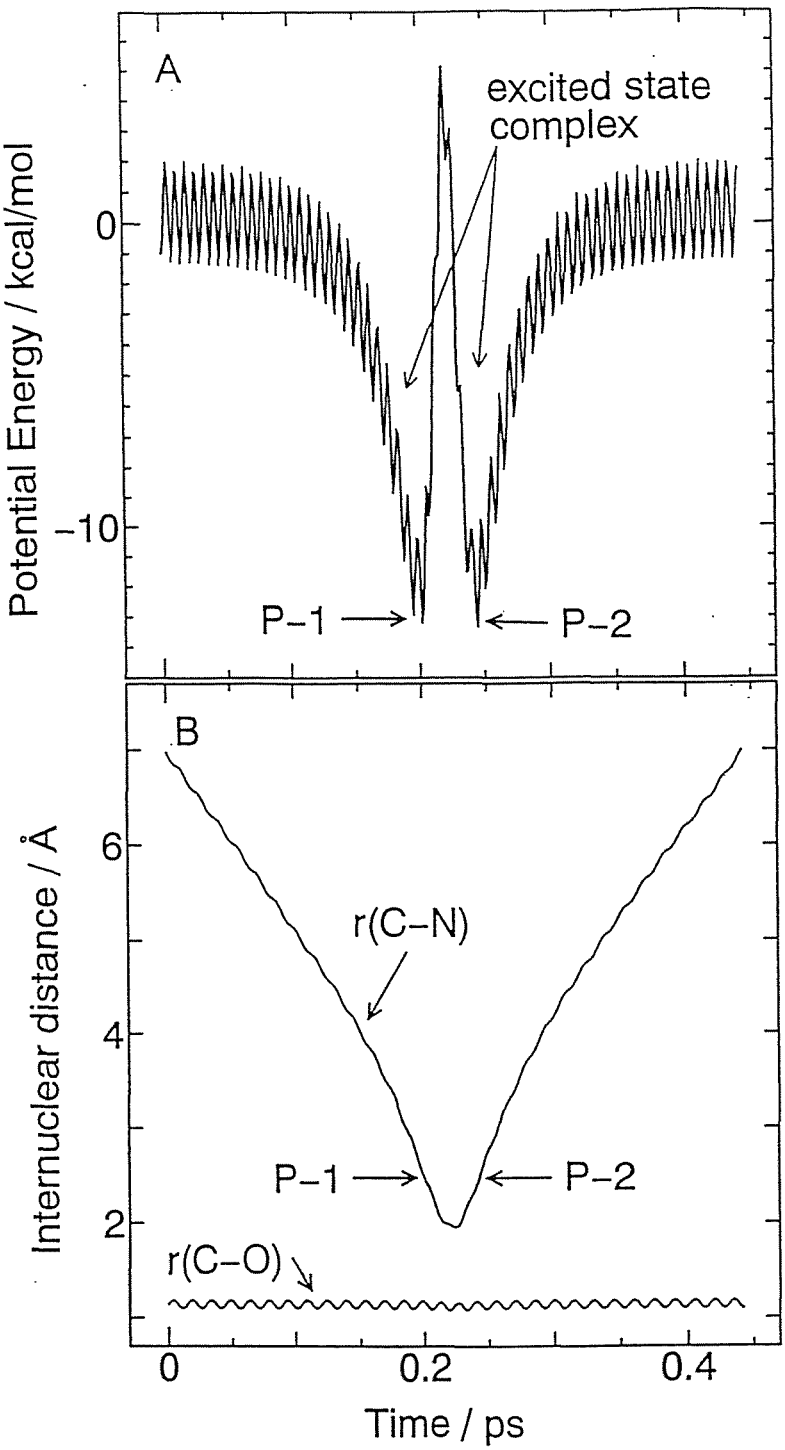

Figure III-7. A sample trajectory plotted for the potential energy (A) and r(C-O) and r(C-N) (B) versus time. The trajectory starts on the excited state at the time zero and forms the excited state complex. The labels *P-1* and *P-2* mean the transition points from the excited PES to the ground state PES. The transition from the *P-1* leads to the intermediate complex channel and the one from the *P-2* leads to the direct channel (See text).

TABLE III-3. LEPS parameters (S, Sato parameter; β, Morse parameter in A^{-1}; De, Dissociation energy in kcal/mol; r_e, internuclear distance in A; α, alpha value in extended LEPS parameter) of the *ab-initio* fitted PES.

parameter	C···N	C···O	N···O
ground state			
S	0.8036	1.000	-0.0832
β	2.067	2.909	1.120
De	266.8	359.2	220.2
r_e	1.2180	1.1064	2.0932
α	0.1252		
excited state			
S	0.4720	1.00	0.7220
β	1.2960	2.410	1.5140
De	23.80	312.10	122.70
r_e	2.5660	1.1400	2.6280
α	0.6080		

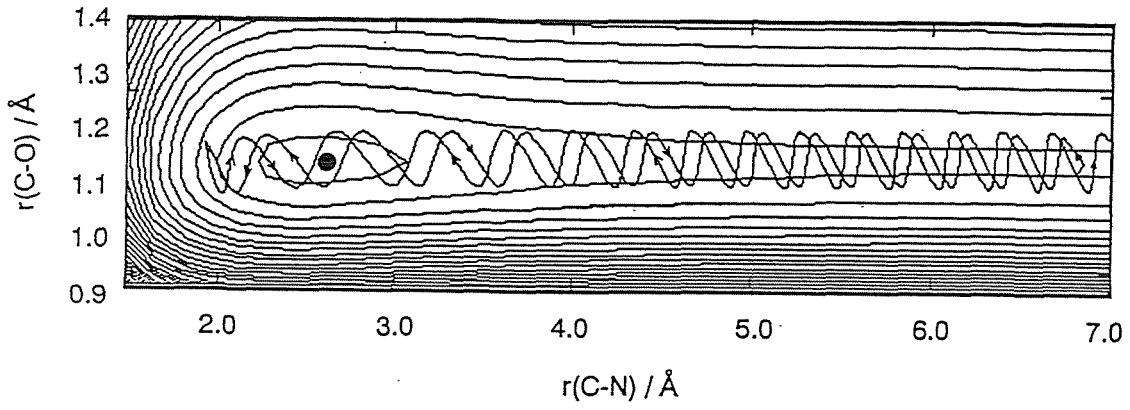

Figure III-6. *Ab-initio* fitted potential energy surface at the excited state (entrance region) and a sample trajectory on the PES. The dot on the PES means the minimum point of the excited state PES and also the transition point (*B*-point) to the ground state.

B. Collinear collision trajectories on the ground state PES.

A trajectory on the excited state PES passes twice through the lowest energy point on the upper PES (B point). They are denoted by *P-1* and *P-2* in the Figure III-7. If a trajectory is dropped at *P-1*, the reaction channel for this trajectory becomes the intermediate complex channel. On the other hand, a trajectory dropped at *P-2* corresponds to the direct channel.

As a simplification of the trajectory calculations, we have assumed that the translational energy of N^+ at the starting point on the ground state PES is fixed to be 1.61eV (37.02 kcal/mol). This energy is estimated as the sum of the energy-difference between the ground (D) and excited (A) state PESs (E(A)-E(D)= 1.45 eV) and the translational energy at the excited state (0.16 eV). Total energy is conserved throughout on the excited state and the ground state PES. This simple treatment is enough to discuss qualitatively the present mechanism. Furthermore we do not take into account the surface hopping trajectory[16] because the theoretical branching ratio of both channels is not required in the present discussion.

Direct channel. A typical trajectory is illustrated on the ground state PES as shown in Figure III-8(A). The trajectory leaves rapidly from the potential basin and goes to the product. The potential energy increases gradually as shown in Figure III-9(A). The internuclear distances of C-N and C-O are plotted in Figure III-9(B). The C-O stretching mode is still in the vibrational ground state. All trajectories proceeding via the direct channel gave the vibrational ground state CO^+ cation.

Intermediate channel. The trajectories along path II are calculated in the same manner used for the direct channel. Only the direction of the momentum vector is changed. A typical trajectory for the intermediate complex channel is plotted in Figure III-8(B). The trajectory starts from the transition point and is trapped in the well. After two collisions with the well, the trajectory goes to the product. Translational energy is transferred to the C-O stretching mode in the well. Figure III-8(B) clearly shows a feature of the energy transfer. Figure III-10 also shows that the C-O stretching mode is enhanced. For one thousand trajectories, almost all the trajectories result in highly vibrationally excited CO^+ (v=1 and 2).

A lifetime of the intermediate NCO^+ is estimated by RRK theory[15] using the parameters listed in Table III-4. The calculated RRK lifetime is 0.21 ps. The corresponding value derived from the trajectory calculations is in the range of 0.2-0.9 ps. This time scale of the lifetime is not enough to lead to a completely statistical rotation distribution of the products, so that this channel leads predominantly to the highly rotationally excited states.

Table III-4. RRK parameters calculated at the MP2/4-31G level.

	this work	Wu[a]
C-N stretching mode, cm^{-1}	635.6	764.8
C-O stretching mode, cm^{-1}	2806.8	
V, kcal/mol	76.7	84.1
E, kcal/mol	92.84	102.2

[a]From Ref. 5.

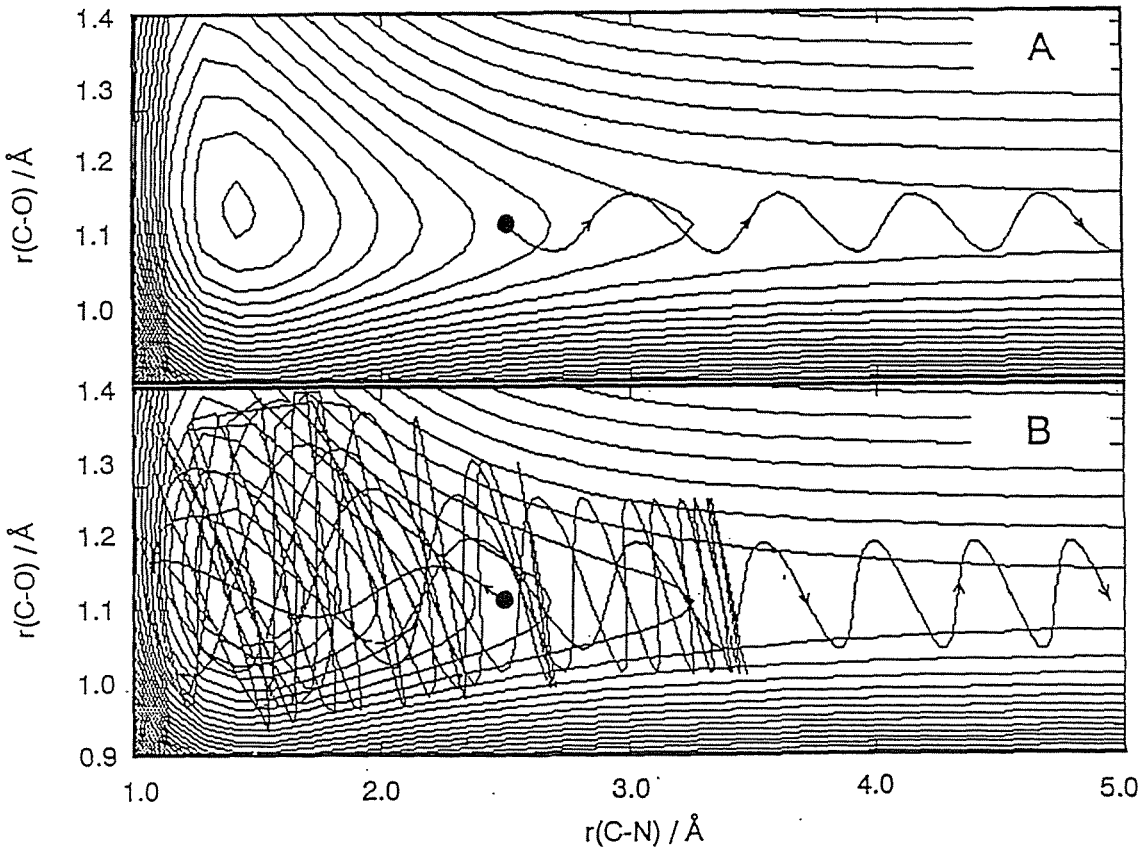

Figure III-8. Ab-initio fitted potential energy surface at the ground state (exit region) and sample trajectories for the direct (A) and the intermediate complex (B) channels.

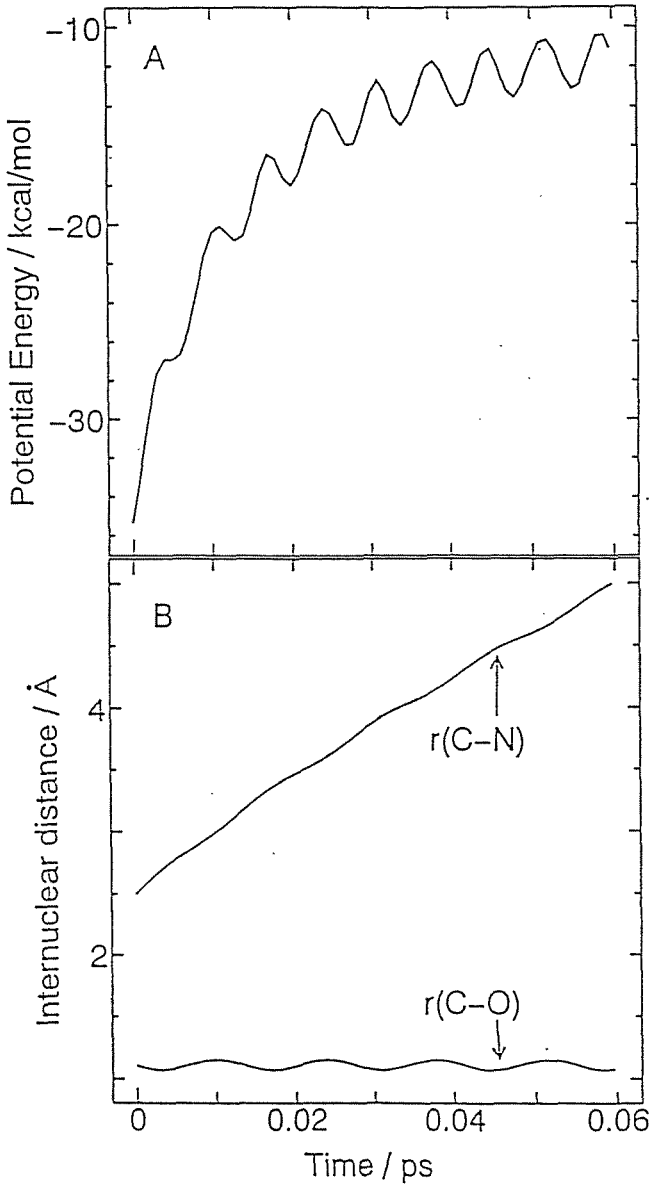

Figure III-9. A sample trajectory for *the direct channel* plotted for the potential energy (A) and r(C-O) and r(C-N) (B) versus time. The trajectory starts on the ground state at the time zero.

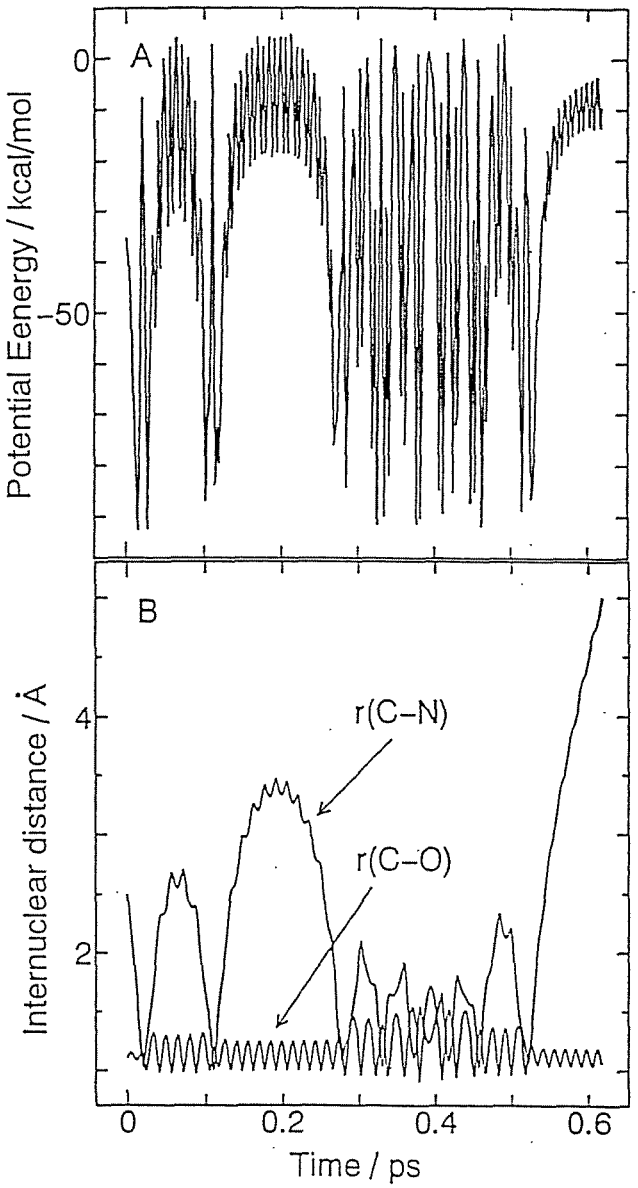

Figure III-10. A sample trajectory for *the intermediate channel* plotted for the potential energy (A) and r(C-O) and r(C-N) (B) versus time. The trajectory starts on the ground state at the time zero.

C. Three dimensional (3D) trajectory calculations

In order to obtain the angle dependency of the vibrational mode of product CO^+, 3D-trajectory calculations are performed. The results of the 3D-trajectory calculation are essentially similar to that of the collinear collision trajectories. One thousand trajectory calculations for non-reactive collision on the excited state PES gave vibrational ground state products. The CO^+ produced via the direct channel is also obtained as a vibrational ground state. The trajectory calculations of the intermediate complex channel gave a vibrational distribution of the CO^+ that is populated in the range of v= 0-3 with the maximum of the distribution located at v=1.

D. Analysis of the trajectory calculations

Figure III-11 shows the vibrational distributions of the product CO^+ for the intermediate complex and direct channels as a function of vibrational quantum number. The collinear and 3D trajectory calculations gave similar results as shown in Figures III-11(A) and III-10(B), although the peak for the 3D-trajectory is located at v=1. One can find that the distributions for the two channels are obviously different from each other. The vibrational quantum number of the CO^+ product via the direct channel is obtained as only v=0. On the other hand, via the intermediate complex channel the vibration is widely distributed in excited states (v= 1, 2). These results indicate that the direct channel and the intermediate complex channel lead to the vibrational ground and excited state CO^+ products, respectively. Furthermore, we have confirmed by the trajectory calculations at collision energies from 0.026 eV to 3.0 eV that the direct channel leads to the vibrational ground state.

The branching ratios of the direct channel vs. the intermediate complex channel are estimated by fitting to the experimental values[3]; they are 0.37 : 0.63 at the collision energy of 0.16 eV and 0.76 : 0.24 at 0.026 eV. This result implies that the direct channel becomes more favorable at lower collision energies.

4. Discussion and Conclusion

In the present work, we have calculated the ground and first excited potential energy surfaces (PESs) of a charge transfer reaction, $N^+ + CO \rightarrow N + CO^+$ and proposed a reaction model based on the results derived from the *ab-initio* calculations. In the model, two reaction channels are considered as the primary pathways during the charge transfer process. In order to confirm the validity of this model, classical trajectory calculations have been carried out on

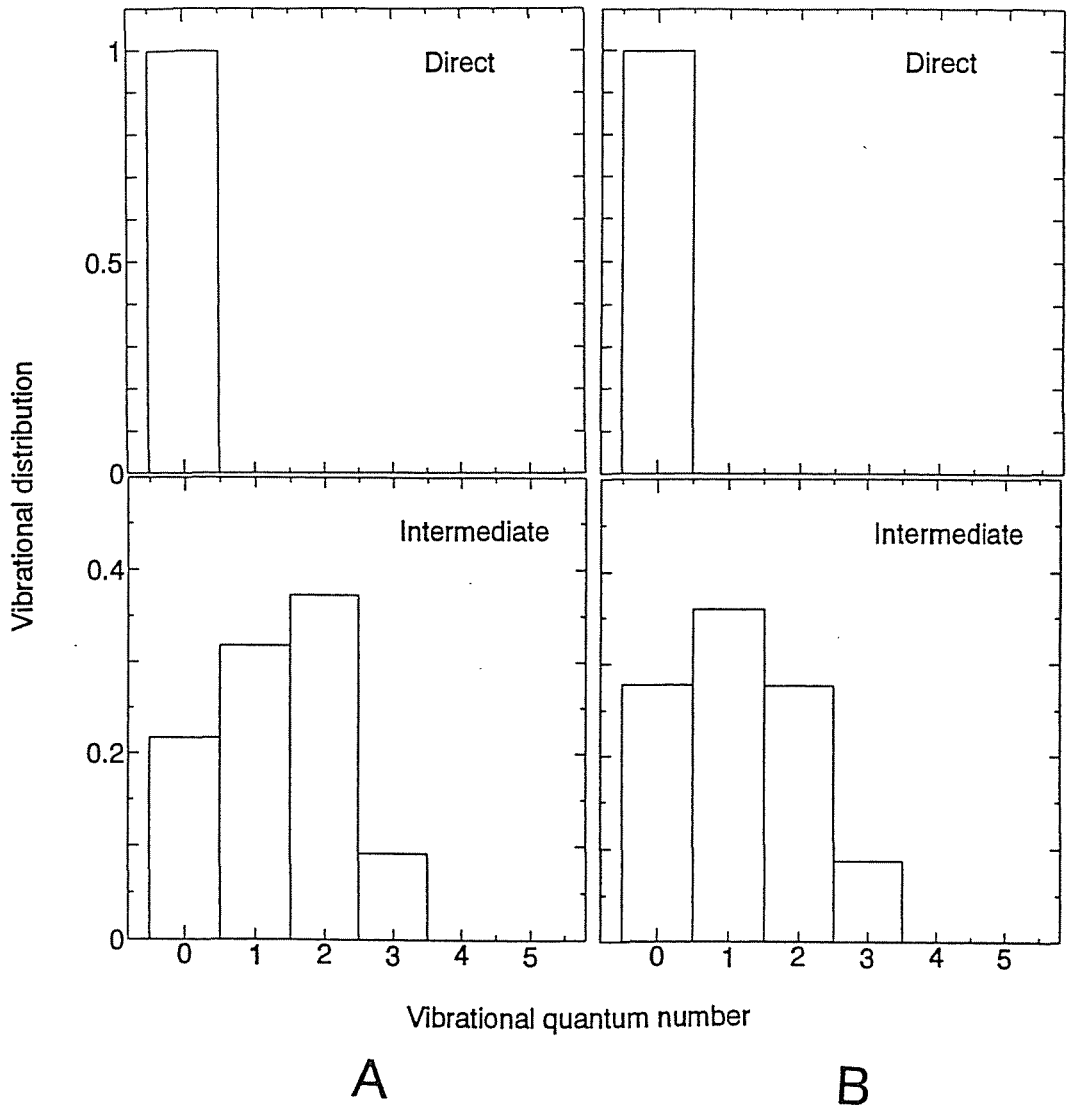

Figure III-11. Vibrational distributions of the product CO^+ as a function of the C-O vibrational quantum number; (A) collinear colision, (B) 3D-trajectory.

the *ab-initio* fitted PESs. It is derived from the trajectory calculations that the CO^+ cation produced via the direct channel leads to the vibrational ground state, whereas the intermediate complex channel gives the vibrationally excited CO^+ product. The collinear trajectories show that the vibrationally excited CO^+ product is formed by collinear collisions as well as side-on attack.

The mechanism of reaction I is still in controversy as described in Sec. 1. The present calculations qualitatively support the dual channel mechanism. The present model is, however, a little different from the previous mechanisms: the excited state complex is involved and plays an important role in the reaction dynamics as described in Sec. 3-E. The model describes quali-tatively the experimental features of the vibrational distribution.

In the present calculation, we have introduced some approximations to treat the reaction dynamics and to construct the potential energy surfaces. It was assumed that the translational energy at the start point on lower PES is fixed to 1.61 eV. This may cause an overestimation of kinetic energy in the product CO^+. A method to treat the energy distribution of the nuclear motions[16] would be required to obtain more reliable results. The surface hopping trajectory[16] was not taken into account. This calculation will be necessary for a quantitative comparison with the experimental values. In the PES calculations, we employed the UHF, MPn (n=2 and 3) and D-CI calculations with split valence 4-31G basis set. Several levels of calculation gave essentially similar results for the shape of PES. The UHF calculations, however, caused a large spin contamination (largest value $<S^2>=2.58$) at the dissociation limit of $N\cdot\cdot CO^+$, which is 30 % larger than exact value. Therefore the D-CI/4-31G PESs were used for the classical trajectory calculation. More elaborate calculations with a larger basis set and more accurate wave function, such as MR-SD-CI or MC-SCF-CI calculations, are needed to obtain a deeper insight for the collision process. Despite the approximations employed here, it was shown that a theoretical characterization of reaction I enables us to obtain valuable information on the mechanism of the collision process.

REFERENCES

1. (a) Sizun, S; Grimbert, D.; Sidis, V.; Baer, M, *J. Chem. Phys.*, **1992**, 96, 307; Baer, M., in *The Theory of Chemical Reaction Dynamics*, edited by M. Baer (Chemical Rubber, Boca Raton, 1985), Vol.II, Chap. 4.
(b) Lin, G.H.; Maier, J.; Leone, S,R, *J. Chem. Phys.* **1985**, *82,* 5527, Hamilton, C.E.; Bierbaum, V.M.; Leone, S.R, *J. Chem. Phys.* **1984**, *83*, 2284
(c) Gislason E.A.; Parlant, G.; Archirel, P.; Sizun, M., *Faraday Discuss.* **1987**, *84*, 325.
(d) Archirel, P.; Levy, B., *Chem. Phys.* **1986**, *106*, 51.
(e) Lin, C.H.; Maier, J.; Leone, S.R, *Chem. Phys. Lett.* **1986**, *125*, 557.
(f) Sonnenfroh, D.M.; Leone, S.R., *J. Chem. Phys.* **1989**, *90*, 1677.
(g) Baer, M.; Nakamura, H., *J. Chem. Phys.*, **1987**, *87*, 4651.
(h) Chapman, S., *J. Chem. Phys.* **1985**, *82*, 4033.
(i) Kusunoki, I; Ishikawa, T, *J. Chem. Phys.* **1985**, *82*, 4991.
(j) Shiraishi, Y.; Kusunoki, I., *J. Chem. Phys.* **1987**, *87*, 6530.
(k) Kusunoki, I; Ottinger, C., *Chem. Phys. Lett.* **1984**, *109*, 554.
(l) Yamashita, K; Morokuma, K; Shiraishi, Y; Kusunoki, I., *J. Chem. Phys.* **1990**, *92*, 2505.
(m) Sakai, S; Kato, S; Morokuma, K.; Kusunoki, I, *J. Chem. Phys.* **1981**, *75*, 5398.
(n) Tachikawa, H; Lunnel, S; Tornkvist, C; Lund, A, *Int. J. Quantum. Chem.* **1992**, *43*, 449.
(o) Tachikawa, H; Shiotani, M; Ohta, T, *J. Phys. Chem.* **1992**, *96*, 165.
(p) Tachikawa, H; Ogasawara, M., *J. Phys. Chem.* **1990**, *94*, 1746.
(q) Tachikawa, H; Ichikawa, T; Yoshida, H., *J. Am. Chem. Soc.* **1990**, *112*, 982.
(r) Tachikawa, H.; Ogasawara, M.; Lund, A., *Can. J. Chem.* **1993**, *71*, 118.
(s) Tachikawa, H; Murai, H; Yoshida, H, *J. Chem. Soc. Faraday Trans.* **1993**, *89*, 2369.
2. (a) Ng, C.Y., in *State-Selected and State-to-State Ion-Molecule Reaction Dynamics*: Part I, Experiment, edited by C.Y. Ng and M.Baer, vol.82 in Advances in Chemical Physics (Wiley, New York, 1992), p.401.
(b) Knutsen, K; Bierbaum, V.M; Leone, S.R, *J. Chem. Phys.*, **1992**, *96*, 298.
(c) Kato, T., *J. Chem. Phys.*, 1984, *80*, 6105.
(d) Conaway, W; Ebata, T; Zare, R.N, *J. Chem. Phys.* **1987**, *87*, 3453.
(e) Tomoda, S; Suzuki, S; Koyano, I, *J. Chem. Phys.*, **1988**, *89*, 7267.

3. (a) Hamilton, C.E; Bierbaum, V.M; Leone, S.R, *J. Chem. Phys.*, **1985**, *83*, 601.
(b) Lin, G.H; Maier, J; Leone, S.R, *J. Chem. Phys.* **1986**, *84*, 2180.
4. Gerlich, D., In *Symposium on Atomic and Surface Physics*, edited by F. Howorka, W. Lindinger, and T.D. Mark, (Studia, Innsburuck, 1984).
5. Wu, A.A, *Chem. Phys.* **1977**, *21*, 173.
6. Cai, Z.L; Wang Y.F; Xiao,H.M, *Chem. Phys. Lett.* **1992**, *190*, 381.
7. Herzberg, G, in *Spectra of diatomic molecules*, (Van Nostarand, Princeton, 1950).; Ch.E. Moore, NBC Circular **1958**, 467.
8. Frish, M.J; Binkley, J.S; Schlegel, H.B; Raghavachari, K; Melius, C.F; Martin, R.L; Stewart, J.J.P; Bobrowicz, F.W; Rohlfing, C.M; Kahn, L.R; DeFrees, D.J; Seeger, R; Whiteside, R.A; Fox, D.J; Fleuder, E.M; Topiol, S; Pople, J.A., Ab-initio molecular orbital calculation program GAUSSIAN86, Carnegie-Mellon Quantum Chemistry Publishing Unit; Pittsburgh, PA.
9. (a) Mϕller, C; Plesset, M.S., *Phys. Rev.* **1934**, *46*, 618.
(b) Bartlett, R.J, *J. Phys. Chem.*, **1989**, *93*, 1697.
(c) Raghavachari, K, *J. Chem. Phys.*, **1985**, *82*, 4607.
10. Ditchfield, R; Hehre, W.J; Pople J.A, *J. Chem. Phys.* **1971**, *54*, 724.
11. Pulay, P, *in Modern Theoretical Chemistry*, edited by H.F. Shaefer (Plenum, New York, Vol.4, Chap.4, 1977).
12. (a) Hariharan, P.C.; Pople, J.A, *Theor. Chim. Acta.* **1973**, *82*, 213. (b) Francl, M.M; Pietro, W.J; Hehre, W.J; Binkley, J.S; Gordon, M.S; DeFrees, D.J; Pople, J.A, *J. Chem. Phys.* **1982**, *77*, 3654.
13. Kwei, G.H; Boffardi, B.P; Sun, S.F, *J. Chem. Phys*, **1973**, *58*, 1722.
14. Bunker, D.L, *Meth. Comput. Phys.* **1971**, *10*, 287.
15. Jonston, H.S, in *Gas Phase Reaction Rate Theory* (Ronald, New York, 1966), Chap.15.
16. (a) Stine, J.R; Muckerman, J.T, *J. Chem. Phys*, **1976**, *10*, 3975., *J. Phys. Chem.* 1987, *91*, 459.
(b) Blais, N.C; Truhlar, D,G, *J. Chem. Phys.* **1983**, *79*, 1134.
(c) Mead, C.A; Truhlar, D.G, *J. Chem. Phys.*, **1986**, *84*, 1055.
(d) Eaker, C, *J. Chem. Phys.*, **1987**, *87*, 4532.

CHAPTER IV.

DYNAMICS OF THE PROTON TRANSFER REACTION $O^- + HF \rightarrow OH(V) + F^-$

1. Introduction.

Proton transfer, hydrogen atom transfer and charge transfer are the most fundamental chemical elementary processes which are observed widely in the gas phase as well as in the condensed phase.[1] Proton transfer reaction in gas phase is one of the simplest reactions including the bond forming and bond breaking processes. Therefore, the reactions have been extensively studied for elucidation of the nature of chemical reaction.[2] Proton transfer reaction in the heavy-light-heavy system,

$$A^- + H\text{-}B \rightarrow A\text{-}H + B^-, \qquad (4.1)$$

where A and B are heavy atoms, has been investigated by means of the crossed molecular beam technique,[3] drift and selected ion flow tubes technique,[4] infrared emission,[5] and laser-induced fluorescence (LIF) technique.[6] These experimental studies show that i) the relative translational energy between the products (A-H and B^-) increases with increasing collision energy, and ii) the energy transfer from translational mode to vibrational mode of the product does not occur effectively.

Recently, an exceptional reaction was found by Knutsen *et al.*[7] They determined using a flow-drift tube technique, the vibrational state populations of product OH radical formed by a proton transfer reaction,

$$O^- + HF \rightarrow OH\,(v=0,1) + F^- \qquad \text{(reaction I)}.$$

The fractional ratio of product OH(v=1),

$$P(v=1) = \frac{OH(v=1)}{OH(v=0)+OH(v=1)} \qquad (4.2),$$

increases monotonically with increasing collision energy. Thus the kinetic feature of this reaction is much different from the previously observed features.

In this chapter, the potential energy surfaces of reaction I are calculated by means of the *ab-initio* MO method, and the vibrational and rotational distributions of the product OH are determined by using the quasi-classical trajectory calculations on the *ab-initio* fitted PESs. Primary aims of the present study are (i) to provide theoretical information on reaction I, and

(ii) to discuss the mechanism of the proton transfer process in reaction I on the basis of both the PES characteristics and the results obtained from the quasi-classical trajectory calculations. In the following section, the method of the calculations is described. In section 3, the *ab-initio* MO calculations are presented. The results of the classical trajectory calculations on the *ab-initio* fitted PESs are also shown. The conclusion and discussion are described in section 4. A new theoretical explanation of reaction I will be also described in summary.

2. Method of calculations

A. *Ab-initio* MO calculations.

Geometries for the neutral HF molecule, the OH radical and the reaction intermediate $[OHF]^-$ are fully optimized by means of the energy gradient method[8] with 4-31G*, 6-31G*, 6-31G** and 6-31++G** basis sets.[9] The electron correlation energy for each geometry is estimated by double-substituted configuration interaction method (D-CI)[10a] and Mϕller-Plesset second- and third-order perturbation methods (MP2 and MP3)[11] within the frozen-core approximation with the 6-31G** and 6-31++G** basis sets. Unlinked cluster quadruple correction (QC) is added to allow for the size-consistency correction.[10b-d]

Adiabatic potential energy surfaces (PESs) for reaction I as functions of the O-H and H-F distances are obtained at the Hartree-Fock (HF) level with 6-31++G** basis sets. Two sets of O-H-F angles (θ), 180° and 135°, are chosen to express the angle dependency. The *ab-initio* MO calculations are carried out at 120 points on the PES.

B. *Quasi*-classical trajectory calculations.

The PESs obtained theoretically are fitted to an analytical equation by means of the least-squares method. The extended-LEPS surface is employed to express the analytical function of the PES. 2000 trajectory calculations on the LEPS surface are computed at each initial condition (HF(v=0,J=0) and collision energies (E_{coll}'s) of 1.198, 3.00, 3.68, 4.10 and 5.34 kcal/mol). Integration of the classical equations of motion is performed at the standard fourth-order Runge-Kutta and sixth-order Adams Moulton combined algorithm[12] with the time increment of 1×10^{-16} s.

C. Lifetime of intermediate complex $[OHF]^-$ ($^2\Pi$).

The lifetime (τ) of $[OHF]^-$ intermediate on the ground state 2D-PES is estimated by using RRK theory.[13] The lifetime as a function of energy E is expressed by

$$\tau = \frac{1}{\langle \nu \rangle} \left[\frac{E - V}{E} \right]^{1-s} \qquad (4.3)$$

where <v> is an average of vibrational frequencies of modes related to the reaction, V is the dissociation energy of the reaction; $[OHF]^- \rightarrow OH + F^-$, *s* is the number of degrees of freedom of vibrations. The <v> is calculated with the OH stretching mode and the HF stretching mode of $[OHF]^-$ obtained at the MP2/6-31++G** level.

3. Results

A. Global features of the proton transfer reaction

To obtain the structures of reactant, product and an intermediate $[OHF]^-$, geometry optimizations are performed. The geometries obtained are listed in Table VI-I. Four independent calculations give a similar geometry. The O-H and H-F bond lengths of the intermediate complex $[OHF]^-$ are 1.0314 A and 1.4003 A in the $^2\Pi$ state, respectively. The H-F distance is much larger than the O-H distance, and the skeleton of O-H-F$^-$ is most stable for a linear form (θ=180°). These features are similar to the previous theoretical results.[14]

Total energies, heat of reaction (ΔH) and the complex formation energies (ΔE) calculated at several levels of theory are given in Table IV-2. The heat of reaction calculated with HF/6-31++G** basis sets (13.19 kcal/mol) is essentially in accordance with the experimental values (10.6 kcal/mol).[15] This agreement implies that one can discuss the reaction mechanism with the HF/6-31++G** level.

Based on the relative energy calculated at the D-CI+QC/6-31++G** level, the energy correlation diagram is illustrated as shown in Figure IV-1. The present proton transfer reaction has an strongly bound intermediate complex $[OHF]^-$ at the collision region. This feature is in good agreement with the prediction from MP2/6-31++G** level.[14]

B. Potential energy surfaces

The adiabatic PESs of the $^2A''$ ($^2\Pi$) state for the O$^-$ + HF reaction are shown in Figure IV-2. A strongly bound complex is formed at r(HF) = 1.30 A and r(OH) = 1.05 A on the ground state PES (θ=180°). The potential basin of the intermediate complex $[OHF]^-$ is deepest for the collinear collision. The stabilization energy of $[OHF]^-$ is calculated to be 1.58 eV with respect to the initial state (r(O$^-$..H)= 4.2 A and r(H-F)= 1.0 A).

The shape of the PES exhibits that the intermediate complex $[OHF]^-$ is strongly and tightly bound along both O-H and H-F directions. Therefore, it could be expected that energy transfer from the translational mode to the O-H stretching mode takes place efficiently in this basin by the collision. The PES clearly indicates the vibrational excitation of product OH.

Table IV-1. Optimized geometries of HF, OH and intermediate complex $[OHF]^-$. Bond length and angles in angstrom and degrees, respectively.

	HF	OH	[OHF]$^-$		
method	r(H-F)	r(O-H)	r(H-F)	r(O-H)	θ
HF/4-31G			1.2981	1.1001	180.0
HF/6-31G*			1.2824	1.0848	180.0
HF/6-31G**	0.9006	0.9549	1.2608	1.0946	180.0
HF/6-31++G**	0.9022	0.9549	1.4003	1.0314	180.0
MP2/6-31++G**[a]			1.35	1.08	180.0

[a]From Ref. 14.

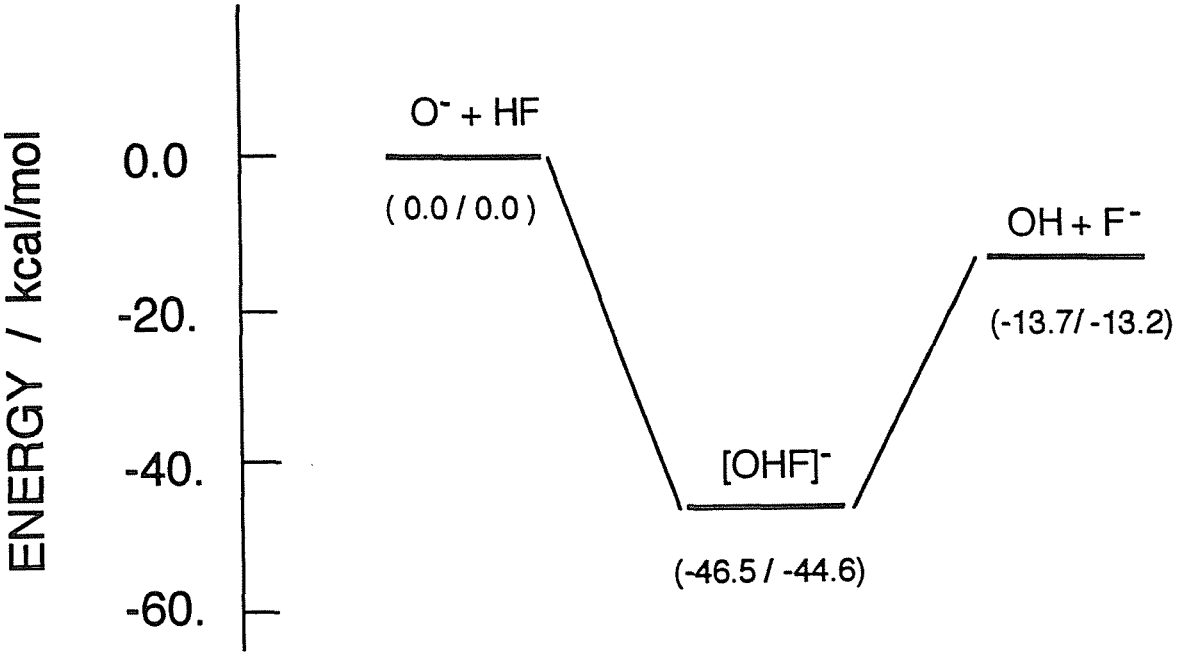

Figure IV-1. Energy diagram of $O^- + HF \rightarrow OH + F^-$ reaction. The numbers in parentheses are the HF/D-CI+QC energies relative to reactant state calculated with 6-31++G** basis set.

TABLE II. Total energies (in a.u), the complex formation energies (ΔE in kcal/mol), and heat of reactions (ΔH in kcal/mol) for the O^- + HF → OH+ F^- reaction system.

method[a]	O^-	HF	$[OHF]^-$	OH	F^-	ΔE	ΔH
HF/6-31G**//HF/6-31G**	-74.718701	-100.011691	-174.812858	-75.388331	-99.350482	51.78	5.28
DCI/6-31G**//HF/6-31G**	-74.865239	-100.191823	-175.134877	-75.541368	-99.523531	48.83	4.92
DCI+QC[b]/6-31G**//HF/6-31G**	-74.869403	-100.197169	-175.156471	-75.546020	-99.528279	56.41	4.85
MP2/6-31G**//HF/6-31G**	-74.857755	-100.194125	-175.143891	-75.531803	-99.526607	57.74	4.10
MP3/6-31G**//HF/6-31++G**	-74.867936	-100.196021	-175.153941	-75.543863	-99.527506	56.47	4.65
HF/6-31++G**//HF/6-31++G**	-74.766619	-100.024312	-174.861814	-75.393364	-99.418586	44.60[c]	13.19
MP2/6-31++G**//HF/6-31++G**	-74.925248	-100.215231	-175.217319	-75.540909	-99.623847	48.22	15.23
MP3/6-31++G**//HF/6-31++G**	-74.930774	-100.214503	-175.219374	-75.552371	-99.61363	46.50	13.00
DCI/6-31++G**//HF/6-31++G**	-74.926957	-100.210064	-175.198087	-75.549628	-99.609462	38.32	13.84
DCI+QC[b]/6-31++G**//HF/6-31++G**	-74.932979	-100.215970	-175.223085	-75.554624	-99.616117	46.52	13.68

[a]" // " means " optimized by ".

[b]Size-consistency correction.

[c]Basis set super position error (BSSE) of the complex formation energy is *0.46* kcal/mol.

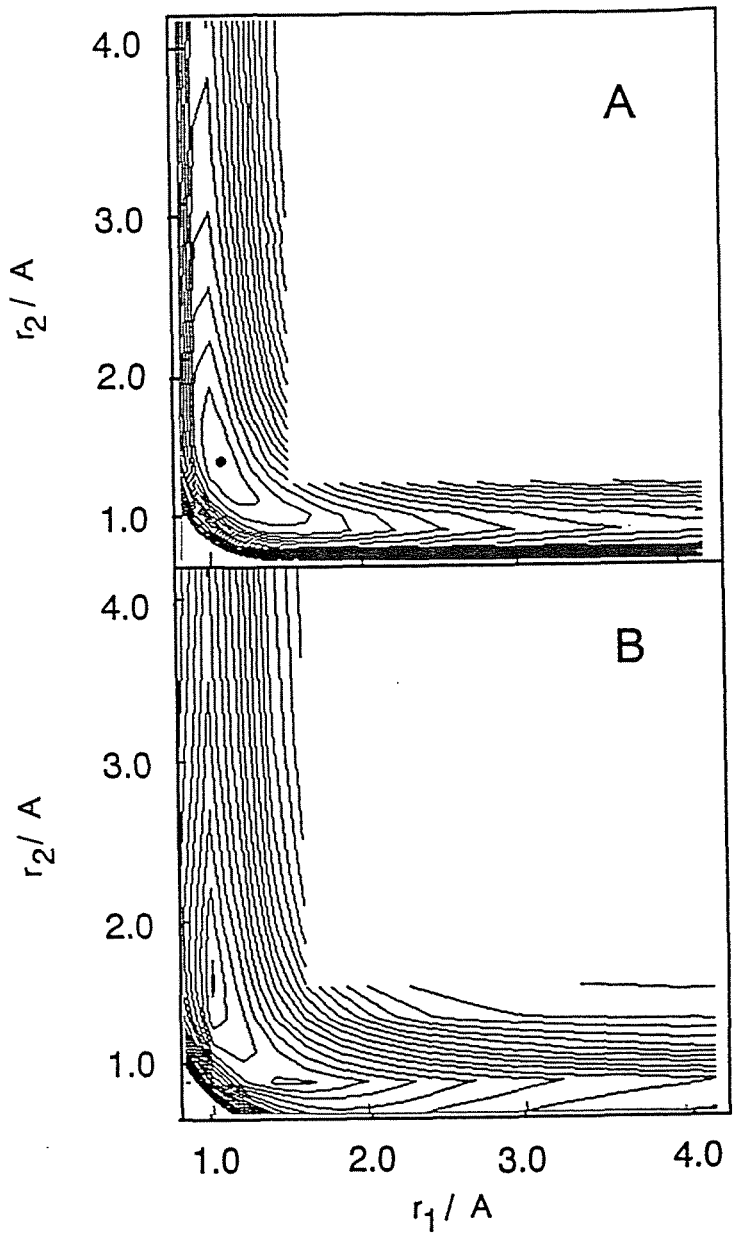

Figure IV-2. Potential energy surfaces of the O^- + HF → OH + F^- reaction calculated at the HF/6-31++G** level. (A) Collinear collision (θ= 180°), (B) Coplanar collision (θ=135°). Contours are drawn for each 5 kcal/mol.

C. *Quasi*-classical trajectory calculation

Table IV-3 shows fitting parameters for the PES determined by the least square method. The well depths, the shape of the PES and ΔH are reasonably reproduced by the *ab-initio* fitted PES.

Potential energy and interatomic distances versus time for a sample trajectory calculated on the fitted PES is shown in Figure IV-3. The trajectory with a collision energy of 3.00 kcal/mol falls down the potential basin, and after two collision with the well the trajectory leads to product ($OH + F^-$). Elapsed time in the intermediate complex region for this trajectory is about 0.05 psec. The lifetime derived from all trajectory calculations is in the range of 0.05-0.9 ps. The corresponding value estimated by RRK theory[15] is 0.22 ps. This means that the excess energy of $[OHF]^-$ is not completely distributed in the rotational and vibrational modes.

Recently, Levandier *et al.*[3b] present the angular and kinetic energy distribution for the products of the proton transfer reaction $O^- + HF \rightarrow OH + F^-$ at a center of mass collision energy of 9.54 kcal/mol. Their results indicate that the reaction proceeds through a transient $[OHF]^-$ complex living several rotational period. The present theoretical result is consistent with their experiments.

TABLE IV-3. LEPS parameters (S, Sato parameter; β, Morse parameter in A^{-1}; De, Dissociation energy in kcal/mol; r_e, internuclear distance in A; α, alpha value in extended LEPS parameter) of the *ab-initio* fitted PES.

parameter	O···H	H···F	O···F
S	1.47263	1.3243	0.7700
De	149.12	135.26	48.91
β	1.8836	1.9011	1.8144
r_e	0.9766	0.9234	2.7739
α	1.000		

D. Analysis of the trajectory calculations

Fractional ratio of the product OH(v=1). The summary of all trajectory calculations is listed in Table IV-4. The fractional ratio of the product OH(v=1) defined by eq.(2), P(v=1),

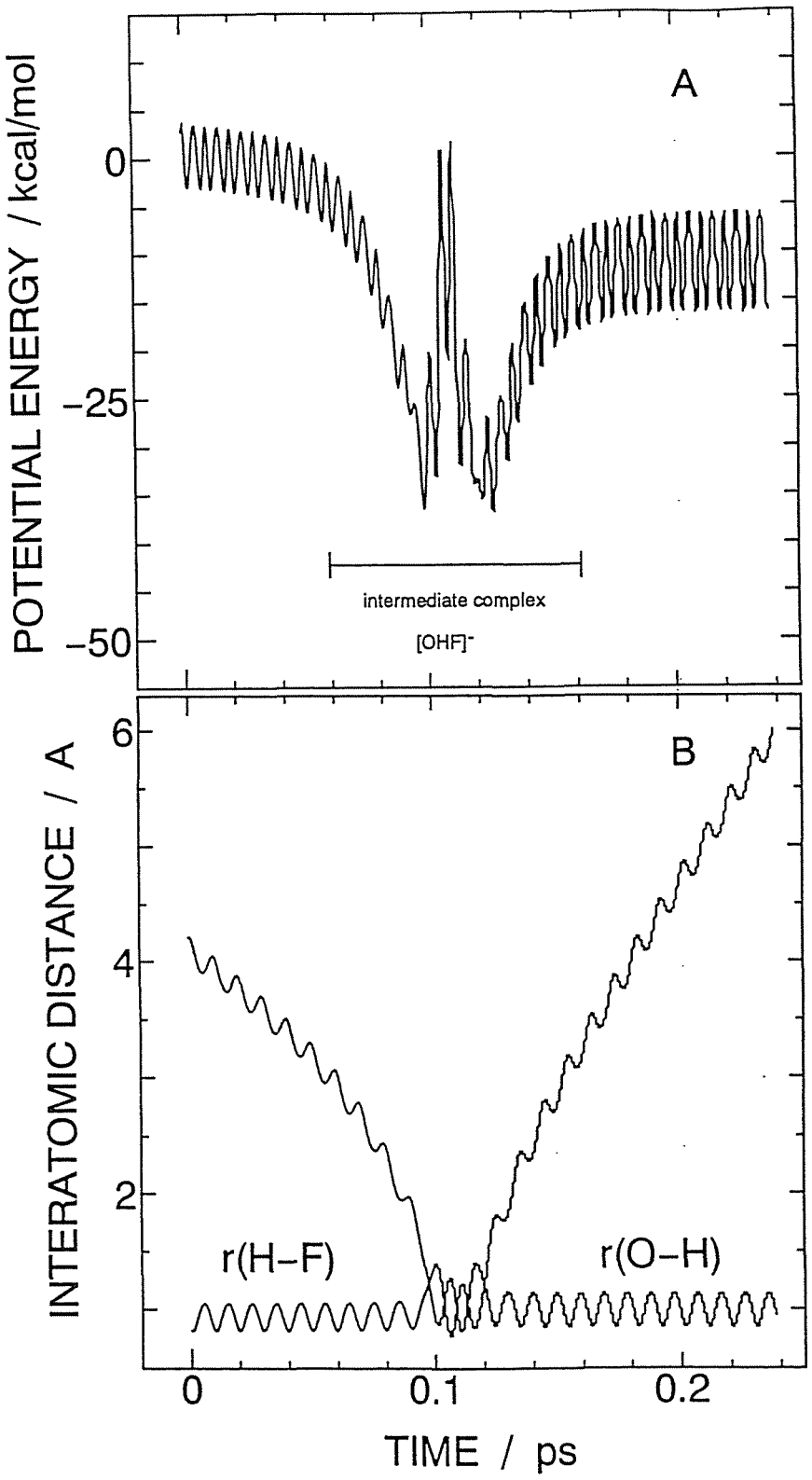

Figure IV-3. Sample trajectory plotted for the potential energy (A) and r(H-F) and r(O-H) (B) versus time. The trajectory starts on the entrance region at the time zero and passes rapidly the intermediate complex region.

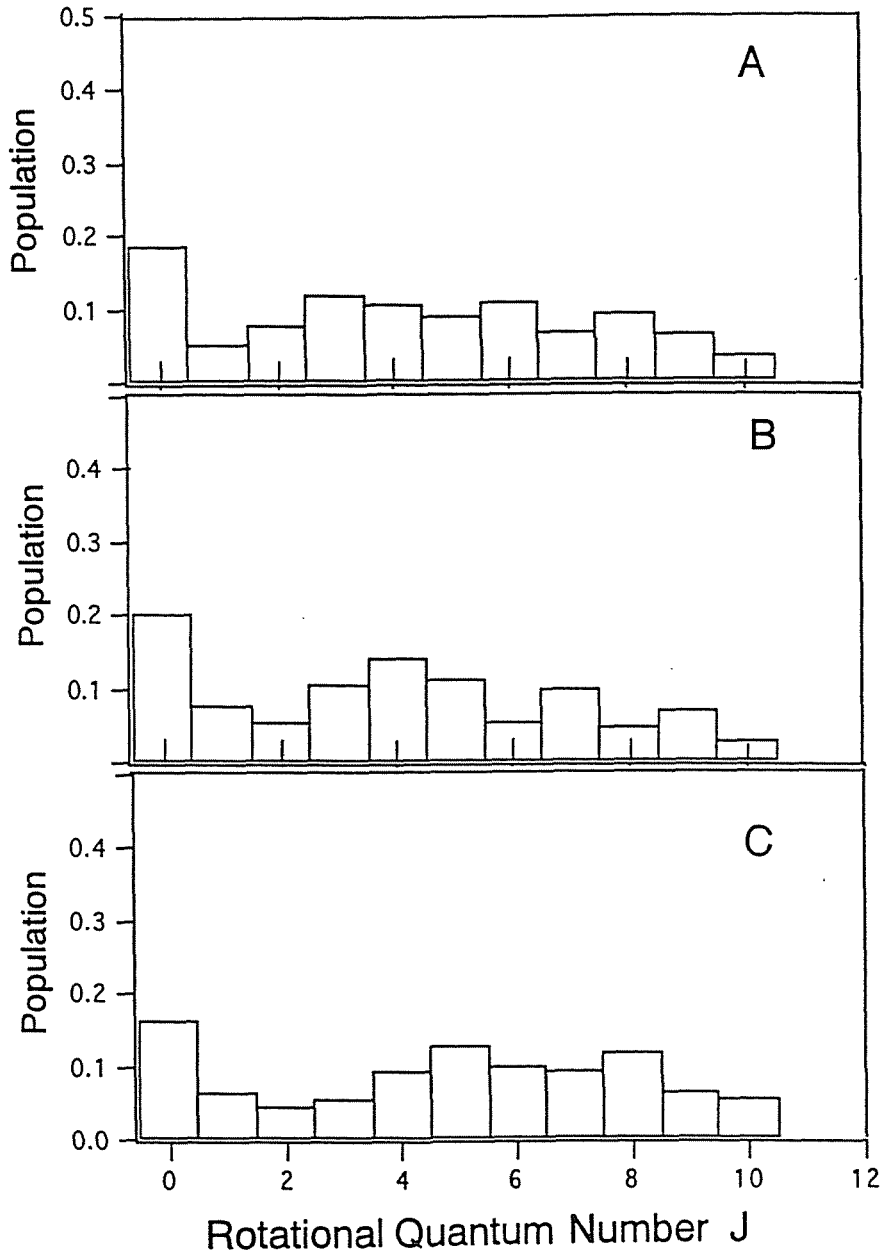

Figure IV-4. Rotational state populations of the OH radical formed by the $O^- + HF \rightarrow OH + F^-$ reaction. The collision energies are (A) 1.198 kcal/mol, (B) 3.00 kcal/mol, and (C) 5.31 kcal/mol.

increases with increasing collision energy from 1.198 to 4.10 kcal/mol. At Ecoll = 5.34 kcal/mol, P(v=1) is suddenly decreased. This reason will be argued in discussion part.

The rotational state populations of the product OH. Figure IV-4 shows the rotational state populations of the product OH calculated at E_{coll} = 1.198, 3.00 and 5.31 kcal/mol. The populations are widely distributed from J = 0 to J = 10. It is clear that the distribution is composed of two components of rotational distribution. Schematic illustration of the two population curves are represented in Figure IV-5. One component denoted by A has a peak at J=0, whereas the other component denoted by B peaks at higher rotational level (J=4-6). The trajectory calculations indicate that A-part and B-part are composed of the vibrationally excited OH(v=1) and the vibrationally ground state OH(v=0), respectively. From an analysis of each trajectory, it is found that the OH(v=1) is mainly formed by a direct mechanism, and the OH(v=0) is formed via a long-lived intermediate complex $[OHF]^-$. As shown in IV-4, the ratio A/B increases monotonically with increasing collision energy and peaks at E_{coll} = 4.10 kcal/mol (A/B=0.43). At Ecoll=5.31 kcal/mol, A-part is slightly decreased (A/B=0.35).

TABLE IV-4. Summary of trajectory calculations.

Ecoll kcal/mol	Nr[a]	P(v=1)[b]	A/B[c]
1.198	0.800	0.12	0.14
3.00	0.70	0.18	0.22
3.68	0.60	0.28	0.39
4.10	0.50	0.30	0.43
5.34	0.40	0.26	0.35

[a]Ratio of reactive trajectories,
Nr = (number of reactive trajectories)/(number of total trajectories)
[b]OH(v=1) fractional ratio, P(v=1)={OH(v=1)/[OH(v=0) + OH(v=1)]}
[c]Ratio of A-part and B-part.

4. Discussion and conclusion

A. Comparison with experimental results.

Recently Leone and co-workers[7] determine relative vibrational state populations for the OH product in the reaction O^- + HF → OH(v=0,1) + F^- as a function of reactant center-of-mass collision energy in a flow-drift tube. At thermal energy, P(v=1) is obtained to be 0.18 ± 0.01. At enhanced average collision energies of 2.29 and 3.68 kcal/mol, P(v=1) increases to 0.25 ± 0.02 and 0.33 ± 0.03, respectively. For comparison, the present theoretical values are plotted

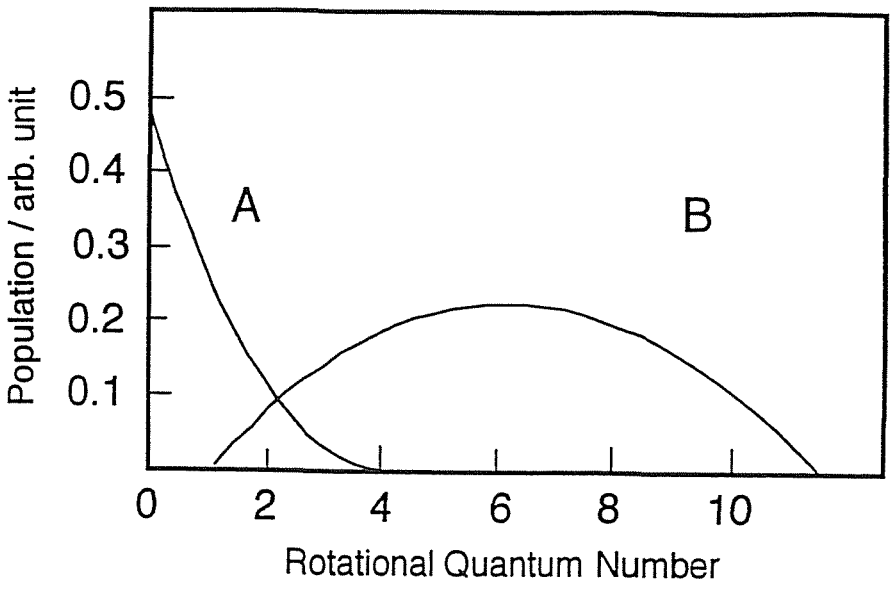

Figure IV-5. Schematic representation of the rotational state population.

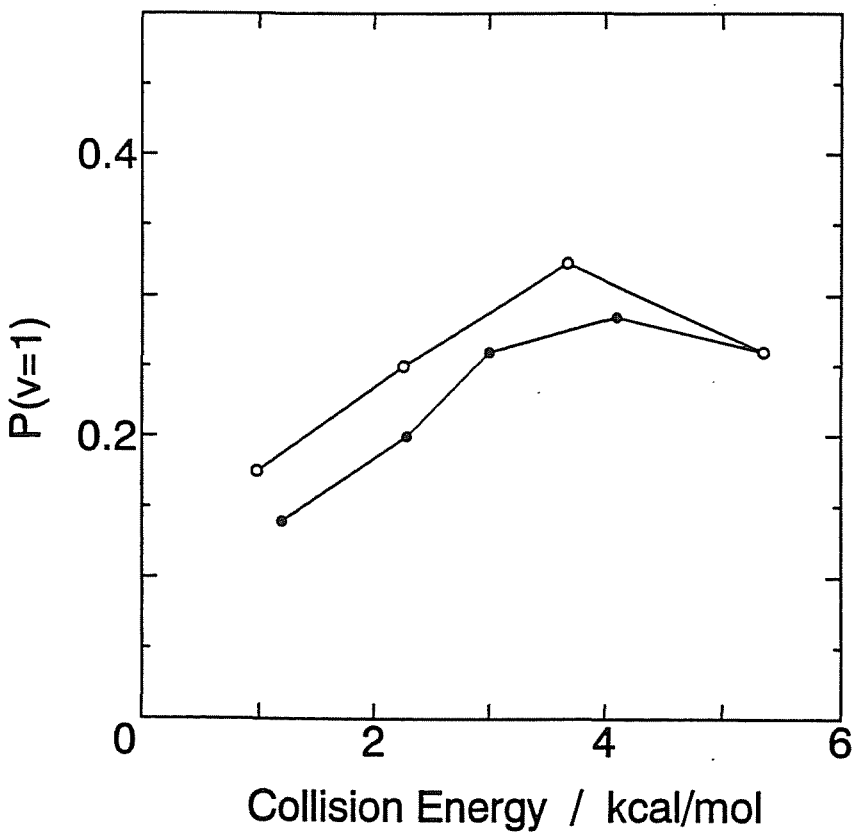

Figure IV-6. The theoretical fraction of total OH population in v=1, P(v=1), vs. center-of-mass collision energy of the reagents (●). The experimental data (O) are cited from Ref. 7.

in Figure IV-6 together with Leone's experimental results.[7] Although the present theoretical values are slightly smaller than the experimental values, a collision energy dependency of P(v=1) is excellently represented by theoretical calculations.

Theoretical OH(v=1) fractional population, P(v=1), increases monotonically up to E_{coll} = 3.68 kcal/mol with increasing collision energy. This increment of P(v=1) is due to the energy transfer at the deep well. In this deep well, the translational energy converts efficiently to the O-H vibrational mode. The deep intermediate complex region causes the vibrational excitation of OH modes.

At E_{coll} = 5.31 kcal/mol, the OH(v=1) fractional population decreases and deviates from the straight-line. This feature is also excellently accordance with experimental one.[7] Let us consider reason why the OH(v=1) fractional population is decreased in this energy region (E_{coll} ≈ 5.31 kcal/mol). As a working hypothesis, we consider here two mechanisms; 1) OH(v=2) product channel is open in this energy region, and 2) the excess energy of $[OHF]^-$ transfers to other internal modes (eg. the rotational mode). Our theoretical calculation indicates that no OH(v=2) product is found at E_{coll} = 5.31 kcal/mol. Therefore, the former mechanism can be rejected. The ratio A/B calculated to be 0.35 at E_{coll}=5.31 kcal/mol is slightly smaller than that of E_{coll} =4.10 kcal/mol (A/B=0.43). This means that the preference of reaction channels is varied in this energy region.

B. The Reaction Model

In this section, we propose a reaction model based on the theoretical results. The *ab-initio* potential energy surface (PES) shows that the strongly and tightly bound intermediate complex $[OHF]^-$ exists in the collision region on the PES. This deeper well causes the energy transfer from the translational mode to the OH vibrational mode. As described in previous section, reaction I is composed of two reaction channels. One is a direct channel,

$$O^- + HF \rightarrow F^- + OH\,(v=1, J=0).$$

The product OH formed by the direct channel is in vibrational excited state (v=1). The rotational state population of the product OH peaks at J=0 (i.e., A-part). The trajectory for this channel passes rapidly in the intermediate complex region. The other channel is a complex channel,

$$O^- + HF \rightarrow F^- + OH(v=0, J=\text{highly excited}).$$

The reaction for the complex channel proceeds via a long-lived intermediate complex $[OHF]^-$. Therefore, the excess energy of $[OHF]^-$ formed by the collision can convert to the rotational energy within a lifetime. The rotational state population of the product OH is widely distributed (i.e., B-part). At low collision energy region such as thermal energy (E_{coll} = 1.198 kcal/mol),

both channels are equivalently dominant. The product OH radical via the direct channel monotonically increases with increasing collision energy up to 4.10 kcal/mol. Further increasing collision energy ($E_{coll} \approx 5.31$ kcal/mol), the product OH via complex channel is dominant. Thus the present model explains the experimentally observed features of reaction I. [6,7]

C. Discussion

The mechanism of proton transfer reaction I is still in controversy as described in Section 1. In this chapter, we propose a new reaction model for reaction I. This model is composed of two reaction channels (direct and complex channels). The model describes qualitatively the experimental features of the vibrational distribution deduced by Leone *et al.* [6,7]

In the present calculation, we have introduced some approximations to construct the potential energy surfaces. In the PES calculations, we employ the UHF calculations with split valence plus polarization and diffuse function type 6-31++G** basis set. Preliminary calculation at the D-CI+QC/6-31++G** level of theory gives essentially similar results for the shape of PES.[16] More elaborate calculations with a larger basis set and more accurate wave function, such as MR-SD-CI or MC-SCF-CI calculations, are needed to obtain a deeper insight for the collision process. Despite the approximations employed here, it is shown that a theoretical characterization of reaction I enables us to obtain valuable information on the mechanism of the collision process.

REFERENCES

1. (a) Baer, M., in *The Theory of Chemical Reaction Dynamics*, edited by M. Baer (Chemical Rubber, Boca Raton, 1985), Vol.II, Chap. 4.
   (c) Tachikawa, H; Ohtake, A.; Yoshida, H., *J. Phys. Chem.* **1993**, *97*, 11944.
   (d) Tachikawa, H; Hokari, N.; Yoshida, H., *J. Phys. Chem.* **1993**, *97*, 10035.
   (e) Tachikawa, H; Murai, H; Yoshida, H, *J. Chem. Soc. Faraday Trans.* **1993**, *89*, 2369.
   (f) Tachikwa, H., *Chem. Phys. Lett.*, **1993**, *212*, 27.
   (g) Tachikawa, H; Lunnel, S; Tornkvist, C; Lund, A, *Int. J. Quantum. Chem.* **1992**, *43*, 449, and *J. Mol. Struct (THEOCHEM)*, (in press).
2. See, for example, *State-Selected and State-to-State Ion-Molecule Reaction Dynamics*: Part I, Experiment, edited by Ng, C.Y. and Baer, M., vol.82 and Part II, Theory, edited by Baer, M. and Ng, C.Y. in Advances in Chemical Physics (Wiley, New York, 1992).
3. (a) Varley, D.F.; Levandier, D.J.; Farrar, J.M., *J. Chem. Phys.*, **1992**, *96*, 8806.
   (b) Levandier, D.J.; Varley, D.F.; Farrar, J.M., *J. Chem. Phys.*, **1992**, *97*, 4008.
   (c) Liao, C.-L.; Xu, R.; Flesch.G.D.; Baer, M.; Ng, C.Y., *J. Chem. Phys.*, **1990**, *93*, 4818.
4. (a) Squires, R. R., Bierbaum, V.M.; Grabowski, J.J.; Depuy, C.H., *J. Am. Chem. Soc.*, **1983**, *105*, 5185.
   (b) Van Doren, J.M.; Barlow, S.C.; Depuy, C.E.; Bierbaum, V.M., *Int. J. Mass Spectrom. Ion Proc.* **1991**, *109*, 305.
5. Langford, A.O.; BierbaumV.M.; Leone, S.R., *J. Chem. Phys.*, **1985**, *83*, 3913.
6. Hamilton, C.E.; Duncan, M.A.; Zwier, T.S.; Weisshaar, J.C.; Ellison, G.B.; Bierbaum; V.M.; Leone, S.R., *Chem. Phys. Lett.*, **1983**, *94*, 4.
7. Knutsen, K.; Bierbaum,V.M.; Leone, S.R., *J. Chem. Phys.*, **1992**, *96*, 298.
8. Pulay, P, *in Modern Theoretical Chemistry*, edited by H.F. Shaefer (Plenum, New York, Vol.4, Chap.4, 1977).
9. (a) Hariharan, P.C.; Pople, J.A, *Theor. Chim. Acta.* **1973**, *82*, 213.
   (b) Francl, M.M; Pietro, W.J; Hehre, W.J; Binkley, J.S; Gordon, M.S; DeFrees, D.J; Pople, J.A, *J. Chem. Phys.* **1982**, *77*, 3654.
(c) Frish, M.J; Binkley, J.S; Schlegel, H.B; Raghavachari, K; Melius, C.F; Martin, R.L; Stewart, J.J.P; Bobrowicz, F.W; Rohlfing, C.M; Kahn, L.R; DeFrees, D.J; Seeger, R; Whiteside, R.A; Fox, D.J; Fleuder, E.M; Topiol, S; Pople, J.A., Ab-initio molecular orbital calculation program GAUSSIAN86, Carnegie-Mellon Quantum Chemistry Publishing Unit; Pittsburgh, PA.
10. (a)Pople, J.A.; Binkley, J.S.; Seeger, R., *Int. J. Quantum Chem.* **1976**, *S10*, 1.

(b) Langhoff, S.R.; Davidson, E.R. *Int. J. Quantum. Chem.* **1974**, *8,* 61.

(c) Davidson, E.R.; Silver, D.W. *Chem. Phys. Lett.*, **1977**, *52*, 403.

(d) Pople, J.A.; Seeger, R.; Krishman, R. *Int. J. Quantum. Chem.* **1977**, *S11*, 149.

11. (a) Moller, C; Plesset, M.S., *Phys. Rev.* **1934**, *46*, 618.

(b) Bartlett, R.J, *J. Phys. Chem.*, **1989**, *93*, 1697.

(c) Raghavachari, K, *J. Chem. Phys.*, **1985**, *82*, 4607.

12. Bunker, D.L, *Meth. Comput. Phys.* **1971**, *10*, 287.

13. Jonston, H.S, in *Gas Phase Reaction Rate Theory* (Ronald, New York, 1966), Chap.15.

14. Bradforth, D.W.; Arnold, D.W.; Metz, R.B., Weaver, A.; Neumark, D.M. *J. Phys. Chem.*, **1991**, *95*, 8066.

15. Heats of formation are cited from Lias, S.G. *J. Phys. Chem. Ref. Data* **1988**, *17*, Suppl. 1.

16. Tachikawa, H. *J. Phys. Chem.*, **1994**, (in press).

CHAPTER V

THE VIBRATIONALLY STATE-SELECTED HYDROGEN ATOM TRANSFER REACTION IN GAS PHASE : $NH_3^+(v) + NH_3 \rightarrow NH_4^+ + NH_2$

1. Introduction

Vibrationally state-selected reactions have recently received much attention from both theoretical and experimental points of view.[1] Ammonia cation (NH_3^+) produced by photo-ionization reacts with neutral ammonia (NH_3) according to three elementary chemical processes:[2,3]

$$NH_3^+(v) + NH_3 \rightarrow NH_2 + NH_4^+ \quad \text{(I)}$$
$$NH_3^+(v) + NH_3 \rightarrow NH_4^+ + NH_2 \quad \text{(II)}$$
$$NH_3^+(v) + NH_3 \rightarrow NH_3 + NH_3^+ \quad \text{(III)}$$

Channels I is a proton transfer reaction from NH_3^+ to NH_3 and channel II is a hydrogen atom abstraction reaction from NH_3 by NH_3^+, respectively. Channel III is an electron (charge) transfer reaction. These channels are known experimentally to depend on the vibrational state; the reactive cross section for channel I is suppressed while channels II and III are enhanced by vibrational excitation of the ν_2 umbrella-bending mode of NH_3^+.[2,3]

Several theoretical calculations have been performed to elucidate the energetics of reactions.[4-6] A theoretical analysis of the potential energy and the geometry of $(NH_3)_2^+$ shows that the ground state potential energy surface (PES) of the dimer cation is quite favorable for the auto proton-transfer reaction (channel-I), and has no activation barrier.[4] This surface has a minimum corresponding to a stable intermediate complex ($NH_4^+ \cdot NH_2$). The complex lies 1.7 and 0.9 eV below the reactant and product, respectively. Recent *ab-initio* MP2/6-311G** calculations show that the reaction energies for channels I, II and III are 15.8, 15.8 and 0.0 kcal/mol, respectively.[6]

Several interpretations have been proposed to account for the vibrational mode specificity in the three channels. For channel I, Tachibana *et al.* apply modified ADO (average dipole orientation) theory to elucidate the mechanism of channel I and show that the experimental feature of channel I can be explained qualitatively by considering a long-range interaction created by a vibration-induced dipole of $NH_3^+(v)$.[7]

For channel II, Conaway *et al.*[2] suggest that a hydrogen bonded structure $(NH_4.NH_2)^+$

may be favorable in the reaction. Tomoda *et al.*[3] propose a model in which the reaction is composed of two microscopic elementary steps: the first is an electron jump from NH_3 to NH_3^+ at long range, and the second is a hydrogen transfer from NH_3^+ to NH_3 in the (NH_4^+..NH_2) intermediate with a hydrogen-bonded structure. Tachibana *et al.*[6] propose a different structural model of the $(NH_3{\cdot}NH_3)^+$ metastable intermediate based on the *ab-initio* MO (HF/4-31G) calculation: the N..N bonding type structure with the in-phase overlap of the HOMO of NH_3 and the LUMO of NH_3^+ in terms of orbital interaction. However, they do not explain the vibrational mode-specificity in channel II. Thus the reaction mechanism of channel II is still in controversy. Channel III also is not clearly understood.[6]

In this chapter, *ab-initio* MR-SD-CI and classical trajectory calculations have been performed to elucidate the detailed reaction mechanism of channel II. Especially we focus our attention on the ν_2 mode specific features on the entrance PES region.

The main purposes of this study are : (i) to provide theoretical information on the entrance PESs for channel II, and (ii) to discuss the mechanism of the hydrogen abstraction process based on both the PES characteristics and the analysis of the classical trajectory calculations. Based on the theoretical results, we propose a simple reaction model for channel II which can explain the experimental observations for channel III as well as those for channel II.

2. Method of the calculations

Ab-initio MO methods and classical trajectory calculations provide useful information about the electronic states and the reaction dynamics of unstable molecules.[8,9] Therefore we use both methods to study the vibrational mode specificity of channel II.

A. Ab-initio MO and MR-SD-CI calculations.

Geometries for the reactant, the product and the intermediate complex are fully optimized by the restricted and unrestricted Hartree-Fock (RHF and UHF) energy gradient method with 6-31G* basis sets.[10] Geometrical parameters for the reaction system are shown in scheme 1.

Potential energy surfaces as functions of r_1 and r_2 are calculated for ground and first excited states by the Multi-reference single and double excitation configuration interaction (MR-SD-CI) method.[11] The hydrogen bonded structure proposed by Conaway *et al.*[2] and Tomoda *et al.*[3] is employed for the reaction system. The geometries of NH_3 (I) and NH_3 (II) in the hydrogen bonded structure are fixed to those of the ammonia cation and neutral ammonia, respectively, except for three variables, r_1, r_2 and θ. In the MR-SD-CI calculations, six reference functions,

which are larger than 0.95 for reference weight, are constructed from ROHF (restricted open-shell HF) configurations.[12] Configuration state functions (CSFs) are chosen to contribute an energy lowering greater than 10^{-6} Hartree by the second-order perturbation method.[13] The final dimension of the MR-SD-CI calculations is about 2000-3000. Fifty points on each PES are calculated for θ = 0.0 and 13.5 degrees, which correspond to the v=0 and v=2 levels of the vibrational quantum number, respectively. These angles are determined from the harmonic frequency of the ν_2 mode of NH_3^+ obtained at the MP2/6-31G* level.

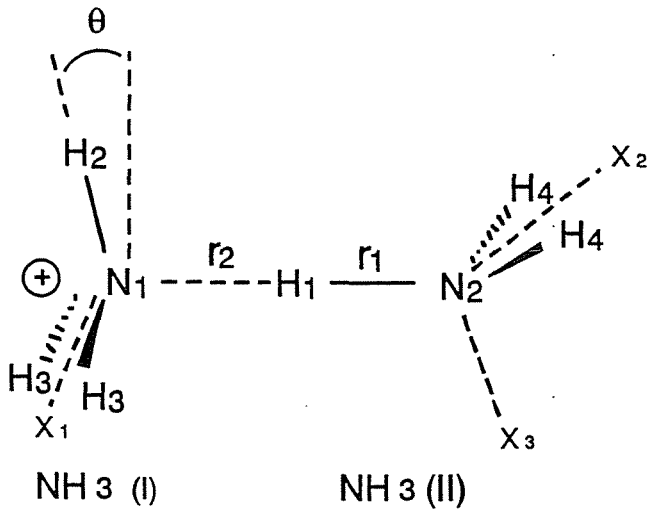

scheme 1

B. Classical trajectory calculations.

In order to compare the reactive cross section for v=0 with that for v=2, we perform the classical trajectory calculation with the PESs (v=0 and v=2) obtained by the *ab-initio* MR-SD-CI calculations. The PESs are fitted to the extended LEPS surface function by using least-squares method. The mean energy differences from the *ab-initio* values is less than 0.1 eV.

Like the previous trajectory calculations,[15] the reaction system is considered as three particles: the ammonia cation NH_3^+ (I), the transferred hydrogen atom, and the NH_2 moiety of NH_3 (II). Therefore, the PES function is expressed by

$$V_v(r_1,r_2,r_3) \qquad (v=0 \text{ and } 2);$$

where r_i is the relative position between two of three particles, NH_3^+(I), H, and NH_2(II); and v is the vibrational quantum number of the ν_2 mode of NH_3^+(I).

Trajectories are initiated at an NH_3(I)..H-NH_2(II) internuclear separation of 7.0 A, with the

H-NH_2 quasi-diatomic molecule in the v=0 and J=0 levels defined by its Morse potential. The orientation of NH_3^+ is randomly selected for each trajectory. The trajectories are integrated over 2000 steps in order to ensure the conservation of the total energy and of the total angular momentum. Integration of the classical equation of motion is performed at the standard fourth-order Runge-Kutta and sixth order Adams-Moulton combined algorithm[14] with a time increment of $1x10^{-16}$ s. The collision energies are 0.9, 1.0, 1.5 and 2.0 eV. One thousand trajectories are sampled for each condition. The lifetime of the $(NH_4 \cdot NH_2)^+$ complex is estimated by both trajectory calculation and RRK theory.[16]

3. Results

A. Global features of the hydrogen abstraction reaction

Optimized geometries, total energies and relative energies for reactant, product and intermediate complex are listed in Tables V-1, V-2 and V-3, respectively. The energetics obtained by several methods are essentially consistent with previous theoretical[4-6] and experimental[2,3] values. The schematic energy diagram of channel II is shown in Figure V-1. This reaction has a minimum corresponding to the intermediate complex (NH_4^+..NH_2), and proceeds under *Cs* symmetry throughout.

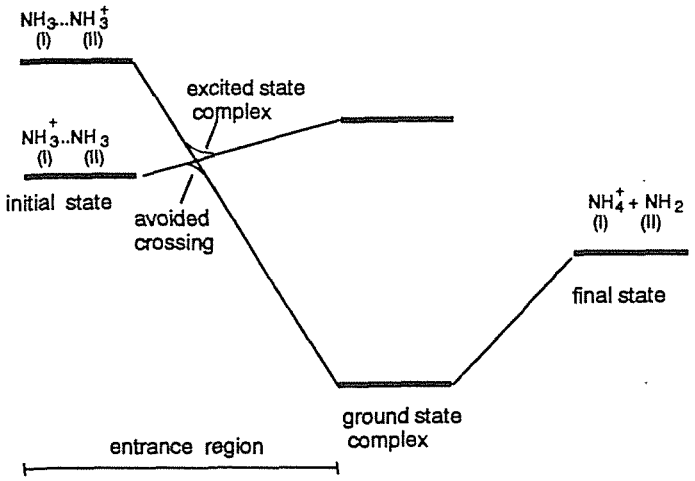

Figure V-1. Schematic energy diagram of the hydrogen abstraction reaction (channel II) : $NH_3^+(v) + NH_3 \rightarrow NH_4^+ + NH_2$.

B. Potential energy surfaces of the reaction.

Ground and first excited state PESs for the reaction (θ = 0.0°) are shown in Figures V-2(A) and V-2(B), respectively. The ground state PES shows that, during the reaction, the N-H bond length of NH_3(II), r_1, is close to 1.0 A in the range of r_2 = 4.0-2.2 A, but increases rapidly for r_2 < 2.0 A. This means that the NH_3 (I) approaches NH_3^+ (II) without geometrical deformation until hydrogen-transfer suddenly occurs in the vicinity of r_2 = 2.0 A.

The activation barrier formed by the avoided crossing (AC), is found at the entrance region of the PES, although the height of the barrier is negligibly small.

The shape of the excited state PES is quite different from that of the ground state PES, with a shallow minimum (r_2 = 2.19 and r_1 = 1.00 A) corresponding to the excited state complex $NH_3^+NH_3]^*$. This minimum is also formed by the AC between the ground and excited state PESs.

Vibrationally excited state PESs, $V_2(r_1,r_2)$, are calculated by assuming a fixed bending angle. The PESs (v=2) obtained are shown in Figures V-3(A) for the ground state and V-3(B) for the excited state. The vibrational excitation from v=0 to v=2 brings about pictorial deformation of the PESs: (1) the position of barrier corresponding to the AC point shifts to an earlier point on the entrance region, and (2) the gradient of the ground state PES at the entrance region increases with increasing vibrational quantum number.

Table V-1. Optimized geometries of the intermediate complex $(NH_4.NH_2)^+$, and the reactant and product molecules for channel II calculated at the HF/6-31G* level. Bond lengths and angles are in angstroms and degrees, respectively.

	$(NH_4.NH_2)^+$	NH_3^+	NH_3	NH_4^+	NH_2
r_1	1.8352		1.0024		
r_2	1.0419			1.0134	
θ	19.87	0.0	19.47		
$r(N_1\text{-}H_2)$	1.0109	1.0124		1.0134	
$r(N_1\text{-}H_3)$	1.0109	1.0124		1.0134	
$r(N_2\text{-}H_4)$	1.0105		1.0024		1.0126
$<H_1N_1X_1$	125.91	90.0			
$<H_3N_1X_1$	54.51	60.0			
$<H_1N_2X_2$	180.0				
$<H_4N_2X_2$	53.15				52.16
$<X_3N_2H_1$			111.70		

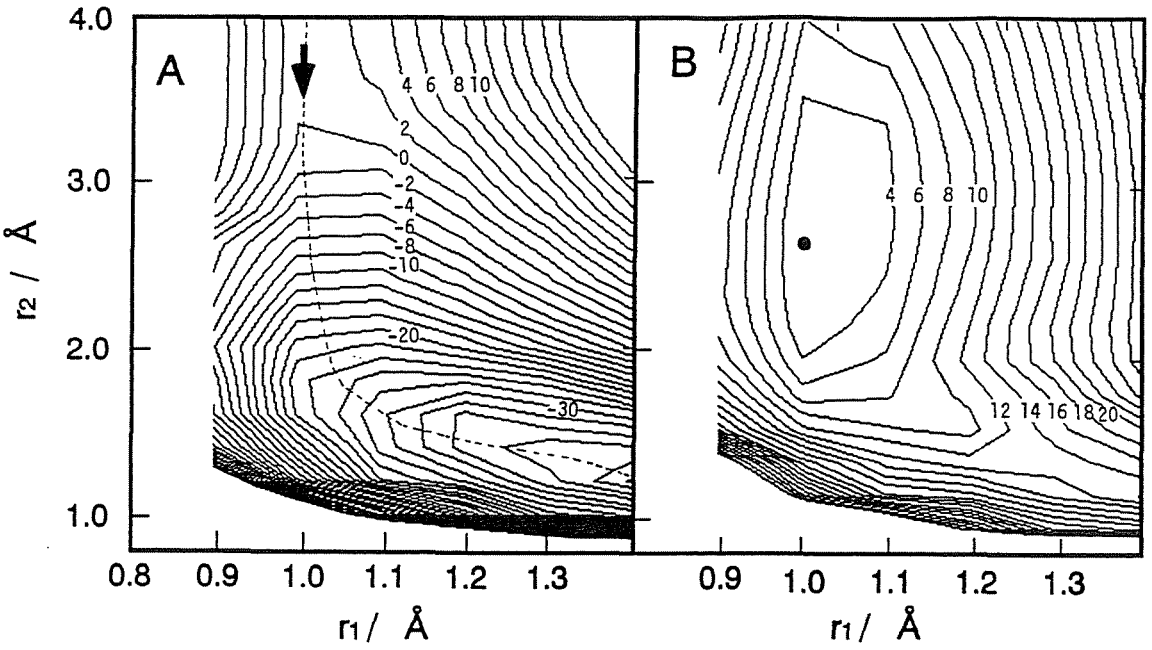

Figure V-2. Potential energy surfaces (PESs) of the hydrogen abstraction reaction (channel II) for $NH_3^+(v) + NH_3 \rightarrow NH_4^+ + NH_2$. (A) v=0 state PES, and (B) v=2 state PES. The intervals of the contours are 2 kcal/mol. The dashed line indicates the minimum energy path on the adiabatic ground state PES. The arrow shows a direction of the reaction on the PES. The calculations are performed at the MR-SD-CI/6-31G* level.

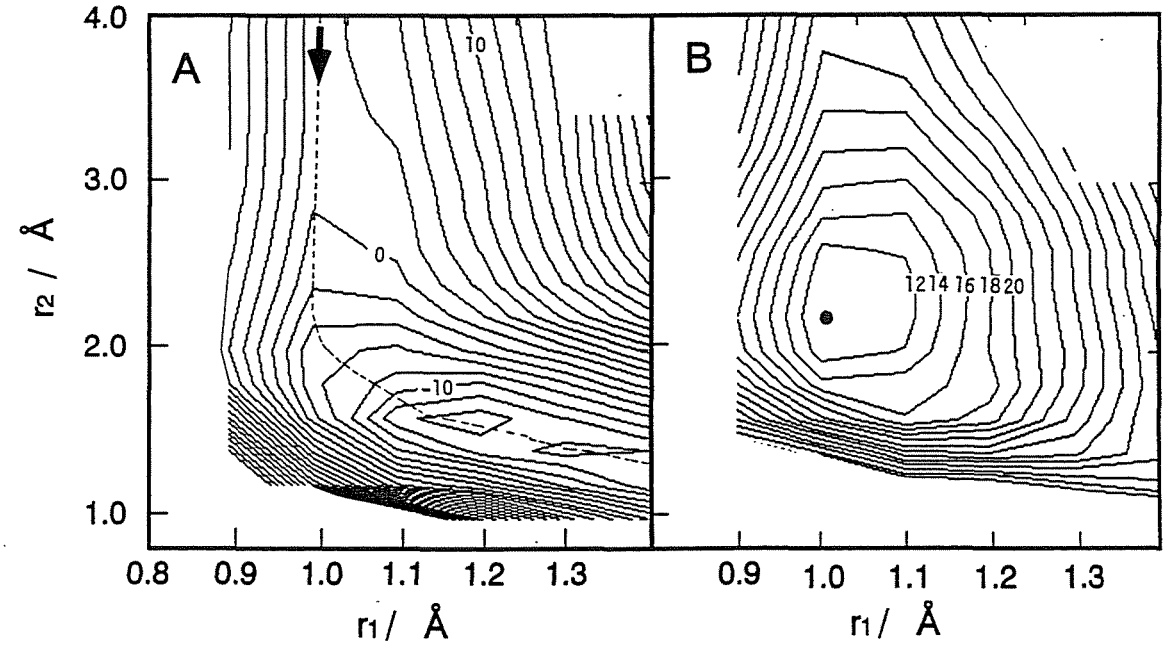

Figure V-3. PESs for vibrationally excited state (v=2): $NH_3^+(v=2) + NH_3 \rightarrow NH_4^+ + NH_2$. (A) Ground state PES, and (B) excited state PES. The intervals of the contours is each 2 kcal/mol. Dashed line indicates the minimum energy path on the adiabatic ground state PES. The arrow show a direction of the reaction on the PES. The calculations are performed at the MR-SD-CI/6-31G* level.

Table V-2. Total energies (in a.u) of the intermediate complex $(NH_4.NH_2)^+$ and the reactant and product molecules for channel II.

	HF/6-31G*	SD-CI/6-31G* [a]	SDCI+QC[b] /6-31G* [a]
NH_3	-56.184356	-56.361381	-56.369063
NH_3^+	-55.873236	-56.018597	-56.023661
$(NH_4.NH_2)^+$	-112.124101	-112.437070	-112.464672
NH_2	-55.557703	-55.704295	-55.7096484
NH_4^+	-56.530771	-56.709133	-56.7167255

[a]At HF/6-31G* optimized structure.
[b]Size consistency correction.

Table V-3. Relative energies (kcal/mol) for channel II.

	reactant	$(NH_4.NH_2)^+$	product
HF/6-31G*//HF/6-31G*[a]	0.	-41.7	-19.4
SD-CI/6-31G*//HF/6-31G*[a]	0.	-35.8	-21.0
SD-CI+QC/6-31G*//HF/6-31G*[a]	0.	-45.2	-21.1
MP4SDQ/6-31G**//HF/6-31G**[a]	0.	-44.7	-20.3
MP2/6-31G*//MP2/6-31G*[b]	0.	-46.1	-20.7
MP3/6-31G*//HF/6-31G*[b]	0.	-45.6	-21.2
MP4/6-31G*//MP2/6-31G*[b]	0.	-45.7	-21.2
MP2/6-311G**//MP2/6-31G*[b]	0.	-43.7	-18.7

[a]Present work, [b]From reference 5

C. Potential energy curves as a function of r2 (v=0 and 2).

To elucidate in detail the effects of vibrational excitation on the PESs at the entrance region, potential energy curves (PECs) as a function of intermolecular distance (r2) are shown in Figure V-4. The solid and dashed lines correspond to PEC(v=0) and PEC(v=2) respectively. The PECs clearly show that the AC point is transferred to the large intermolecular separation due to the vibrational excitation of NH_3^+(v), (r2 = 2.75 A for v=0 vs. r2 = 3.20 A for v=2). This

effect plays an important role in the dynamics of channel II, as seen later. Other interesting points of the vibrational excitation effect are the uplift of the ground PEC and the lowering of the upper PEC. Consequently the energy difference between upper and lower PESs becomes significantly lower due to the vibrational excitation.

Charges on ammonia molecules before and after the AC are summarized in Table V-4. The NH_3(I) before the AC has a cationic character in $1^2A'$ and a neutral character in the $2^2A'$ state. On the other hand, the NH_3(II) has no charge in the $1^2A'$ state, but has a positive charge (+1e) in the $1^2A'$ state. These results strongly indicate that the transition, $1^2A' \rightarrow 2^2A'$, at the AC point corresponds to an electron jump from neutral NH_3^+ (II) to cationic NH_3^+ (I). After the AC point, the positive charge is equivalently delocalized on both ammonia molecules. These results show that a charge transfer takes place before and after the AC point.

The electron density of the excited state complex is given in Table V-5. Positive charges are equivalently populated to be +0.57e on NH_3(I) and +0.43e on NH_3(II). This means that the complex is mainly stabilized by charge-resonance interaction between ammonia molecules.

Table V-4.Total electron densities on each atom and total charges on the ammonia molecules[a] calculated by MR-SD-CI method.

	before AC[b]		after AC[c]	
	$^2A'$	$2^2A'$	$^2A'$	$2^2A'$
N_1	7.7349	8.0394	7.9023	7.8943
H_2	0.4348	0.6526	0.5214	0.5334
H_3	0.4152	0.6540	0.5080	0.5187
NH_3(I)	+1.0	0.0	+0.44	+0.47
N_2	7.9377	7.6782	7.8185	7.8205
H_1	0.7040	0.4496	0.6257	0.6203
H_4	0.6792	0.4361	0.5580	0.5470
NH_3(II)	0.0	+1.0	+0.56	+0.53

[a] r_1 is fixed to 1.0 A
[b] r_2 = 6.0 A
[c] r_2 = 2.0 A

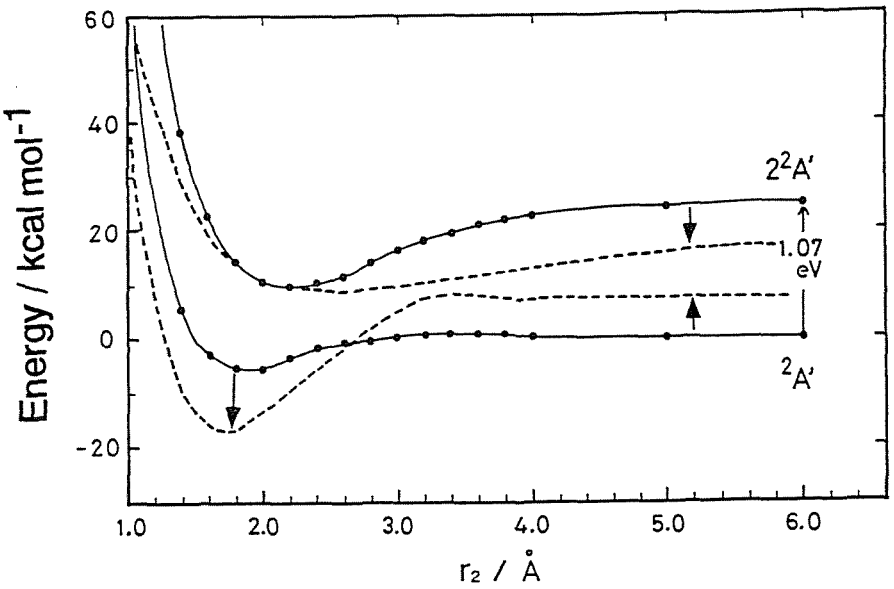

Figure V-4. Potential energy curves for the ground ($^2A'$) and the first excited ($2^2A'$) states calculated as a function of intermolecular distance (r_2). Solid and dashed curves indicate the vibrational ground (v=0) and excited (v=2) state PECs, respecti-vely. The arrows mean "shift of PEC" due to the vibrational excitation from v=0 to v=2. The calculations are performed at the MR-SD-CI/6-31G* level.

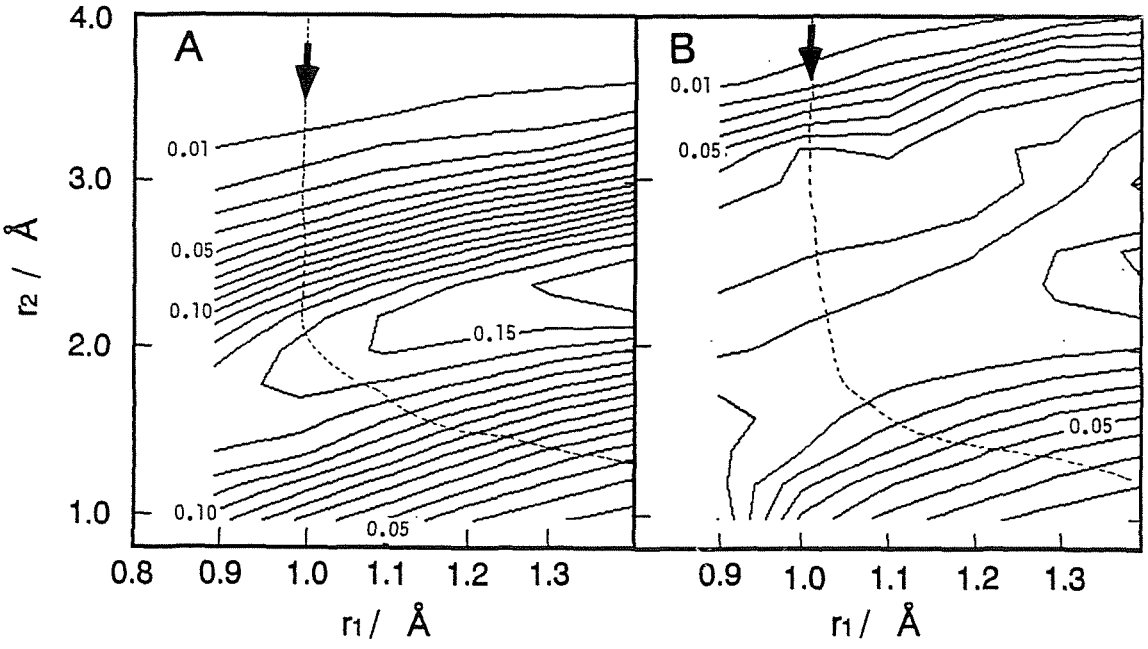

Figure V-5. Contour maps for the transition moments of the $1^2A'$-$2^2A'$ transition. (A) NH_3^+(v=0) + NH_3 → NH_4^+ + NH_2, and (B) NH_3^+(v=2) + NH_3 → NH_4^+ + NH_2. The contour is drawn for each 0.01 a.u. The calculations are performed at the MR-SD-CI/6-31G* level.

Table V-5. Atomic electron densities and charges for the excited state complex.[a]

	atom	electron density	charge
NH_3 (I)			+0.57
	N_1	7.7843	
	H_2	0.5923	
	H_3	0.5251	
NH_3(II)			+0.43
	N_2	7.9279	
	H_1	0.5565	
	H_4	0.5444	

[a]Energy difference from the ground state PES is 0.57 eV.

D. Transition moments for $1^2A'$-$2^2A'$ excitation during the reaction.

Transition moments between adiabatic ground and excited state PESs are plotted in Figures V-5(A) for v=0 and V-5(B) for v=2. The shapes of the curves for v=0 and v=2 are quite different. The transition moments at the AC points along the minimum energy paths for v=0 (r_2 = 2.75A) and v=2 (r_2 = 3.20 A) are calculated to be the same (0.05 a.u). This indicates that the hopping probability between surfaces, which is proportional to square of transition moment, is the same at each AC point. Therefore an increase in the vibrational quantum number of NH_3^+(v) causes only movement of the AC point.

E. Trajectories on the adiabatic $^2A'$ state PES.

Ab-initio PESs are fitted by the extended LEPS surface with the parameters listed in Table V-6. Using the ab-initio fitted PESs, classical trajectory calculations are performed. Time dependences of the potential energy and interparticle distances for a sample trajectory are plotted in Figures V-6 and V-7, respectively. These figures show that, after four collisions with the well in the $(NH_4.NH_2)^+$ complex region, the trajectory proceeds to the exit region. Almost all trajectories in the exit region lead to N-H vibrationally excited NH_4^+. This excitation may be caused by energy transfer from exthothermic energy to vibrational energy.

The translational energy of the products gradually increases with increasing collision energy, which is consistent with previous experimental and theoretical studies for a heavy-light-

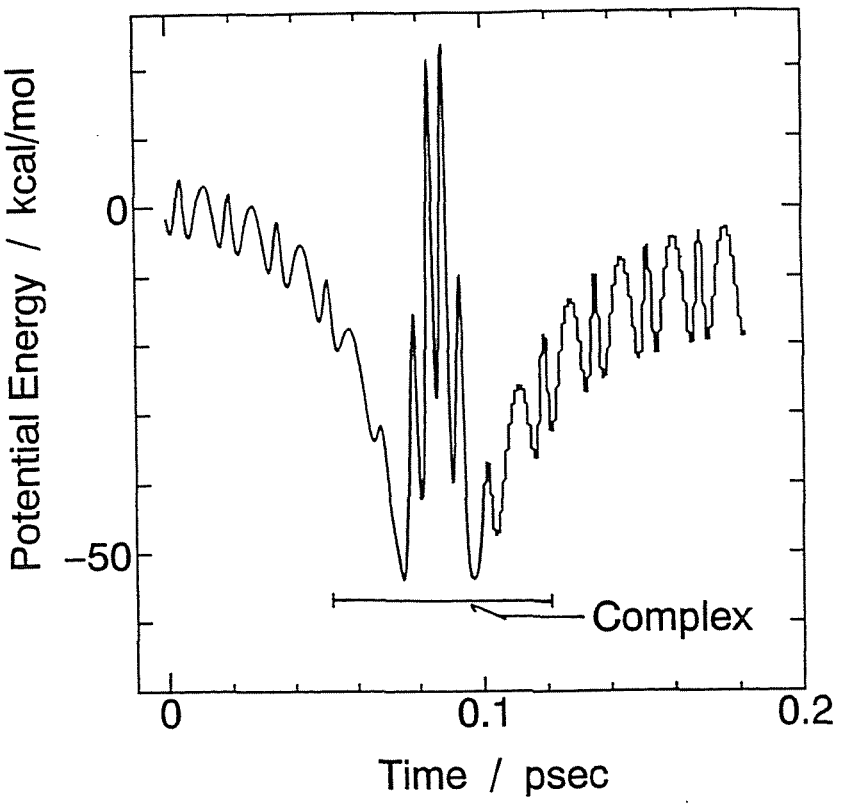

Figure V-6. A sample reactive trajectory on the PES (v=0) plotted for potential energy versus time. The trajectory starts at the time zero and is trapped in the ground state complex during 0.05 to 0.12 ps. After four collisions with the well, the trajectory proceeds to the exit region.

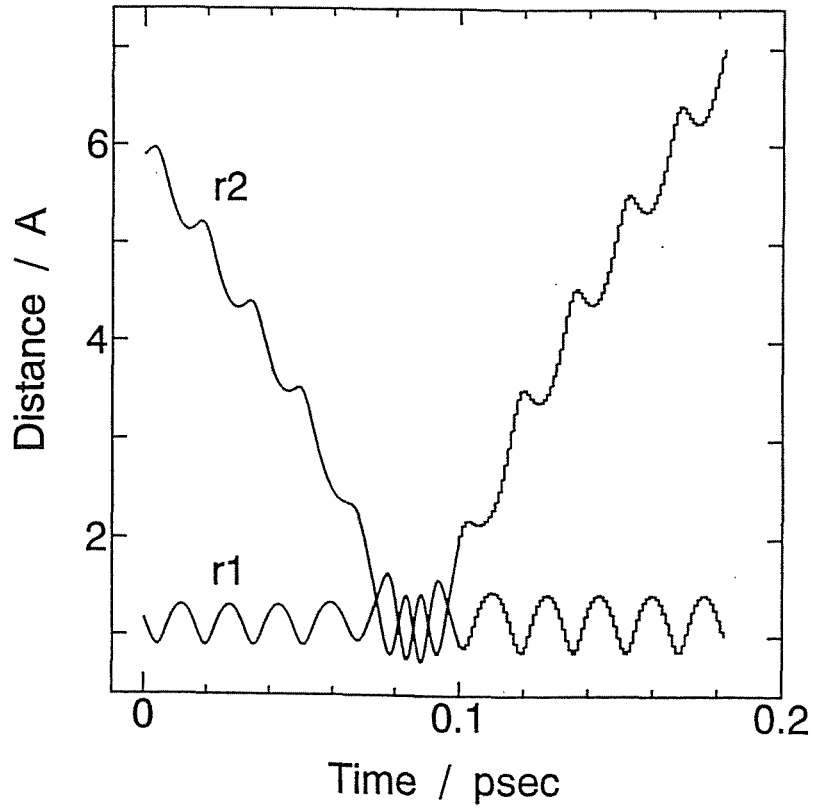

Figure V-7. A sample reactive trajectory on the adiabatic ground state PES (v=0) plotted for the interparticle distances, r1 and r2, versus time. The trajectory starts at the time zero and is trapped in the ground state complex during 0.05 to 0.12 ps.

heavy reaction system.[17]

Table V-6. LEPS parameters (*S*, Sato parameter; β, Morse parameter in A^{-1}; *De*, dissociation energy in kcal/mol; r_e, interperticle distance in A; and α, alpha value in the extended LEPS parameter) of the PESs for vibrational ground (*v=0*) and excited (*v=2*) states.

parameter	NH_3 (I)..H_1	H_1..NH_2 (II)	NH_3 (I)..NH_2 (II)
ground state (v=0)			
S	-0.0264	0.1477	0.5940
β	1.2732	2.6049	1.5932
De	176.7	120.5	28.8
r_e	0.8207	0.9379	2.703
α	0.5102		
excited state (v=2)			
S	0.7786	1.0487	1.4520
β	1.899	2.2029	0.7972
De	147.3	87.7	34.5
r_e	0.9977	1.0760	3.6090
α	0.0197		

The lifetime of the complex at a collision energy of 1.0 eV is calculated to be 0.04-0.08 ps, which agrees with the RRK estimated lifetime (0.05 ps). The trajectory reaches the AC point within 0.06-0.08 ps if an intermolecular distance of 6.0 A is chosen as a starting point.

F. Analysis of the trajectories.

Collinear trajectories are 70 % reactive for v=0 and 100 % reactive for v=2. The results of these three-dimensional (3D) trajectory calculations are summarized in Table V-7. The ratio of reactive trajectories to total trajectories (N_r/N_t) for v=2 is larger than that for v=0 at each energy. The maximum value of the impact parameter (b_{max}) is 4.2 A for v=0 and 5.4 A for v=2. The location of the AC point causes this difference.

Table V-7. Summary of the trajectory calculations.

collision energy / eV	N_r / N_t			b_{max} / A	
	v=0	v=2	v=2/v=1	v=0	v=2
0.90	0.131	0.222	1.69	4.2	5.4
1.00	0.127	0.212	1.67	4.2	5.4
1.50	0.122	0.165	1.35	4.2	4.8
2.00	0.126	0.171	1.36	4.2	4.8

4. The reaction model for channel II

Based on the results derived from theoretical calculations, we propose a simple model for reaction channel II. The *ab-initio* calculations show that an electron jump takes place at the AC point on the entrance PES. The AC moves to larger intermolecular separation with vibrational excitation to the ν_2 mode. The classical trajectory calculations show that bmax also increases. A scheme is illustrated in Figure V-8 for a better understanding of the situation. The effect of vibrational excitations of the ν_2 mode is considered as an expansion of the electron capturing (EC) volume of the NH_3^+. The reactive cross section increases with increasing vibrational quantum number v. Straight lines A and B indicate trajectories with impact parameters of 2.0 and 3.5 A, respectively. In the vibrational ground state (v=0), trajectory A (small impact parameter) reaches the EC zone, whereas trajectory B (large impact parameter) does not cross the EC zone. On the other hand, both trajectories cross the EC zone in the vibrationally excited state. Thus the present model qualitatively explains the experiments.

5. Discussion and Conclusion

In the present work, we have calculated the ground and first excited potential energy surfaces (PESs) of a hydrogen abstraction reaction, $NH_3^+(v) + NH_3 \rightarrow NH_4^+ + NH_2$ (channel II), and performed the classical trajectory calculation with ab-initio fitted PESs. Based on the results derived from these *ab-initio* MO and classical trajectory calculations, we propose a simple model to explain the vibrational mode specificity of channel II. The present model interprets the enhancement of the reactive cross section for channel II as an expansion of EC

zone of the NH_3^+. This model reasonably explains the experimental features observed.

We consider two vibrational levels of NH_3^+ (v=0 and v=2) in the present calculations. A potential energy curve as a function of θ, which is preliminary calculated,[18] shows that an avoided crossing is occurred at θ= ca.18.0 degree if r2 is 4.2 A. This angle corresponds to v=5 level of NH_3^+(v). The avoided crossing of θ direction may be important as well as that of r2 direction in case of the reaction in the higher vibrational level. The present model is dominant at low vibrational level.

Although channel II is the principal focus of the present work, the model reasonably explain the vibrational mode-specificity of channel III.[18] The preliminary calculation of the reaction system for channel III reveals that the N-N bonding structure proposed by Tachibana *et al.* is most favorable to channel III.[18]

In the present calculation we have introduced approximations to treat the reaction dynamics and construct the PESs. It is assumed that the vibrationally excited PES is constructed by a frozen bending-angle approximation. This may cause an overestimation of the reactive cross section. A method to treat the multi-dimensional potential surface requires a quantitative comparison with experiments. Despite the approximations employed here, it is shown that a theoretical characterization of channel II enables us to obtain valuable information concerning the mechanism of the hydrogen transfer process.

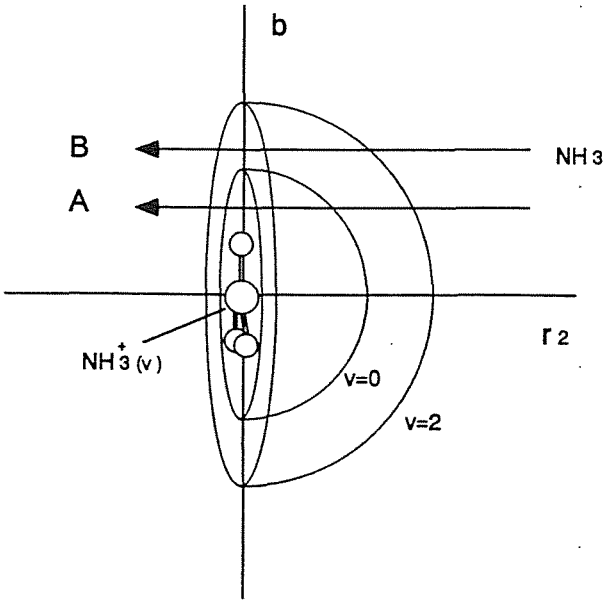

Figure V-8. Schematic representation of the model for the hydrogen abstraction reaction (channel II), $NH_3^+(v) + NH_3 \rightarrow NH_4^+ + NH_2$. Arrows A and B indicate trajectories with small and large impact parameters, respectively. Small and large domes indicate the electron capturing volumes of NH_3^+ for vibrational ground (v=0) and excited (v=2) states, respectively. Both trajectories cross the electron capturing zone for vibrational excitation to the ν_2 umbrella-bending mode of NH_3^+.

References

1. For review: Ng,C.y., in :*State-Selected and State-to-State Ion-Molecule Reaction Dynamics*, eds, Ng, C. Y. and Baer, M., vol.82, In Advances in Chemical Physics (Wiley, New York, 1992), p. 401.
2. Conaway, W. E.; Ebata, T.; Zare, R.N., *J. Chem. Phys*, **1987**, *87,* 3453.
3. Tomoda, S.; Suzuki, S.; Koyano, I., *J. Chem. Phys*, **1988**, *89*, 7268.
4. (a) Tomoda, S., *Chem. Phys*, **1986**, *110*, 431.
   (b) Tomoda, S.; Kimura, K., *Chem. Phys. Lett.*. **1985**, *121*, 159.
5. (a) Bouma, W. J.; Radom, L., *J. Am. Chem. Soc.* . **1985**, *107*, 4931.
   (b) Gill, P. M.; Radom, L., *J. Am. Chem. Soc.* . **1988**, *110*, 4931.
6. Tachibana, A.; Kawauchi, S.; Kurosaki, Y.; Yoshida, N.; Ogihara, T.; Yamabe, T., *J. Phys. Chem.* **1991**, *95*, 9647.
7. (a) Tachibana, A.; Suzuki, T.; Yoshida, N.; Teramoto, Y.; Yamabe, T., *Chem. Phys.*. **1991**, *156*, 79.
   (b) Tachibana, A.; Suzuki, T.; Teramoto, Y.; Yoshida, N.; Sato, T.; Yamabe, T., *J. Chem. Phys.*, **1991**, *95*, 4136.
8. (a) Tachikawa,H.; Lunell,S.; Tornkvist, C.; Lund, A., *Int. J. Quantum Chem.*. **1992**, *43*, 165.
   (b) Tachikawa, H.; Shiotani, M.; Ohta, K., *J. Phys. Chem.*. **1992**, *96*, 118.
   (c) Tachikawa, H.; Murai, H.; Yoshida, H., *J. Chem.Soc. Faraday Trans.* **1993**, *89*, 2369.
   (d) Tachikawa, H.; Lund, A.; Ogasawara, M. *Can. J. Chem.*, **1993** , *71*, 118.
   (e) Tachikawa,H.; Hokari, N.; Yoshida, H., *J. Phys. Chem.*, **1993**, *97*, 10035.
   (f) Tachikawa, H., *Chem. Phys. Lett.*. **1993**, *212*, 27.
9. See for instance: (a) Yamashita, K.; Morokuma,K.,*J. Phys. Chem.* **1988**, *92*, 3109.
   (b) Tachikawa, H.; Ohtake, A.; Yoshida, H., *J. Phys. Chem.*. **1993**, *97*, 11944..
10. (a) Frisch, M. J.; Binkley, J. S.; Schlegel, H. B.; Raghavachari, K.; Melius, C. F.; Martin, R. L.; Stewart, J. J. P.; Bobowicz, F.W.; Rohlfing, C.M.; Kahn, L.R.; DeFrees, D.J.; Seeger, R.; Whiteside, R.A.; Fox, D.J.; Fleuder, E.M.; Pople, J.A., An Ab-initio molecular orbital calculation program; GAUSSIAN 86.
    (b) Gordon, M.S.; Binkley, J.S.; Pople, J.A.; Pietro, W.J.; Hehre, W.J., *J.Am. Chem. Soc.* . **1982**, *104*, 2797.
    (c) Francl, M.M.; Pietro, W.J.; Hehre, W.J.; Binkley, J.S.; Bordon, M.S.; DeFrees, D.J.; Pople, J.A., *J. Chem. Phys.* **1982**, *77*, 3654.

11. Murakami, A.; Iwaki, H.; Terashima, H.; Shoda, T.; Kawaguchi, T.; Noro, T., MR-SD-CI calculation program, MICA3, 1985.

12. H. Kashiwagi, T. Takada, E. Miyoshi, S. Obara and F. Sasaki, RHF calculation program JAMOL4, 1985.

13. Chang, D.P.; Herring, F.G.; Williams, D.J., *J. Chem. Phys.*. **1974**, *61*, 958.

14. Bunker, D.L., *Math. Comput. Phys.*. **1971**, *10*, 287.

15. (a) Han, K.; Zheng, X.; Sun, B.; He, G.,, *Chem. Phys. Lett.*. **1991**, *181*, 474.
(b) Blais, N.C.; Bernstein, R.B., *J. Chem. Phys.* **1986**, *85*, 7030.
(c) Sayos, R.; Aguilar, A.; Sole, A.; Virgili,J., *Chem. Phys.***1985**, *93*, 265.
(d) Park, J.; Lee, Y.; Hershberger, J.F.; Hossenlopp, J.M.; Flynn., G.W., *J. Am. Chem. Soc.* **1992**, *114*, 58.

16. Jonston, H.S., In: *Gas Phase Reaction Rate Theory* (Ronald, New York, 1966), Chap. 15.

17. (a) Levandier, D.J.; Varley, D.F.; Carpenter, M.A.; Farrar, J.M., *J. Chem. Phys.* **1993**, *99*, 148.
(b) Knutsen, K.; Bierbaum, V.M.; Leone, S.R., *J. Chem. Phys*, **1992**, *96*, 298.
(c) Chapman, S., *Chem. Phys. Lett.*. **1981**, *80*, 275.

18. Tachikawa, H.; Tomoda, S., (To be published)

CHAPTER VI

HYDROGEN ATOM ABSTRACTION FROM METHANOL BY METHYL RADICAL

1. Introduction

The abstraction of H-atom from methanol by methyl radical is one of the reactions which attract interest of chemists from both the experimental and theoretical points of view. A particular feature of this reaction is that two reaction channels,

$$CH_3 + CH_3OH \rightarrow CH_4 + CH_2OH \qquad (I)$$

and

$$CH_3 + CH_3OH \rightarrow CH_4 + CH_3O, \qquad (II)$$

possibly compete with each other; the elucidation of factors determining the branching between the two reaction channels is of general importance. This reaction gives a typical example where the contribution of quantum tunneling effect causes the deviation of kinetic feature from that expected from the classical theory. This is another interesting feature of the reaction.

Both the reaction channels I and II have actually been observed to proceed in gas phase at high temperature.[1] Although the H-atom abstract-ion from the methyl group (channel I) dominates over the H-atom abstraction from the hydroxyl group (channel II) in the gas phase at high temperatures, the extrapolation of the observed temperature dependence of the rate constants ($cm^3 \cdot molecule^{-1} \cdot s^{-1}$), $k_I = 3.24 \times 10^{-13} \exp(-5035/T)$ and $k_{II} = 1.0 \times 10^{-13} \exp(-4884/T)$,[2] predicts the predominance of the latter below 300 K. However, no positive evidence for the occurence of reaction through the reaction channel II in liquid and solid methanol has been experimentally obtained so far, and it seems to be generally believed that the H-abstraction from methanol occurs exclusively through the reaction channel I at low temperatures.

The experimental studies on the H-atom abstraction from methanol by the methyl radical in solid state at low temperatures has been made by using the electron spin resonance (ESR) method. Williams and his co-workers have shown that in solid methanol H-atom is abstracted exclusively through the reaction channel I,[3] and that the Arrhenius plot of the rate constant deviates from straight line below 100 K and approaches to a limiting value.[4] The isotope effect has also been examined by comparing the rate of the H-abstraction from CH_3OH with the rate of the D-abstract-ion from CD_3OD. They have also shown that the H-abstraction is 1000 times faster than the D-abstraction at 77 K.[3] Doba *et al.* have reconfirmed the isotope effect: the H-abstraction proceeds even at 5 K, whereas the D-abstraction is too slow to be observed below 77 K.[5] The big isotope effect can be interpreted in terms of the quantum tunneling effect.

Although the quantum tunneling effect on this reaction has been shown unequivocally by the previous ESR experiments, no theoretical study on it has not been reported yet. The importance of the quantum tunneling effect on chemical reactions has previously been shown experimentally[6] and theoretically[7] for several reactions. The H-atom abstraction reaction of the present interest is a prototype reaction for studying the quantum tunneling effect on organic radical reactions.

The primary aim of the present investigation is to understand, on the basis of *ab-initio* MO and reaction rate theories, the reason why reaction II does not prevail at low temperature in contradiction with the simple, straight extrapolation of the kinetic data at high temperature. With this respect, the rate constant has been studied for both the reaction channels I and II, on the purely theoretical basis, in taking account the quantum tunneling contribution. The present results of the theoretical calculations show that the quantum tunneling effect is important at low temperature for both the reaction channels, but the predominance of the channel I over the channel II at low temperature is not attributed to the quantum tunneling effect but to the influence of the hydrogen-bonding in condensed phase methanol.

2. Method of Calculations

Ab initio MO calculation. The MO calculation for the reaction system, $CH_3OH + CH_3$, was carried out with 3-21G and 6-31G** basis sets[8] by using GAUSSIAN-82[9] and GAUSSIAN-86[10] programs in the Computer Center of the Institute for Molecular Science. Recent theoretical study of a hydrogen abstraction from methanol by OH radical shows that the geometry optimizations at the MP2/6-31G level give a reasonable transition state structure.[7(o)] Therefore the geometry at the reactant, transit-ion, and product states along the reaction coordinate was fully optimized by using the unrestricted Hartree-Fock (UHF)[11] and second-order Moller-Plesset perturbation (MP2)[13] energy gradient methods. The theoretical vibrational frequencies were numerically calculated with the 3-21G basis set under the harmonic approximation.[12] These frequencies were used for calculating the RRKM rate constant. The electron correlation energy was estimated for each geometry at a high accuracy by applying second-, third- and forth-order Moller-Plesset perturbation (MP2, MP3 and MP4) theories[13] and the double substituted coupled cluster (CCD) thoery,[14] because the height of reaction barrier strongly depends on the electron correlation interaction.[15] As doublets, the expectation value of the spin operator $\langle S^2 \rangle$ should be 0.75; this value in the UHF calculations presented here did not exceed 0.780.

Rate constant calculation. Although the present reaction is actually a bimolecular thermal reaction, it can be regarded as a unimolecular process proceeding through the complexed intermediate states as shown in Figure VI-1, so that its reaction rate can be estimated based on the

unimolecular reaction theory.[16] We have assumed that the motion along the reaction coordinate is separable from the other degree of freedom.[15,19]

According to RRKM theory,[17,18] the rate constant for the unimolecular reaction is given as

$$k(E) = N(E) / h\, N_0'(E), \qquad (6.1)$$

where N(E) and $N_0(E)$ are the integral densities of state for the transition state and for the reactant state, respectively. Applying the harmonic approximation to estimate N(E) and $N_0(E)$,[19] equation (1) can be reduced into the following expression:

$$k(E) = \frac{(s-1)!\prod_i^s h\omega_i}{2\pi\, h\, E^{s-1}} \Sigma P[E-V_0-h\omega^+(n+1/2)] \qquad (6.2)$$

where s is the degree of freedom ($s=3n-6$), V_0 is the barrier height, ω_i and ω^+ are the normal mode frequencies of the reactant molecule and the transition state, and $P(E_1)$ is the tunneling probability for total energy E_1. The tunneling probability was calculated in approximating the reaction barrier with the Eckart potential[20] as described in section 3.2. We actually calculated by using the integral expression:

$$k(E) = A\int_{-V_0}^{E-V_0} \frac{(s-1)\, P(E_1))\, (E-V_0-E_1)^{s-2}}{E^{s-1}}\, dE_1 \qquad (6.3)$$

instead of eq.(6.2) in the RRKM rate calculation, where A is the frequency factor derived from the harmonic vibrational frequencies. As will be discussed in the Section 3.2, this approximation seem to be enough to compare the relative reaction rates in the present perpose.

The rate calculation was made with the short cut paths[21] on the two-dimensional potential surface (2D-PES) and compared with the RRKM calculation. The short cut path contains a straight line connecting a point on the minimum energy path (MEP) in the entrance valley to an isoenergetic point on the MEP in the exit valley. The short cut path is important in the case of light-particle tunneling reaction.[21] The reactions of the present interest, the reaction channels I and II, are regarded as the H-atom (light particle) transfer between heavy particles.

Based on the 2D-PES for the reaction channels I and II calculated at the HF/3-21G level, the canonical rate constant was calculated along short cut paths as

$$k_i(T) = \nu \frac{\int_0^\infty P(E-V_i) \exp(-E/kT)\, dE}{\int_0^\infty \exp(-E/kT)\, dE} \qquad (6.4)$$

where n is the vibrational frequency corresponding to the harmonic frequency of the C-H or O-H streching mode in the reactant state, and V_i is the barrier height for the i-th short cut path. The probability of tunneling, P(E), was calculated analytically by assuming a parabolic barrier. Fitting parameters for the parabolic barrier are the barrier hight and the negative frequency, i.e., a curveture at the saddle point along the short cut path.

The overall rate constant should properly be obtained by summing $k_i(T)$ for all the possible short cut paths:

$$k(T) = \Sigma\, k_i(T) \qquad (6.5)$$

However, $k_i(T)$ significantly varies depending on the height and width of reaction barrier to be tunneled, so that the reaction proceeds almost exclusively along a particular path giving the maximum $k_i(T)$. Therefore, the overall rate constant was approximated with the maximum $k_i(T)$ at each temperture;

$$k(T) = k_{i,max}(T), \qquad (6.6)$$

from which the temperature dependence of reaction rate was examined.

3. Results and Discussion

3. 1. Optimized Geometries and Total Energies

The fully optimized geometries of the reaction system in the reactant state and the transition state are shown in Figure VI-1 for both the reaction channels I and II. The numerical parameters for these optimized geometries are given in Tables VI-1 and VI-2. The geometry optimization was made in presuming the *Cs* symmetry.

The optimized geometries for the reactant states indicate that the methyl radical coordinated with a methanol molecule is distored from the well-known planer conformation. The distortion angle (the deviation of the direction of the C-H bonds from the molecular plane) calculated at the HF/6-31G* level is 1.04 and 3.94 degrees for the reaction channels I and II, respectively. The distortion of the methyl radical has qualitatively been indicated by a slight increase in the ^{13}C hyperfine coupling constant of the methyl radical in solid methanol matrix compared with that in the gas phase: the increase is attributed to the *2s-2p* orbital mixing.[22]

The intermolecular distance in the reactant state is given by $r(C_2\text{-}H_1)$ for the reaction channel I and $r(C_2\text{-}H_4)$ for the reaction channel II. They are 3.3485 A and 2.6480 A. The methyl radical approaches the methanol molecule more closely in the reaction channel II than in

the reaction channel I. This will be due to the repulsive interaction between the methyl group in methanol and the methyl radical in the channel I.

In the transition state (TS), the distance between the methyl radical and the methanol molecule is almost the same for both the reaction channels: r(C_2-H_1)=1.3592 A for the channel I and r(C_2-H_4)=1.3331 A for the channel II.

The deformation of the methanol molecule in the TS is in the same magnitude for both the reaction channels. The C-H bond of the methanol, r(C_1-H_1), in the reaction channel I stretches by 24.7 %, from 1.0807 A in the reactant state to 1.348 A in the TS. The O-H bond of the methanol, r(O-H_4), in the reaction channel II stretches by 24.6 %, from 0.9471 A to 1.1803 A. This is in agreement with the observation for the H-abstraction from methanol by methylene, $CH_3OH + CH_2 \rightarrow CH_2OH + CH_3$.[23]

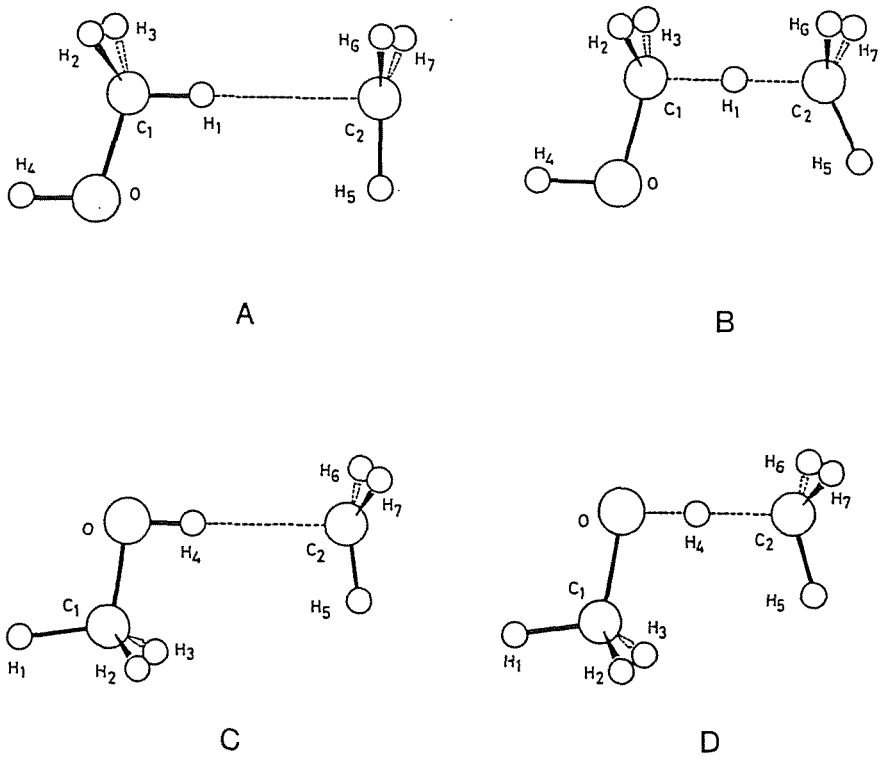

Figure VI-1. Illustration of optimized geometries for (A) reactant state and (B) TS for the reaction channel I, $CH_3 + CH_3OH \rightarrow CH_4 + CH_2OH$, and (C) reaction state and (D) TS for the reaction channel II, $CH_3 + CH_3OH \rightarrow CH_4 + CH_3O$. Corresponding geometrical parameters are given in Tables VI-1 and VI-2.

Table VI-1. Optimized parameters at the reactant state and the transitionstate (TS) for the reaction channel I. Bond length and angles are in angstrom and in degree.

	reactant			TS		
	HF/3-21G	HF/6-31G*	MP2/6-31G	HF/3-21G	HF/6-31G*	MP2/6-31G
r(C_1-H_1)	1.0782	1.0807	1.0912	1.3452	1.3480	1.3348
r(C_2-H_1)	3.0670	3.3485	2.9990	1.3575	1.3592	1.3431
r(C_1-C_2)	4.1452	4.4292	4.0902	2.7027	2.7072	2.6779
r(C_1-O)	1.4418	1.4002	1.4719	1.4248	1.3852	1.4513
r(O-H_4)	0.9658	0.9463	0.9786	0.9678	0.9482	0.9803
r(C_2-H_5)	1.0717	1.0726	1.0834	1.0797	1.0806	1.0922
r(C_2-H_6)	1.0718	1.0727	1.0834	1.0787	1.0798	1.0929
r(C_1-H_2)	1.0853	1.0875	1.0994	1.0814	1.0841	1.0973
∠H_1C_1O	106.32	107.21	105.21	103.48	104.66	102.50
∠C_1OH_4	110.30	109.43	110.10	111.23	110.07	111.48
∠$H_2C_1H_3$	108.72	108.66	109.29	119.06	112.53	113.12
∠$H_1C_1H_2$	108.66	108.43	109.35	104.66	105.16	105.88
∠$C_1C_2H_5$	75.25	71.37	68.65	105.35	105.73	103.85
∠$H_6C_2H_7$	119.93	119.92	119.93	119.54	113.17	113.39
∠$C_1C_2H_6$	98.75	100.88	101.72	104.38	105.16	105.71

Table VI-2. Optimized parameters at the reactant state and the transitionstate (TS) for the reaction channel II. Bond length and angles are in angstrom and in degree.

	reactant			TS		
	HF/3-21G	HF/6-31G*	MP2/6-31G	HF/3-21G	HF/6-31G*	MP2/6-31G
r(O-H_4)	0.9663	0.9471	0.9800	1.1601	1.1803	1.2193
r(C_2-H_4)	2.4702	2.6480	2.4687	1.3752	1.3331	1.2844
r(O-C_2)	3.3465	3.5951	3.4487	2.5353	2.5134	2.5037
r(C_1-O)	1.4389	1.3980	1.4684	1.4484	1.3963	1.4669
r(C_1-H_1)	1.0790	1.0814	1.0921	1.0819	1.0844	1.0971
r(C_1-H_2)	1.0856	1.0878	1.0998	1.0833	1.0866	1.0989
r(C_2-H_5)	1.0723	1.0733	1.0841	1.0775	1.0788	1.0924
r(C_2-H_6)	1.0724	1.0733	1.0841	1.0779	1.0792	1.0923
∠H_4OC_1	110.23	112.09	109.97	107.02	106.94	108.16
∠OC_1H_1	106.48	107.31	105.45	105.61	106.22	104.78
∠$H_2C_1H_3$	108.58	108.56	109.12	109.35	109.14	109.7
∠$H_1C_1H_2$	108.50	108.33	109.16	108.68	108.35	109.06
∠OC_2H_5	88.77	87.73	84.93	101.70	102.89	102.70
∠$H_6C_2H_7$	119.72	119.56	119.73	114.69	113.99	113.52
∠$H_4C_2H_6$	95.59	97.04	97.21	104.74	105.41	106.35

Table VI-3. Total energies (a.u.) and activation energies (kcal·mol^{-1}) for the reaction channel I, $CH_3 + CH_3OH \rightarrow CH_2OH + CH_4$, calculated by several methods.

Method	TS	Reactant	Ea
HF/3-21G//HF/3-21G	-153.6987216	-153.7414536	26.80
MP2/3-21G//HF/3-21G	-153.9948339	-154.0271592	20.28
MP3/3-21G//HF/3-21G	-154.0172932	-154.0507750	21.00
MP4D/3-21G//HF/3-21G	-154.0268262	-154.0600097	20.81
MP4DQ/3-21G//HF/3-21G	-154.0256817	-154.0590526	20.93
CCD/3-21G//HF/3-21G	-154.0287721	-154.0621646	20.94
HF/6-31G*//HF/6-31G*	-154.5476984	-154.5948776	29.61
MP2/6-31G*//HF/6-31G*	-154.9809751	-155.0145300	21.06
HF/6-31G//MP2/6-31G	-154.5600766	-154.6062004	28.94
MP2/6-31G//MP2//6-31G	-154.7951818	-154.8306875	22.28
MP3/6-31G**//MP2/6-31G	-155.0777721	-155.1094295	19.87
MP4DQ/6-31G**//MP2/6-31G	-155.0790612	-155.1133555	21.52
MP4SDQ/6-31G**//MP2/6-31G	-155.0946819	-155.1256748	19.45

Table VI-4. Total energies (a.u.) and activation energies (kcal·mol^{-1}) for the reaction channel II, $CH_3 + CH_3OH \rightarrow CH_3O + CH_4$, calculated by several methods.

Method	TS	Reactant	Ea
HF/3-21G//HF/3-21G	-153.7147544	-153.7431610	17.83
MP2/3-21G//HF/3-21G	-154.0110176	-154.0294918	11.59
MP3/3-21G//HF/3-21G	-154.0336491	-154.0530620	12.18
MP4D/3-21G//HF/3-21G	-154.0434414	-154.0622888	11.83
MP4DQ/3-21G//HF/3-21G	-154.0420772	-154.0613054	12.07
CCD/3-21G//HF/3-21G	-154.0449994	-154.0643614	12.15
HF/6-31G*//HF/6-31G*	-154.5561103	-154.5964090	25.29
MP2/6-31G*//HF/6-31G*	-154.9892087	-155.0168927	17.37
HF/6-31G//MP2/6-31G	-154.5010814	-154.5339983	20.66
MP2/6-31G//MP2//6-31G	-154.8050128	-154.8326619	17.35
MP3/6-31G**//MP2/6-31G	-155.0843807	-155.1115079	17.02
MP4DQ/6-31G**//MP2/6-31G	-155.0848642	-155.1115407	16.74
MP4SDQ/6-31G**//MP2/6-31G	-155.1023760	-155.1278877	16.01

Total energies at the reactant state and the TS were calculated with several methods and they are listed in Table VI-3 for the reaction channel I and in Table VI-4 for the reaction channel II together with activation energies. All the calculation methods show that the activation energy is comparatively larger for the reaction channel I than for the channel II. According to the most accurate calculation (MP4/6-31G**// MP2/6-31G), the activation energy of the channel II is only 85% of that of the channel I (16.01 kcal/mol vs. 19.47 kcal/mol). These results seem to indicate that the calculation at the higher level does not give the reverse order of activation energy values. They are qualitatively in agreement with the activation energies experimentally observed for the gas-phase reactions at high temperatures, though the MO calculations generally give the absolute value of activation energy too large compared with that observed experimentally.

According to the MP2/6-31G*//HF/6-31G* calculation, the isolated methanol+methyl radical system has a total energy of -155.013601 a.u. This turns out that the association energy between the methyl radical and methanol molecule (in the reactant state) is 0.58 kcal/mol for the reaction channel I and 2.07 kcal/mol for the channel II. This means that the methyl radical associates more preferably to the hydroxyl group than to the methyl group of the methanol molecule.

3. 2. Vibrational Modes of Reaction Complexes and RRKM Rate Constant

The harmonic vibrational frequencies of normal mode are listed in Table VI-5 for the reactant state and the TS of both the reaction channels. The normal mode having the imaginary frequency at the TS is the C-H-C asymmetric stretching and the O-H-C asymmetric stretching for the reaction channels I and II, respectively. They correspond to the direction of the reaction coordinate. The magnitude of the imaginary frequency inversely correlates to the thickness of the potential barrier in the vicinity of the TS along the reaction coordinate. Comparing the imaginary fre-quencies in Table VI-5, the tunneling probability is expected to be larger for the reaction channel II than for the channel I.

The frequencies of the bending and rocking vibrations of the methyl radical are higher in the TS of both the reaction channels than those in the reactant state. This is due to a sp^3-like orbital on the C-atom of the methyl radical (C_2) created by the interaction with the 1s-orbital of the abstracted H-atom (H_1 or H_4) in the vicinity of the TS.

Microcanonical rate constants were calculated for both the reaction channels I and II on the basis of the above-mentioned results of the vibration analysis and the Miller's corrected version[24] of the RRKM theory. Because the activation energies with zero-point energy correction (Ea+ΔZPE) obtained by the present *ab-initio* calculation are larger than the experimentally-determined values by ca. 10 kcal/mol, the calculated activation energies

(Ea+ΔZPE) were scaled down, as shown in Table VI-6, using a common scaling factor. The scaling factor has been so determined that the scaled activation energy fits to the experimental value (8.14 kcal/mol) for the reaction channel I. The scaled activation energy thus determined is 6.43 kcal/mol for reaction channel II. The rate constant calculation was made by fitting the reaction barrier with the Eckart potential.[20] Parameters used for fitting the potential are shown in Table VI-6. The negative frequencies at the TSs and the frequency factors for both channels are obtained at the HF/3-21G level.

Figure VI-2 (curves A and B) shows the microcanonical rate constants obtained by the above calculation. These rate constant values include the tunneling effect through the Eckart reaction barrier (See, Table VI-6). The rate constant is much larger for reaction channel II (curve B) than for reaction channel I (curve A) in the whole energy region. This means that the reaction channel II dominates over the channel I at any temperature. In this rate constant calculations, we used the integral expression eq.(6.3) for simplification. The large difference of the reaction rate constant (10^3~10^4) predicts that the rate calculation by using eq.(6.2) does not change above conclusion.

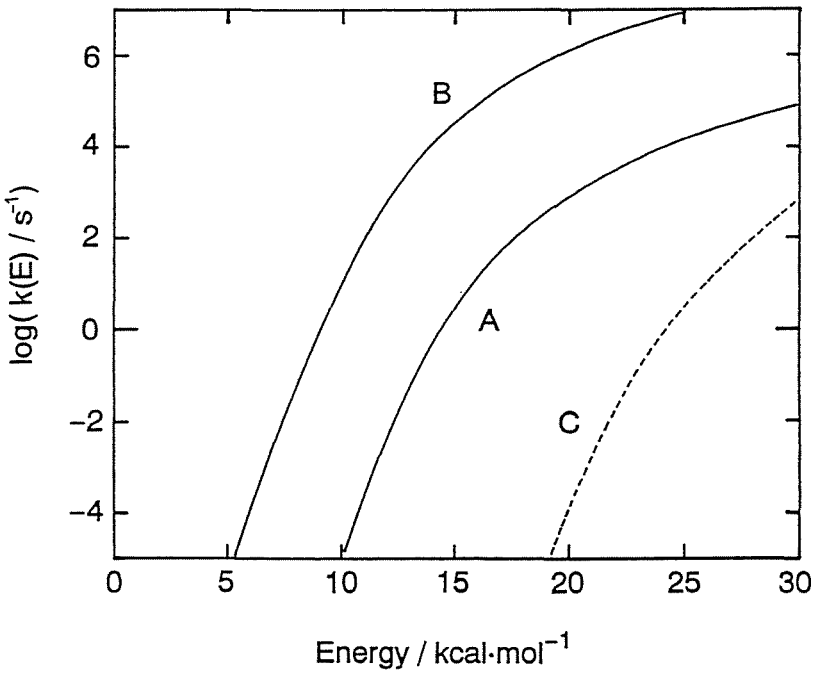

Figure VI-2. Microcanonical rate constant calculated for the modified RRKM theory for (A) the reaction channel I, $CH_3 + CH_3OH \rightarrow CH_4 + CH_2OH$, (B) reaction channel II, $CH_3 + CH_3OH \rightarrow CH_4 + CH_3O$, for isolated reaction system, and (C) reaction channel II in condensed phases (the methoxyl group of methanol brocked with hydrogen-bonding).

Table. VI-5. Descriptions of normal mode and corresponding harmonic vibrational frequencies (cm-1) calculated by the HF/3-21G method for the reaction channel I, $CH_3OH + CH_3 \rightarrow CH_2OH + CH_4$, and for the reaction channel II, $CH_3OH + CH_3 \rightarrow CH_3O + CH_4$, at the stationary points along the reaction coordinate.

			reaction I		reaction II	
mode	description	sym	Reactant	TS	Reactant	TS
1	OH str.	a'	3867.5	3828.3	3855.0	3080.5 i
2	$\cdot CH_3$ asym.str.	a'	3428.8	3348.5	3424.0	3364.6
3	$\cdot CH_3$ asym.str.	a"	3426.9	3339.5	3422.6	3358.7
4	$\cdot CH_3$ asym.str.	a'	3302.9	2542.1 i	3288.8	3266.0
5	$\cdot CH_3$ sym.str.	a'	3250.9	3220.9	3247.9	3230.2
6	CH_3(MeOH)asym.str.	a"	3215.9	3283.8	3210.6	3243.7
7	CH_3(MeOH)sym.str.	a'	3177.3	3209.0	3174.0	3190.3
8	CH_3(MeOH)asym.bend.	a'	1698.6	1658.7	1699.3	1694.6
9	CH_3(MeOH)asym.bend.	a"	1688.9	1648.2	1686.3	1669.9
10	CH_3(MeOH) sym.bend.	a'	1639.8	1645.0	1638.6	1614.0
11	$\cdot CH_3$ asym.bend.	a'	1543.9	1557.4	1544.7	1602.4
12	$\cdot CH_3$ asym.bend.	a"	1543.6	1562.7	1543.9	1593.0
13	OH in-plane bend.	a'	1481.5	1412.3	1494.8	1515.1
14	CH_3(MeOH) rock.	a"	1254.4	1258.9	1254.7	1247.7
15	CH_3(MeOH) rock.	a'	1153.9	1199.5	1164.2	1227.6
16	CO str.	a'	1089.2	1111.9	1096.2	1069.8
17	$\cdot CH_3$ sym.bend.	a'	454.2	1312.9	581.2	1311.0
18	OH out-of-plane bend.	a"	365.7	199.1	451.5	1224.7
19	$\cdot CH_3$ rock.	a'	106.7	651.6	186.3	646.8
20	$\cdot CH_3$ rock.	a"	97.1	806.8	174.3	453.3
21	$\cdot CH_3$-H-MeOH sym.str.	a'	55.3	485.0	97.4	509.1
22	$\cdot CH_3$-H-MeOH out-of-plane bend.	a"	51.7	399.3	75.1	160.2
23	$\cdot CH_3$-H-MeOH in-plane bend.	a'	17.3	138.0	35.5	39.1
24	$\cdot CH_3$ rotation	a"	8.2	27.6	20.0	177.1

Table VI-6. Activation energies with zero-point energy correction (kcal/mol) and RRKM parameters.

	reaction channel	
	I	II
Ea (MP4/6-31G**//HF/6-31G)	19.45	16.01
ΔZPE(HF/3-21G)	-0.88	-1.34
Ea + ΔZPE	18.57	14.67
V_0[a]	8.14	6.43
Ea' (MP4/6-31G**//HF/6-31G)	22.00	15.68
ΔZPE' (HF/3-21G)	-1.29	-1.68
Ea'+ ΔZPE'	20.73	14.00
V_1[a]	9.08	6.13
ω_i[c], cm^{-1}	2542.1i	3080.5i
A[d], s^{-1}	1.14×10^8	7.77×10^9

[a]Scaling factor is 0.538. V_0=0.438(Ea+ΔZPE), V_1=0.538(Ea' + ΔZPE).
[b]Activation energy and zero-point energy for the reverse reaction,
$CH_4 + CH_2OH \rightarrow CH_3OH + CH_3$ or $CH_4 + CH_3O \rightarrow CH_3OH + CH_3$
[c] Unscaled harmonic vibrational frequency obtained at the HF/3-21G level.
[d]Frequency factor calculated with the harmonic frequencies in Table VI-5.

3. 3. Short-cut path Rate Constant

In order to take into account all the possible short cut paths in the potential energy surface for the calculation of rate constants, the two-dimensional energy surface was derived for both the reaction channels I and II at the HF/3-21G level. The results are shown in Figures VI-3 and VI-4. The mass-weighted poten-tial energy surface is given as a function of two large-amplitude parameters: those primarily related to r(C_1-H_1) and r(C_2-H_1) for the reaction channel I, and to r(O-H_4) and r(C_2-H_4) for the reaction channel II. The geometry of the reaction systems was fully optimized at each set of the two large-amplitude parameters by using the energy gradient method. The short cut paths are the shortest lines connecting the isoenergetic points of the reactant and product regions.

The canonical rate constants for the reaction channel I was calculated, to examine the fundamental feature of the reaction process, under the assumption that the reaction proceeds through a particularly selected short cut path. The results of calculation are demonstrated in the Arrhenius plots in Figure VI-5 typically for three reaction paths (shown by broken lines in Figure VI-3): the minimum energy (ME) path through the suddle point (line A in Fig. VI-3), the

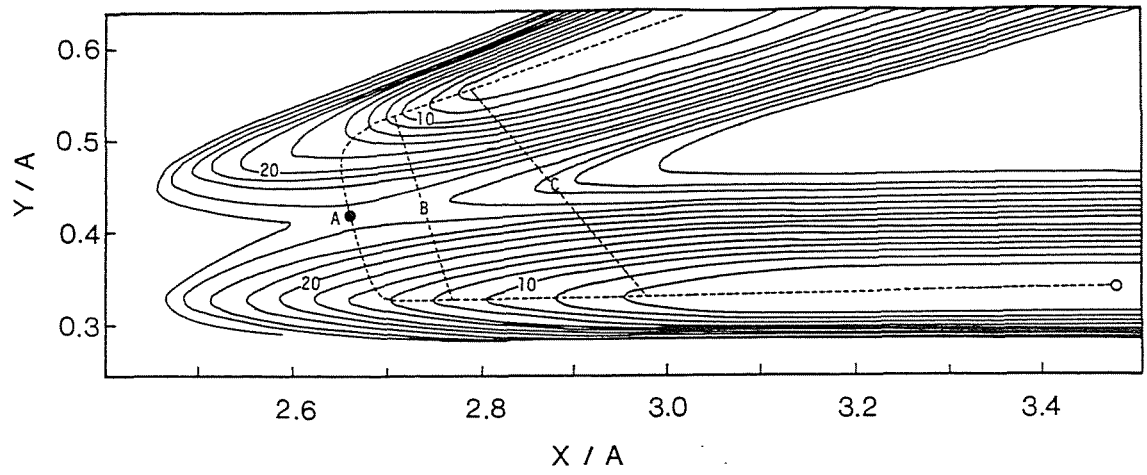

Figure VI-3. The potential energy surface for the reaction channel I, $CH_3 + CH_3OH \rightarrow CH_4 + CH_2OH$, calculated at the HF/3-21G level. Line A is the minimum energy path, and lines B and C are the short cut paths with energy of 11.09 kcal/mol and 5.58 kcall/mol (the zero-point energy of the reactant state). The dot point indicates the transition state with the activation energy of 26.80 kcal/mol.

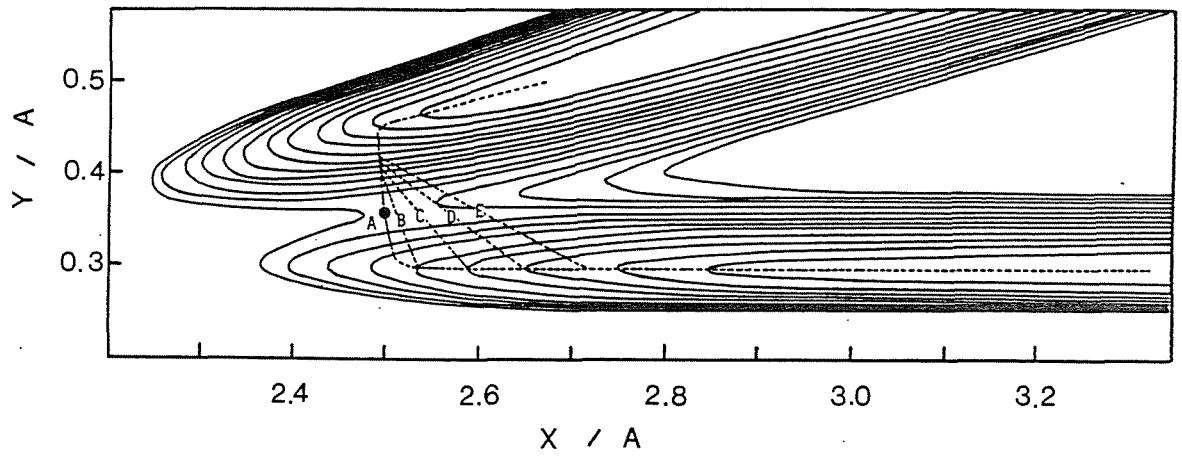

Figure VI-4. The potential energy surface for the reaction channel II, $CH_3 + CH_3OH \rightarrow CH_4 + CH_3O$, calculated at the HF/3-21G level. Line A is the minimum energy path, and lines B, C, D, and E are the short cut paths of the energy 10.0, 8.0, 6.0, and 4.71 kcal/mol (the zero-point energy of the reactant state). The dot point indicates the transtion state with the activation energy of 17.32 kcal/mol.

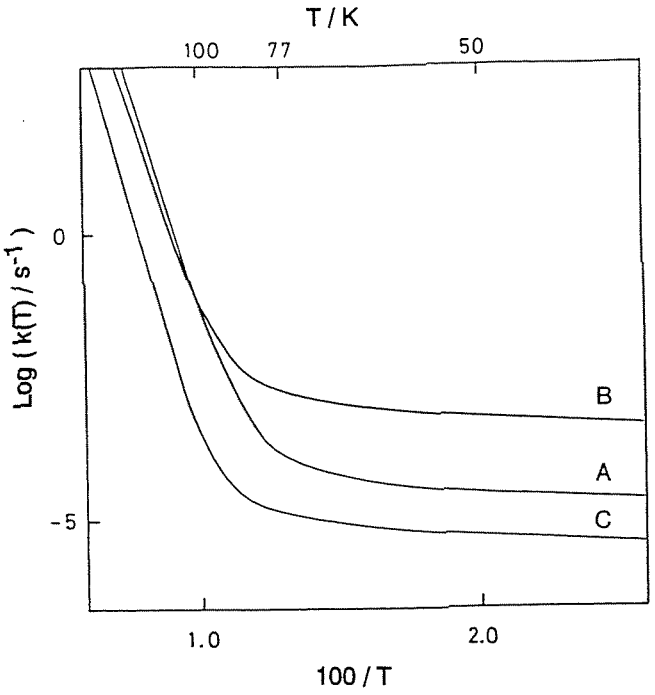

Figure VI-5. Dependence of canonical rate constant on reciprocal temperature for reaction channel I. The reaction is assumed to proceed along one of fixed reaction paths shown in Fig. 3. A: the minimum energy path, B: the short cut path of 11.09 kcal/mol energy, C: the short cut path of 5.58 kcal/mol the (the zero-point energy of the reactant state).

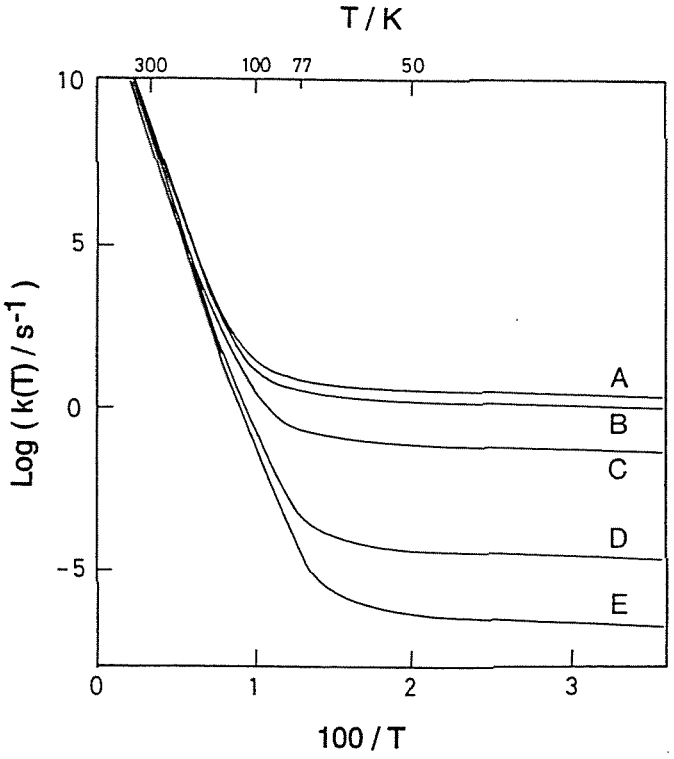

Figure VI-6. Dependence of canonical rate constant on reciprocal temperature for reaction channel II. The reaction is assumed to proceed along one of fixed reaction paths shown in Fig. 4. A: the minimum energy path, B, C, D, and E: the short cut paths 10.0, 8.0, 6.0, and 4.71 kcal/mol. The path E corresponds to the zero-point energy of the reactant state.

short cut paths of 11.09 kcal/mol energy (line B) and of 5.58 kcal/mol (zero-point energy of the reactant state, line C). In the high temperture region where the Arrhenius plot shows typical straight lines, the ME path with the lowest barrier is preferred to either of the short cut paths. In the low-temperature region (T<100 K), the rate constants for all the reaction paths approach a limiting value and become independent of temperature. The rate constant for the ME path is signifi-cantly lower than that for the short cut path of 11.09 kcal/mol. It is indicated that the reaction channel I proceeds almost exclusively through the short cut paths at low temperture, as in the case of $H + H_2$ reaction where the quantum tunneling effect has previously been shown to be essentially important at low temperatures based on the detailed theoretical considerations of rate constant.[7]

It should be noted that, in the above calculation of the rate constant, the absolute value of the energy surface was scaled down by a common scaling factor, so that the theoretical activation barrier (26.80 kcal/mol at the saddle point in Fig.VI-3) coincides to the activation energy of the reaction, 8.14 kcal/mol, observed at high temperatures.[2] It is still now a difficult task to reproduce purely on theoretical basis the activation energy of a reaction.

The canonical rate constants along some particular reaction paths for the reaction channel II were also calculated in the same manner as for the reaction channel I by using the common scaling factor for adjusting the activation barrier. The results of calculation are demonstrated in the Arrhenius plots in Figure VI-6 typically for five reaction paths shown by broken lines in Figure VI-4. The rate constants for all the reaction paths tend to a limitting value. This indicates that the tunneling effect is important at low temperature for the reaction channel II also. The ME path through the suddle point (line A in Fig. VI-4) gives the highest rate constant irrespective of temperature. However, the ME path rate constant is very close to that for some of the short cut paths. This suggests that the reaction channel II proceeds through either of the ME path and the short cut paths at low temperatures.

Comparison of the rate constants between Figure VI-5 and VI-6 gives an theoretical estimate of the branching between the raction channels I and II. The rate constant for the most preferable reaction path of the reaction channel II (in Figure VI-6) is 2-3 orders of magnitude larger than that of the reaction channel I in the low-temperature range. This means that the inclusion of the quantum tunneling effect does not explain the experimental observation that the H-abstraction by the methyl radical occurs exclusively from the methyl group of methanol (reaction channel I) at low temperatures, i. e., in liquid and solid state.

The actual dependence of the theoretical rate constant for the reaction channel I on temperature is derived by plotting the rate constant for the most preferable path (the path giving the maximum rate constant) at each temperature instead of integrating contribution from all the possible reaction paths, as shown in Figure VI-7. The rate constants observed in the ESR studies on the methyl radical in solid methanol[5] are also shown in Figure VI-7. The

experimental data agree with the results of present theoretical calculation. Deviation from the classical value (the dashed straight line) again shows the importance of the tunneling effect in the low-temperature region. The isotope effect on the reaction of present interest is studied by calculating the theoretical rate constant for

$$CD_3OD + CH_3 \rightarrow CH_3D + CD_2OD \qquad \text{(III)}$$

and comparing it with the rate constant observed by the ESR[5] in Figure VI-7. The agreement between theory and experiment again indicates the feasibility of the present treatment of rate constant for the reaction channel I.

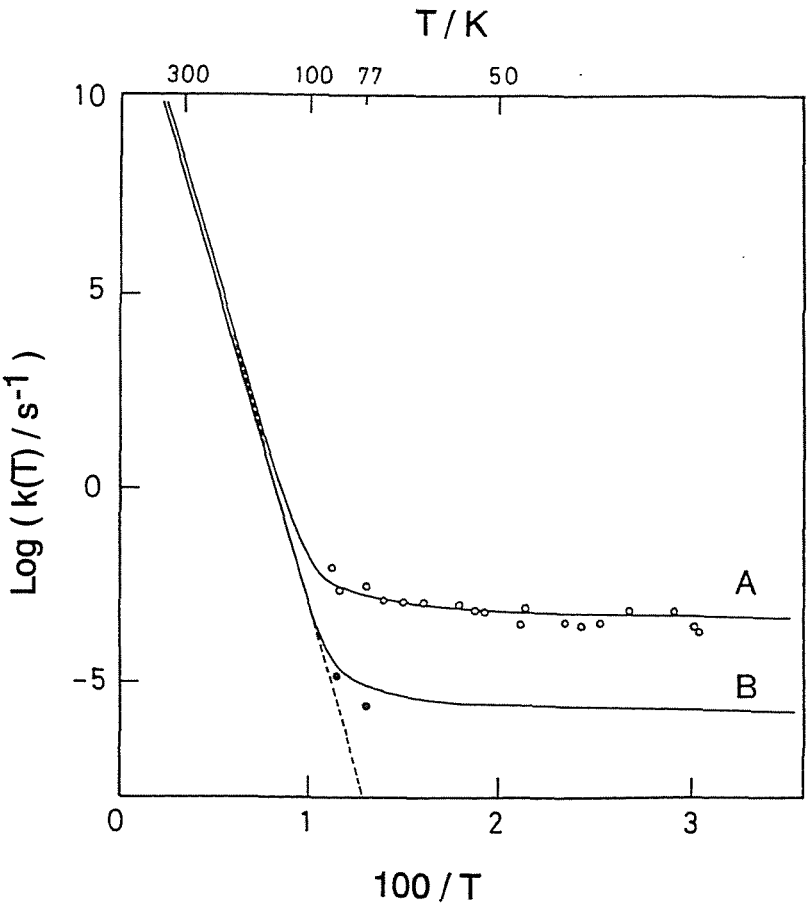

Figure VI-7. Actual dependence of the rate constant for the reaction channel I on reciprocal temperature together with isotope effect: (A) $CH_3 + CH_3OH \rightarrow CH_4 + CH_2OH$, and (B) $CH_3 + CD_3OD \rightarrow CH_3D + CD_2OD$. Open and closed circles shows the corresponding ESR results reported previously (ref. 5). Dashed straight line shows the expected line for the protiated methanol based on the classical theory without the tunneling effect for comparison.

3. 5. Effect of Matrix Interactions

The theoretical treatments for the isolated reaction system, CH_3+CH_3OH, described hereinbefore seem to require an additional factor to explain the actual absence of the reaction channel II at low temperatures. Since all the experiments at low temperatures have necessarily been made in condensed phases, the hydrogen-bonding is the most plausible factor which blocks the reaction site, the hydroxyl group of methanol, from the attack of the methyl radical and effectively inhibits the reaction channel II. The effect of the hydrogen-bonding has been examined by calculating the RRKM rate constant for the channel II under the assumption that the hydrogen-bonding should be broken before the hydroxyl H-atom is abstracted by the methyl radical, so that the activation barrier is raised by the magnitude of the hydrogen-bond energy.

To estimate the hydrogen-bond energy, a simpler model system, $CH_3OH..O(H)CH_3$, was taken for the calculation at the MP2/6-31G* level. The calculation gave the hydrogen-bonding energy of 7.31 kcal/mol. It turns out that the scaled activation barrier is raised from 6.47 to 13.78 kcal/mol. The microcanonical rate constant for the latter barrier was calculated with the modified version of the RRKM theory[24] and is shown in Figure VI-2 (curve C). It is indicated that the blocking of the hydroxyl group by the hydrogen-bonding reduces con-siderably the rate constant for the reaction channel II, so that it is much lower than the rate constant for the reaction chennel I in all the energy region. This means that the reaction channel I proceeds much more faster than the channel II in condensed phases, as observed experimentally.

The electrostatic effect of the medium (solvent) molecules[25] is seemingly another possible factor to modify the rate constant in condensed phases. This effect was modeled by 30 point charges (10 water molecules) surrounding the reaction system, according to the fractional charge model,[25] and calculated the RRKM rate constant for both the reaction channels I and II. However, the rate constant values were found to be modified in reverse direction: the rate constant for the reaction channel I is increased, while that for the channel II is decreased by the electrostatic effect. Therefore, this effect is not important for explaining the dominance of the reaction channel I at low temperatures.

References

1. Tsang, W., *J. Phys. Chem. Ref. Data.* **1987**, *16*, 471.
2. Kerr, J. A.; Parsonage, M. J., In *Evaluated Kinetic Data on Gas Phase Hydrogen Transfer Reactions of Methyl Radicals,* Butterworths, London, 1976, p. 95.
3. Campion, A.; Williams, F., *J. Am. Chem. Soc.* **1972**, *94*, 7633.
4. Hudson, R.L.; Shiotani, M.; Williams, F., *Chem. Phys. Lett.* **1977**, *48*, 193.
5. (a) Doba, T.; Ingold, K. U.; Siebrand, W.; Wildman, T. A., *Faraday Discuss. Chem. Soc.* **1984**, *78*, 175.
   (b) Doba, T.; Ingold, K. U.; Siebrand, W.; Wildman, T. A., *J. Phys. Chem.*, **1984**, *88*, 3165.
6. (a) Tsuruta, H.; Miyazaki, T.; Fueki, K.; Azuma, N., *J. Phys. Chem.* **1983**, *87*, 5422.
   (b) Miyazaki,T.; Hiraku, T.; Fueki,K.; Tsuchihashi,Y., *J. Phys. Chem.* **1991**, *95*, 26.
7. (a) Truhlar, D.G.; Isaacson, A. D.; Garrett, B. C., In *Theory of Chemical Reaction Dynamics*; Baer, M., Ed.; CRC Press: Boca Raton, FL, 1985; Vol.4.
   (b) Miller, W. H., *J. Phys. Chem.* **1983**, *87*, 3811.
   (c) Miller, W. H., In *The Theory of Chemical Reacton Dynamics,* Clary, D. C., Ed., D. Reidel, Boston, **1986**, p. 27.
   (b) Miller, W. H.; Ruff, B. A.; Chang, Y., *J. Chem. Phys.* **1988**, *89*, 6298.
   (c) Carrington, T.; Miller, W. H., *J. Chem. Phys.* **1987**, *86*, 1451.
   (d)Gray, S. K.; Miller, W. H.; Yamaguchi, Y.; Schaefer, H.F., *J. Am. Chem. Soc.* **1981**, *103*, 1900.
   (e)Osamura, Y., Schaefer, H. F.; Gray, S. K.; Miller, W. H. *J. Am. Chem. Soc.* **1981**, *103*, 1904.
   (f) Okuyama, S.; Oxtoby, D.W., *J. Chem. Phys.* **1988**, *88*, 2405.
   (g) Ovchinnikova, M. Ya, *Chem. Phys.* **1979**, *36*, 85.
   (h) Babamov, V. K.; Marcus, R. A., *J. Chem. Phys.* **1981**, *78*, 1790.
   (i) Truhlar, D. G.; Kuppermann, A., *J. Am. Chem. Soc.* **1971**, *93*, 1840.
   (j) Bosch, E.; Moreno, M.; Llunch, J. M.; Bertran, J., *J. Chem. Phys*, **1990**, *93*, 5685.
   (k) Shida, N.; Almlof, J.; Barbara, P.F, *J. Phys. Chem.*, **1991**, *95*, 10457.
   (l) Marcus, R. A.; Coltrin, M. E., *J. Chem. Phys.* **1977**, *67*, 2609.
   (m) Hancock, G. C.; Mead, C. A.; Truhlar, D. G.; Varandas, A. J. C., *J. Chem. Phys.* **1989**, *91*, 3492.
   (n) Takayanagi, T.; Sato, S., *J. Chem. Phys.* **1990**, *92*, 2862.
   (o) Pardo, L.; Banfelder J. R.; Osman, R., *J. Am. Chem. Soc.*, **1992**, *114*, 2382.
8. (a)Gordon, M. S.; Binkley, J. S.; Pople, J. A.; Pietro, W. J.; Hehre, W. J., *J. Am. Chem. Soc.* **1972**, *104*, 2797.

(b) Francl, M. M.; Pietro, W. J.; Hehre, W. J.; Binkley, J. S.; Bordon, M. S.; Defrees, D. J.; Pople, J. A., *J. Chem. Phys.* **1982**, *77*, 3654.

9. Binkley, J. S.; Frisch, M. J.; DeFrees, D. J.; Raghavachari, K.; Whiteside, R. A.; Schlegel, H. B.; Fluder, E. M.; Pople, J. A., An ab-initio molecular orbital calculation program; *GAUSSIAN-82.*

10. Frisch, M. J.; Binkley, J. S.; Schlegel, H. B.; Raghavachari, K.; Melius, C. F.; Martin, R. L.; Stewart, J. J. P.; Bobowicz, F. W.; Rohlfing, C. M.; Kahn, L. R.; DeFrees, D. J.; Seeger, R.; Whiteside, R. A.; Fox, D. J.; Fleuder, E. M.; Pople, J. A. An ab-initio molecular orbital calculation program; *GAUSSIAN-86.*

11. Pulay, P. In *Modern Theoretical Chemistry*, Schaefer, H. F. III, Ed.; Plenum; New York, 1977; Vol. 4, Chapter 4.

12. Pople, J. A.; Krishnan, R.; Schlegel, H. B.; Binkley, J. S. *Int. J. Quantum. Chem. Symp.* **1979**, *13*, 325.

13. Mϕller, C.; Plesset, M. S., *Phys. Rev.* **1934**, *46*, 618; Krishnan, R.; Frisch, M. J.; Pople, J. A., *J. Chem. Phys.* **1980**, *72*, 4244, and reference therein.

14. (a) Bartlett, R. J., *J. Chem. Phys.* **1989**, *93*, 1697.
(b) Lee, Y. S., Kucharski, S. A.; Bartlett, R. J. *J. Chem. Phys.* **1984**, *81*, 5906.
(c) Raghavachari, *J. Chem. Phys.* **1985**, *82*, 4607.

15. Francisco, J. S. *J. Am. Chem. Soc.* **1989**, *111*, 7353.
(b) Kakumoto, T.; Saito, K.; Imamura, A., *J. Phys. Chem.* **1987**, *91*, 2366.

16. Tachibana, A.; Fueno, H.; Tanaka, E.; Murashima, M.; Koizumi, M.; Yamabe, T., *Int. J. Quantum. Chem.* **1991**, *39*, 561.

17. Johnson, H. S., In *Gas Phase Reaction Rate Theory*, Ronald Press, New York, **1966**, p. 37.

18. Robinson, P. J.; Holbook, K. A., In *Unimolecular Reaction*, Wiley, New York, **1972**, p. 131.

19. Miller, W. H., In *Tunneling*, Jortner, J.; Pullman, B. eds. D. Reidel, Boston, **1986**, pp. 91-101.

20. Eckart, C. *Phys. Rev.* **1930**, *35*, 1303.

21.(a) Garrett, B. C.; Truhlar, D. G., *Int. J. Quantum. Chem.* **1987**, *31*, 17.
(b) Garrett, B. C.; Truhlar, D. G., *J. Phys. Chem.*, **1991**, *95*, 10374.
(c) Garrett, B. C.; Truhlar, D. G.; Wagner, A. F.; Dunning, T. H., *J. Chem. Phys.* **1983**, *78*, 4400.

22. Stratt, R. M.; Destjardins, S. G., *J. Am. Chem. Soc.* **1984**, *106*, 256.

23. Oikawa S.; Tsuda, M., *J. Am. Chem. Soc.* **1985**, *107*, 1940.

24. Miller, W. H., *J. Am. Chem. Soc.* **1979**, *101*, 6810.

25. Noell, J. O.; Morokuma, K., *Chem. Phys. Lett.* **1975**, *36*, 465.

CHAPTER VII

THE SOLVENT EFFECTS IN HYDROGEN ATOM TRANSFER REACTIONS IN CONDENSED PHASE

1. Introduction

Solvent effects play a major role in chemical reactions and have been extensively studied both experimentally and theoretically.[1] In recent years, theoretical models of the effect of solvents on chemical properties and reactions have been developed by several groups.[2] In 1975, Noell and Morokuma proposed a fractional charge model[3] of the solvation shell, in which the solvent is represented by point charges at the solvent atomic centers, and applied this method to some solvation systems. More recently, Lunell and co-workers[4] have made *ab-initio* MO calculations of electronic states of solid ammonia on the basis of the fractional charge model, and could successfully interpret several experimental phenomena. Newton developed a continum model[5] for solvation systems at the Hartree-Fock (HF) level and applied it to hydrated electrons. In his model, the solvation system is constructed from the first solvation molecules calculated by molecular orbital theory and a dielectric medium for calculation of the long-range interaction with the first solvation molecules.

Also, solvent effects in chemical reactions have been extensive investigated theoretically. In 1984, Clark[6] studied the dissociation reaction due to electron capture for $CH_3Cl + e^- \rightarrow \cdot CH_3 + Cl^-$, in a lattice of helium atoms, and pointed out the significance of the medium in chemical reactions. Noell and Morokuma[7] applied their fractional charge model to the reaction $NH_3 + HF \rightarrow NH_4^+ + F^-$, and showed that the solvents significantly changed the potential surface for the reaction.

Among other methods that are able to include the solvent effects, the self-consistent reaction field (SCRF),[8] has been widely used in molecular calculations. Karelson *et al.* [9] applied this method to the potential curves for the dissociation reaction of HF in the gas phase and in solution. More recently, Steinke *et.al.*[10] discussed the electronic nature of 1,3-dipoles in some solvents on the basis of results obtained by this method.

Thus, several models and methods to treat solvent effects have been applied to static properties and to chemical reactions, and have succeeded in interpreting experimental phenomena. A limitation in these method, however, when used for calculating the chemical reaction rate constant at the microscopic level, is that they do not explicity consdider the solvent

effects on the difference of the vibrational energies in the reactant (RC) and in the transition state (TS).

In this chapter, we examine a simple model to estimate the rate constant in the condenced phase and discuss the solvent effects on the chemical reaction rate. This model is based on the RRKM theory,[11,12] as extended by Miller,[13] and includes the vibrational coupling between the reaction system and the surrounding solvent molecules. This model is used to calculate the rate constant of the unimolecular reaction, $CH_3O\cdot \rightarrow \cdot CH_2OH$ in the condensed phase.

2. Theory

According to the transition state theory, in case of angular momentum J=0, the standard expression of the unimolecular rate constant[11] is

$$k(E) = N(E)/[2\pi\hbar\, \partial No(E)/\partial E] \tag{7.1}$$

where N(E) and N_0(E) are the integral densities of state in the transition state and in reactant molecules, respectively. (∂No/∂E) can be calculated from the classical Whitten-Robinowich equation[14]

$$(\partial N_0 / \partial E) = E^{3N-7}\left[(3N-7)!\,\hbar^{3N-6}\prod_{i=1}^{3N-6}\omega_i\right]^{-1} \tag{7.2}$$

where N is the number of atoms and $\{\omega_i\}$ are the vibrational frequencies of the reactant molecule. Following Miller's theory,[15] the quantum mechanical expression that involves tunnel effects is given by

$$N(E) = \sum_n P(E - \varepsilon_n^+) \tag{7.3}$$

where P(E) is the one dimensional tunneling probability[16] as a function of the energy E, and ε_n is the vibrational energy level of the transition state. The vibrational energy can be written

$$\varepsilon_n^+ = V_0 + \sum_{i=1}^{3N-7}\hbar\,\omega_i^+\left(n_i + \frac{1}{2}\right) \tag{7.4}$$

where V_0 and $\{\omega_i\}$are the barrier height and the vibrational frequencies of the transition state molecule, respectively.

For the final equation, the integral form of the microcanonical rate constant including Miller's tunneling correction is given by [16]

$$k(E) = \frac{1}{2\pi}\int_{-V0}^{E-V0} \cdot dE_1 \left(\frac{\prod_{i=1}^{s} \omega i}{\prod_{i=1}^{s-1} \omega i^{\pm}} \right) \cdot \left(\frac{\partial P(E1)}{\partial E1} \right) \cdot \left(\frac{E\text{-}V0\text{-}E1}{E} \right)^{S-1} \qquad (7.5)$$

or

$$k(E) = A \cdot \int_{-V0}^{E-V0} \cdot dE_1 \cdot \left(\frac{s-1}{E} \right) \cdot P(E_1) \cdot \left(\frac{E - V_0 - E_1}{E} \right)^{S-1} \qquad (7.6)$$

where s is the degree of freedom and A is the frequency factor:

$$A = \left(\prod_{i=1}^{s} \omega_i \right) / 2\pi \left(\prod_{i=1}^{s-1} \omega_i^{+} \right) \qquad (7.7)$$

The temperature dependent rate constant (canonical rate constant) is given by

$$k(T) = \frac{1}{\hbar} \int_0^{\infty} N(E) \cdot \exp(-E/kT) \cdot dE \; / \int_0^{\infty} \left(\frac{\partial N_0(E)}{\partial E} \right) \cdot \exp(-E/kT) \cdot dE \qquad (7.8)$$

Since the unimolecular rate constant is dependent on the activation energy V_0 and the vibrational frequencies $\{\omega_i\}$, one should estimate those values in the solution system in order to obtain the rate constant.

In our simple model, the effect of solvents in a chemical reaction is regarded as a perturbation to the normal mode frequencies of the isolated reaction system. Although the eigenstates of a vibrational mode in the isolated reaction system are orthogonal to each other, this orthogonality is broken if the solvent molecules exist. Indeed, the energy shifts of the vibrational modes for the isolated system may be caused through the eigenstate of the solvent.

In order to consider the vibrational coupling between the isolated reaction system and solvent molecules, we modify the Hessian matrix or force constant matrix, which is calculated by means of the second derivative of the potential energy V. To include the effect of the solvent, the matrix is expressed as

$$K^S = \begin{bmatrix} R_{ij} & I_{ij}^1 \cdots & I_{ij}^n & \cdots I_{ij}^k \\ \vdots & S_{ij}^{11} \cdots & S_{ij}^{1n} & \cdots S_{ij}^{1k} \\ & \cdots & S_{ij}^{nn} & \\ & \cdots & & \cdots S_{ij}^{kk} \end{bmatrix} \tag{7.9}$$

where each matrix component is calculated for the 3N X 3N cartesian coordinates by[17]

$$K_{ij} = \frac{\partial^2 V}{\partial X_i \cdot \partial X_j} \tag{7.10}$$

R_{ij} and $S_{ij}^{n,n}$ are the matrix elements of the reaction system and of the *n-th* solvent molecule, respectively. I_{ij}^n and $S_{ij}^{n,j}$ are the cross-terms between the reaction system and the n-th solvent molecule and between the n-th and l-th solvent molecules, respectively. Especially, if all solvent molecules and the reaction system are sufficiently away from each other, eq. (7.9) is reduced to

$$K^S = R + \sum_{n=1}^{k} \sum_{m=1}^{k} S^{m,n} \tag{7.11}$$

Thus, the vibrational energy shifts caused by the solvent molecules occur through the term $\{I_{ij}^n\}$. If the vibrational coupling interaction between solvent molecules is negligibly small as compared with the interaction with the reaction system, we can make eq. (7.9), that has a form of many-body system, into a linear combination of two-body systems.

On the basis of those considerations, we calculate the rate constant in the solvation system with the following steps: (i) calculation of the second derivative matrix element in the reaction system $\{R_{ij}\}$; (ii) calculation of the second derivative matrix elements in a reduced system; for example, a system composed of R_{ij} and the first solvation shell, or of R_{ij} and one solvent molecule. (iii) continuation of step (ii) up to the number of solvent molecules. (iv) construction of second derivative supermatrix $\mathbf{K}^S$. (v) calculation of the **D** matrix according to

$$\mathbf{D} = \mathbf{M}^{-1/2}\, \mathbf{K}^S\, \mathbf{M}^{-1/2} \tag{7.12}$$

where M_{ij} is the mass of the atom i; (vi) calculation of the eigenvalues and eigenstates in the solvation system by diagonalizing the **D** matrix.

$$\mathbf{L} = \mathbf{U}^T \mathbf{D}\, \mathbf{U} \tag{7.13}$$

(vii) calculation of the microcanonical rate constant with eq. (7.5). Thus, by using this simple approximation, one can obtain easily the effect of vibrational coupling between the reaction system and surrounding solvent molecules, i.e. one can add the effect of solvation to the reaction system.

3 Application to the chemical reactions

A. Intramolecular hydrogen atom transfer reaction $CH_3O\cdot \rightarrow \cdot CH_2OH$ in water matrix.

To apply our model, we consider the hydrogen atom rearrangement reaction from the methoxy radical ($CH_3O\cdot$) to the hydroxy methyl radical ($\cdot CH_2OH$) in gas phase and in condensed phase.

$$CH_3O\cdot \rightarrow \cdot CH_2OH \qquad (7.14)$$

Since those radical molecules play an important role not only in gas phase reactions in combustion chemistry[18] but also in radiation chemistry in low-temperature matrix reactions,[19] this reaction has received considerable attention experimentally and theoretically. So far, however, the solvent effect has not been investigated in detail because it is complicated to monitor the proceeding of this reaction in the condensed phase.

Concerning the present reaction in the gas phase, some experiments have been performed to obtain thermochemical and kinetics data,[20] In 1969, Handy and Franklin[21] showed that CH_2OH lies energetically on the order of 5 ± 5 kcal/mol below CH_3O. Batt *et. al.*[22] estimated an upper limit of the rate constant for the gas phase reaction, based on investigations of the pyrolysis of dimethyl peroxide.

The magnetic interaction parameters of CH_3O in irradiated methanol at 4 K were determined for the first time by Iwasaki and Toriyama in 1978.[23] Furthermore, they investigated experimentally the reactions occuring by radiolysis of polycrystalline methanol and interpreted that the formation of $\cdot CH_2OH$ is caused by a unimolecular process from $CH_3O\cdot$, i.e., according to reaction (7.14).[24]

Some excellent theoretical investigations on the methoxy radical, the hydroxymethyl radical and the isomerization reaction have been performed during the years. In 1983, Schaefer and co-workers studied systematically this isomerization reaction by means of accurate *ab-initio* calculations (MP3/6-31G**) and predicted theoretically that the hydroxymethyl radical energetically lies 5.0 kcal$\cdot$ mol^{-1} lower than methoxy radical and that the activation energy for the isomerization reaction (7.14) is about 36 kcal$\cdot$ mol^{-1}.[25] By using the reaction path

Table VII-1. Optimized parameters obtained at the HF/D95V** level. Bond lengths and angles are in Angstrom and in degrees, respectively.

	reactant	TS	Product
r(C-H_1)	1.087	1.080	1.075
r(C-H_2)	1.087	1.080	1.079
r(C-H_3)	1.090	1.269	1.909
r(O-H)	1.986	1.188	0.944
r(C-O)	1.386	1.369	1.361
<OCH_1	111.61	117.27	113.11
<OCH_3	106.10	53.40	110.53
<H_1CH_2	110.61	117.12	119.28
<OCH_2	111.61	113.11	117.89
<PCH_1			72.92
<$PCOH_3$			106.01

Table VII-3. Total energies (a.u.) at the stationary points on the potential surface of $CH_3O\cdot$ / $\cdot CH_2OH$ rearrangement reaction in vacuo. The basis set used is the Huzinaga-Dunning DZP (D95V**) basis.

Method	Reactant	TS	Product
HF	-114.45252	-114.36803	-114.44716
MP2	-114.73021	-114.67668	-114.74719
MP3	-114.75467	-114.69240	-114.76331
MP4DQ	-114.75711	-114.69507	-114.76612
CCD	-114.75780	-114.69550	-114.76660
CCD + ST4	-114.76684	-114.70801	-114.77618

Table VII-2. Theoretical and experimental vibrational frequencies (cm^{-1})[a] of the stationary points (reactant; RS, transition state; TS and product; PD) of the $CH_3O\cdot \rightarrow \cdot CH_2OH$ rearrangement reaction at the HF/95V** level, as well as isotope (all protons substituted by deuterons) and matrix effects on the vibrational frequencies.

	Reaction in vacuo[e]					Isotope		in matrices	
Symmetry	RC	Expt.[c]	TS	PD[b]	Expt.[d]	RC	TS	RC	TS
a´	3247 (3255)		3264	4214 (4125)	3650	2403	2360	3249	3267
	3170 (3188)		2484	3421 (3427)		2271	1805	3173	2486
	1640 (1668)		1604	3283 (3289)		1279	1289	1631	1578
	1557 (1585)	1325±30	1265	1608(1626)	1459	1113	1117	1535	1264
	1204 (1226)		1073	1459 (1483)	1334	1073	835	1203	1097
	1098 (1130)	1015	2564 i	1285 (1155)	1183	870	1899 i	1094	2565 i
a´´	3266 (3274)		3380	1143 (1287)	1048	2423	2523	3343	3381
	1560 (1604)		1235	804 (850)	569	1157	951	1543	1227
	806 (1283)		942	402 (411)	420	631	677	872	979

[a]Values are unscaled.

[b] The *molecule has* C_1 symmetry.

[c]Values are taken from Ref. 33 and Ref. 34.

[d]Values are taken from Ref. 35.

[e] 6-31G* values from Ref. 25 shown in parentheses.

Hamiltonian developed by Miller *et.al.*,[26] Colwell and Handy [27] investigated the curvature effects on this reaction and showed that this effect decreased the rate constant about 5 % .

Thus, although several properties of this reaction have been studied theoretically, so far there is no study of the solvent effects on the rate constant of this reaction at the *ab-initio* CI level. In this section, we show the results of the solvent effect on the rate constants derived from the application of our simple model.

a. Method of the calculation and the model cluster

The basis sets used here are Huzinaga-Dunning valence double-zeta Gaussian base[28] to which are added a set of p functions to hydrogen and a set of d functions to the heavy atoms ($D95V^{**}$ basis). In order to obtain the potential surface associated with the reaction, geometry optimization of the reactant, transition state and product molecules are performed by using the energy gradient method[29] with the $D95V^{**}$ basis. To gain the electron correlation, the coupled cluster theory[30] in which the configurations included are single and double excitations relative to the HF configuration, and Moller-Plesset many-body perturbation theory (MP2, MP3 and MP4DQ),[31] are employed in the present study. In order to include the solvent effect in the activation energy calculations, the fractional charges ($39H_2O$) representing the water molecule are located in the surrounding reaction system. For the values of the point charges and the geometry of the water molecules, $MP2/D95V^{**}$ optimized values (R(O-H)=0.962 Å, < HOH=104.41°, q_O=-0.66, q_H=+0.33) are employed in this calculation. The vibrational couplings between the reaction system (RS) and the solvent molecules are accounted for in the interaction between RS and ten water molecules in the first solvation shell. The reduced system (which is explicitly considered by *ab-initio* calculations) is composed of RS and two water molecules, and the overall system (i.e. the $\mathbf{K}^S$ matrix) is made of five reduced systems.

Since the solvation structure of this system is unknown, we assume that the structure of the first solvation shell is constructed from ten water molecules with the dipole oriented toward the oxygen or carbon atoms of $CH_3O\cdot$ radical, as shown in Figure VII-1. The distances between RS and a coordinating water molecule, which are roughly estimated from HF/3-21G calculations (r_1 = 2.969 Å, r_2 = 2.976 Å r_3 = 3.793 Å and r_4 = 3.350 Å), are used.

b. Reactions in gas phase and in the model cluster

Figure VII-2 shows a schematic illustration of the $CH_3O\cdot/\cdot CH_2OH$ rearrangement reaction on the basis of the present calculation. As predicted by Saebo *et al.*,[25] the symmetry of

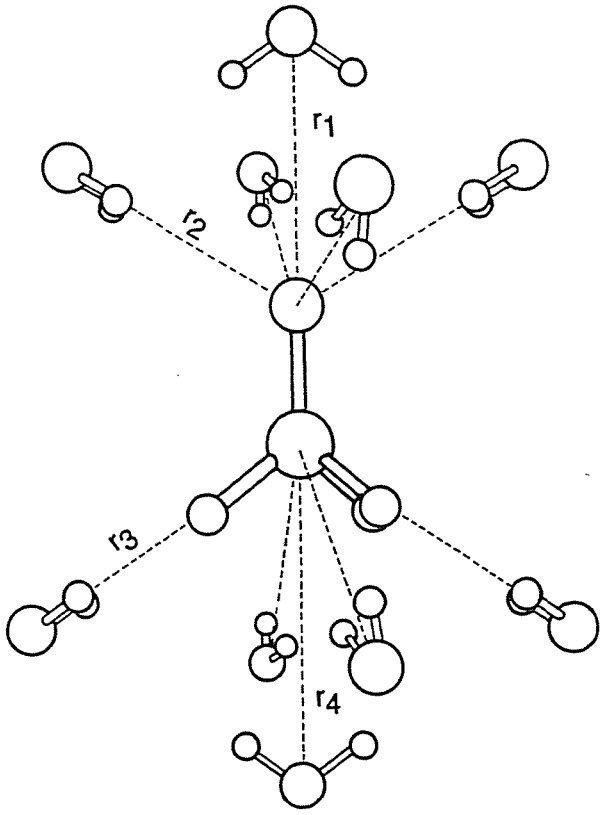

Figure VII-1. Assumed structural model of the first solvation shell of the reaction system. (r_1 = 2.969 Å, r_2 = 2.976 Å, r_3 = 3.793 Å, r_4 = 3.350 Å). The complex has *Cs* symmetry.

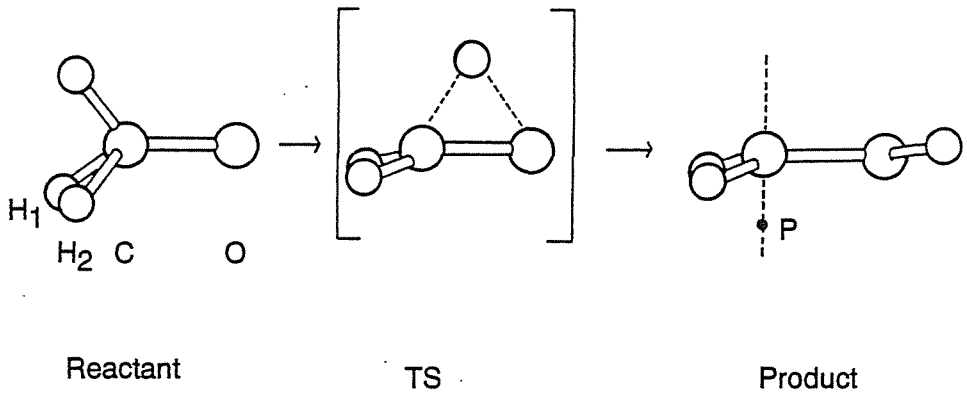

Figure VII-2. Schematic illustration of the reaction process for the $CH_3O\cdot/\cdot CH_2OH$ hydrogen rearrangement reaction predicted by the HF/D95V** calculations.

Table VII-4. Total energies (a.u.) in the condensed phase at the stationary points on the potential surface of $CH_3O\cdot/\cdot CH_2OH$ rearrangement reaction. The basis set used is the Huzinaga-Dunning DZP ($D95V^{**}$) basis.

Method	Reactant	TS	Product
HF	-122.20685	-122.13229	-122.19322
MP2	-122.48453	-122.44270	-122.49328
MP3	-122.50900	-122.45759	-122.50950
MP4DQ	-122.51144	-122.46030	-122.51234
CCD	-122.51213	-122.46068	-122.51284
CCD + ST4	-122.52118	-122.47310	-122.52257

Table VII-5. Barrier heights[a] and reaction energies (ΔH)[a] (in kcal mol^{-1}) calculated with the $D95V^{**}$ basis set.

	Non-solvent system		Solvated system	
Method	Ea	ΔH	Ea	ΔH
HF	53.0	-3.4	46.8	-8.6
MP2	33.6	10.7	26.3	5.5
MP3	39.1	5.4	32.3	0.3
MP4DQ	38.9	5.7	32.1	0.6
CCD	39.1	5.5	32.3	0.4
CCD + ST4	36.9	5.9	30.2	0.9

[a]values are not including zero point vibrational contributions

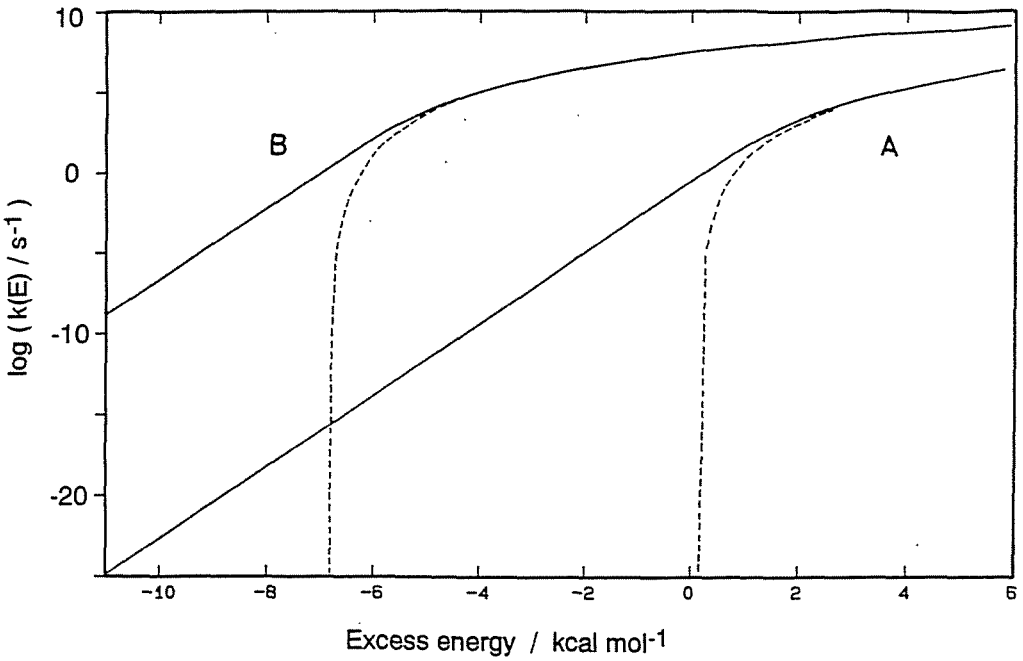

Figure VII-3. Solvation effects on the microcanonical rate constants as a function of the excess energy (E-V_0; see text). Solid and dashed lines indicate the calculated rates including the tunnel effect and classically, respectively. (A) Non-solvated system (B) Solvated system including the vibrational coupling between the reaction system and the solvent molecules.

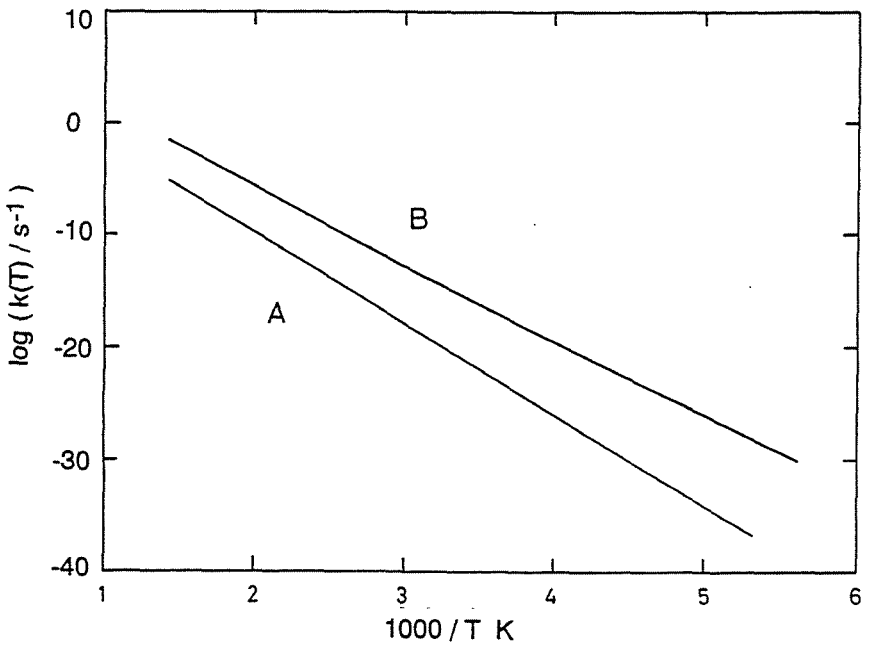

Figure. VII-4. Arrhenius plots of the thermally averaged rate constants (canonical rate constants) calculated by eq. (7.8) in text. (A) Non-solvated system (B) Solvated system

Table VII-6 The vibrational coupling effect on the microcanonical rate constants in the solvated system. A: Without the vibrational coupling, B: Allowing vibrational couplings between the reaction system ($CH_3O \rightarrow CH_2O$) and solvent molecules (10 H_2O) in the first solvation shell..

Excess energy (kcal/mol)	log (k(E) / sec^{-1})	
	A	B
-6.0	1.88	2.13
-4.0	4.88	5.02
-2.0	6.45	6.54
0.0	7.43	7.50
2.0	8.12	8.18
4.0	8.64	8.69
6.0	9.05	9.10

Table VII-7. Calculated canonical rate constants in gas and condensed phases as a function of temperature.

	log(k(T)/s^{-1})	
T/K	Gas phase	condensed phase
200	-34.90	-25.83
300	-20.65	-14.95
400	-13.86	-9.27

[a]Values include the vibrational coupling between RS and the coordinating water molecules.

the reactant keeps the irreducible representation $^2A'$ of the C_S point group until the transition state, and is broken by the Jahn-Teller effect in the product.

The fully optimized geometrical parameters, which are obtained at the HF/D95V** level, are listed in Table VII-1. The structures are essentially in accordance with the prediction from the 6-31G** level. The harmonic vibrational frequencies of the reactant, TS and the product, which are predicted theoretically, are summarized in Table VII-2. The non-scaled harmonic frequencies obtained here are each 10 % higher than the corresponding experimental values.

The total energies of the stationary points on the reaction surface are given in Table VII-3 for the non-solvated system, and in Table VII-4 for the solvated system. The geometries used for the solvated system are those obtained by optimization at the HF/D95V** level in the non-solvated system. As shown in Table VII-5, the activation energies in the solvation system are significantly affected and reduced by about 6.7 kcal/mol by the solvent effects. Based on the results concerning ΔH (= $E_{reactant}$ - $E_{product}$), we predict theoretically that this reaction occurs exothermally by about 6 kcal/mol in the gas phase. This is in good agreement with Saebo's calculation[25] and some experimental pieces of evidence.[21,32] On the other hand, ΔH is close to zero in the solution system, that is, this reaction might proceed isothermally in the condensed phase.

Figure VII-3 shows the microcanonical rate constants in the non-solvated system (A) and in the solvated system (B) which includes the vibrational couplings between the reaction system and the solvent molecules as a function of the excess energy. This result indicates that the solvent effect is significant in this reaction system, and that the rate constant is augmented by the solvation effects. The reason why the rate constant increases in the solvation system is mainly due to two different factors; i.e., the activation energy and the vibrational coupling terms. As shown in Figure VII-3, the lowering of the activation energy causes a translation of the microcanonical rate constant curve towards the low-energy region. In this case, the solvation effect on the activation energy contributes significantly to the increase of the rate constant.

In order to estimate the contribution of the vibrational coupling terms, we have made a calculation of the rate constant which does not involve the vibrational coupling. Table VII-6 reveals that this coupling effect changes the microcanonical rate constant in the tunneling region. On the other hand, the vibrational coupling effect is not so important in the high energy region where the activation energy mainly controls the reaction rate. The thermally averaged rate constants (canonical rate constants) calculated by eq.(7.8) are shown as Arrhenius plots in Figure VII-4. As expected from the comparison of the micro-canonical rate constants with and without solvents, strong solvent effects are also observed in the Arrhenius plots. Furthermore, these effects become greater in the low-temperature region.

In 1978, Iwasaki and Toriyama interpreted the formation of $\cdot CH_2OH$ radical at 77 K in polycrystalline methanol by assuming that the $CH_3O\cdot$ radical disappeared by a unimolecular process, i.e. according to reaction (7.14).[24]

To elucidate this phenomenon, we attempted to simulate the rate constant by using a usual tunneling calculation. The rate constant should be at least of the order 10^{-5} - 10^{-10} sec^{-1} at 77 K to be observed experimentally. Using the activation energy as a parameter, its value was determined so as to fit those rate constants at 77 K and the rate constant was then extrapolated to high temperature. The results of this rough calculation are given in Table VII-7. There is a large difference between the simulated and theoretical lines. This might be too large even if we consider the approximations of this calculation. On the basis of those results, we suggest that the decay of $CH_3O\cdot$ radical in a methanol matrix at low temperature might be caused by a bi-molecular process.

c. Conclusion

A simple model to estimate the rate constant in solvated systems was proposed in this section. In the model, the effects of solvation are included as the vibrational coupling between the reaction system and the solvent molecules. Although we considered ten water molecules as the surrounding solvent in the vibrational coupling calculation, it is equally possible to include more solvent molecules in the model because one does not need to obtain the force constant matrix elements for the supermolecule. In this model it is only necessary to calculate those for the reduced system.

By applying this model to the unimolecular reaction; $CH_3O\cdot \rightarrow \cdot CH_2OH$ in the condensed phase, we obtained the result that the rate constant in solvated system would be slightly increased by the effect of the vibrational coupling in the tunneling region.

B. Intramolecular hydrogen atom transfer reaction $CH_3O\cdot \rightarrow \cdot CH_2OH$ in frozen methanol.

The influence of the medium on the dynamics of a chemical reaction has been extensively studied experimentally and theoretically. As far as theoretical approaches based on the the molecular orbital theory are concerned, several models have been examined.[36] Tachibana *et. al* proposed the string model in which the solvent effects are treated as a perturbation to the intrinsic reaction coordinate (IRC) and applied it to an isomerization reaction; $H_2CO \rightarrow HCOH$ and to a hydration of CO_2; $CO_2 + H_2O \rightarrow H_2CO_3$.[36,37] Although this model is mathematically sophisticated, it seems to be difficult to extend to large reaction systems.

In the previous section, we have proposed the vibrational coupling (VC) model, which takes into account the solvent-induced shifts of the vibrational frequencies of the reaction system.[39] These shifts are caused by the vibrational couplings between the reaction system and the solvent molecules. Since a Hessian matrix is directly solved in the VC-model, one can extend the model to large reaction systems. This model becomes a good approximation if solvent molecules interact weakly with the reaction system. In the previous section, we applied this model to an isomerization reaction of the methoxy radical;

$$CH_3O\cdot \rightarrow \cdot CH_2OH \qquad (I)$$

in a water cluster composed of ten water molecules, and concluded that the solvent molecules cause an increase of the rate constants due to shifts of the vibrational frequencies and that this coupling effect on the reaction rate was most important in the tunneling region .[39]

In the present section, we have attempted to extend the VC model to the same reaction in solid methanol in order to elucidate the crystal field effects on the reaction rate. This reaction system has been investigated using ESR spectroscopy by Iwasaki and Toriyama.[23] They found on the basis of ESR spectra that the methoxy radical converted to the CH_2OH radical by annealing from 4 K to 77 K in methanol polycrystalline phase. The reaction rate of the radical conversion observed seems to be slightly faster than that extrapolated from the corresponding high temperature gas phase data[22] and significantly slower than that in methanol-water matrices.[23] This means that not only the tunnel effect, but also the medium effect, affect the reaction rate. Therefore the system is a good example to test the vibrational coupling in a crystal field environment. In this work, we have treated both effects on the isomerization reaction using the vibrational coupling model and RRKM theory. The primary aims of this study are to elucidate a role of the vibrational couplings on the reaction in frozen methanol and to provide a theoretical information on the reaction mechanism of CH_3O/CH_2OH isomerization in frozen methanol.

a. Structure of the Model Cluster

A cluster composed of eighteen methanol molecules was considered as a model of the methanol polycrystalline phase. The structure of the model cluster was constructed based on crystallographic data.[40] The model cluster obtained has a layer structure as shown in Figure VII-5. The reactant molecule, CH_3O, is replacing a methanol molecule in the lattice. A geometry of the methanol molecules around the reaction molecule is shown in Figure VII-6. Intermolecular distances between the CH_3O radical and neighbor methanol molecules were

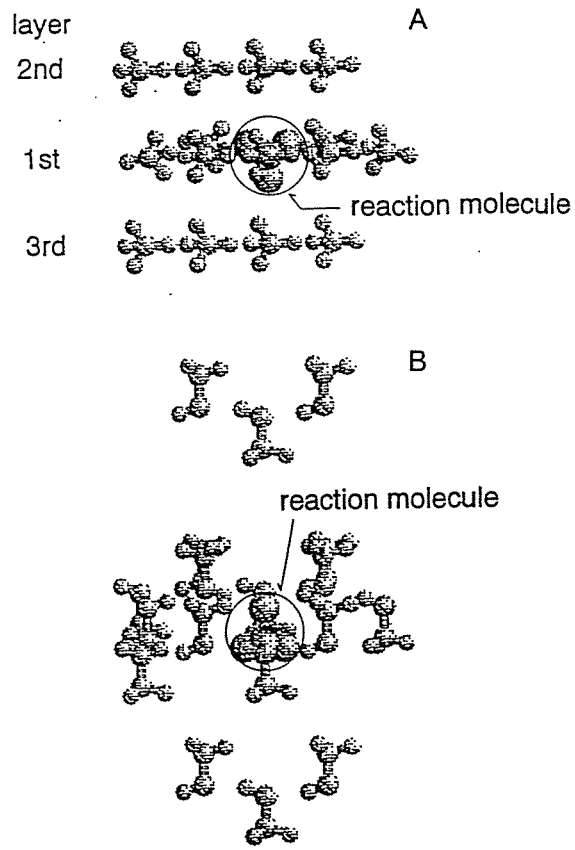

Figure VII-5. Structures of the model cluster and the position of the reaction molecule.

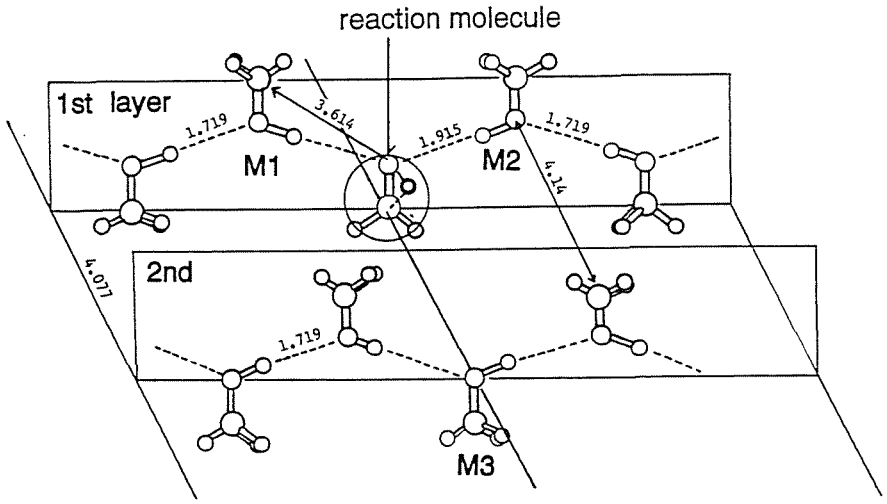

Figure VII-6. Geometry of the methanol molecules around the reaction molecule. Eight methanol molecules on the first and second layers are sketched. The M_1, M_2 and M_3 mean the methanol molecules considered in the vibrational coupling with the reactant molecule. The position of oxygen atom of the reaction molecule is fixed during the reaction.

optimized at the HF/3-21G level. The distance obtained is 1.915 A for the oxygen-hydrogen distance. The geometry of the isolated methanol molecule is optimized at the HF/3-21G level.

b. Ab-initio MO calculations

The *ab-initio* MO theory has been provided valuable information on the structure and the electronic states of the unstable radicals in matrix.[41] Hence all calculations are done at the ab-initio Hartree-Fock (HF) and post-HF (MP2, MP3 and Coupled cluster methods) levels of theory.[42] Geometries of the isolated reaction molecule at the stationary points along the reaction coordinate; reactant (RC), product molecules (PD) and the structure at the transition state (TS) were fully optimized at the HF/3-21G, HF/D95V** and MP2/3-21G levels using the UHF energy gradient method.[43]

The geometries of the reaction molecule at the RC and TS states in the model cluster were assumed to have the structures obtained in vacuo. An additional assumption is that the geometry of the methanol model cluster does not change throughout during the reaction. These approximations are usually employed to test the solvent effects on a chemical reaction[37,38,44] and effective in this case because the interaction between the reaction system and the medium molecule is comparatively small and the reaction occurs at very low temperature (4K-77K).[39] Total energies of the reaction molecule in the model cluster were calculated based on the fractional charge (FC) model [3]; a methanol molecule is described by effective point charges on each atom as shown in Table VII-8. Values of the point charge were determined by the HF/D95V** calculation for an isolated methanol molecule. Eighteen methanol molecules surrounding a reactant molecule were represented by the point charges in the energy calculations.

The continuum model[45] was employed to estimate the activation energy including the matrix effects for comparison. According to the continuum model, solvation energy for a dipole in a dielectric cavity is expressed by

$$E_{solv} = \frac{\varepsilon - 1}{2\varepsilon + 1} \cdot \frac{\mu^2}{r^3} \qquad (7.15)$$

where, ε is the dielectric permittivity (roughly 2 for methanol matrix), μ is the molecular dipole moment and r is the cavity radius. The dipole moments of the reaction molecule are calculated by the HF/D95V** level. The oxygen-hydrogen distance (1.915 A) was chosen as a cavity radius in this calculation.

Table.VII-8. Fractional charges used for the atoms in the methanol molecule. The values are calculated at the HF/D95V** level.

atom	charge
O	-0.52
C	-0.13
H(O-H)[a]	0.32
H(C-H)[b]	0.11

[a]Hydrogen in hydroxy group
[b]Hydrogen in methyl group

Table VII-9. Optimized parameters obtained at the HF/95V** and MP2/3-21G levels. Bond lengths and angles are in Angstrom and in degrees, respectively.

	HF/D95V**[a]			MP2/3-21G		
	reactant	TS	product	reactant	TS	product
r(C-H_1)	1.087	1.080	1.075	1.094	1.084	1.080
r(C-H_2)	1.087	1.080	1.079	1.094	1.084	1.086
r(C-H_3)	1.090	1.269	1.909	1.099	1.277	1.974
r(O-H)	1.986	1.188	0.944	2.044	1.214	0.990
r(C-O)	1.386	1.369	1.361	1.458	1.472	1.412
<OCH_1	111.61	117.27	113.11	111.97	117.67	112.02
<OCH_3	106.10	53.40		105.25	51.88	
<$H1CH_2$	110.61	117.12	119.28	110.55	111.96	119.30
<OCH_2	111.61	113.11	117.89	111.97	117.67	119.61
<PCH_1			72.92			77.31
<$PCOH_3$			106.01			102.20

[a]From reference 4.

c. Estimation of the vibrational frequencies in the model cluster.

In order to calculate the reaction rate constant including the medium effect, the vibrational coupling (VC) model was employed. The detailed procedure of the VC model approach is described in our previous paper.[39] This model considers the perturbations to the vibrational frequencies in the RC and TS states caused by the medium, as schematically shown in Figure VII-7. Although the modes ω_i and ω_j are orthogonal to each other in the gas phase, these modes can be coupled to each other through the mode of a solvent molecule in the environment of the medium. If one can estimate the modes ω_i' and ω_j' (or $\Delta\omega_i$ and $\Delta\omega_j$), the rate constant including medium effects is given on the basis of the unimolecular rate theory.[46]

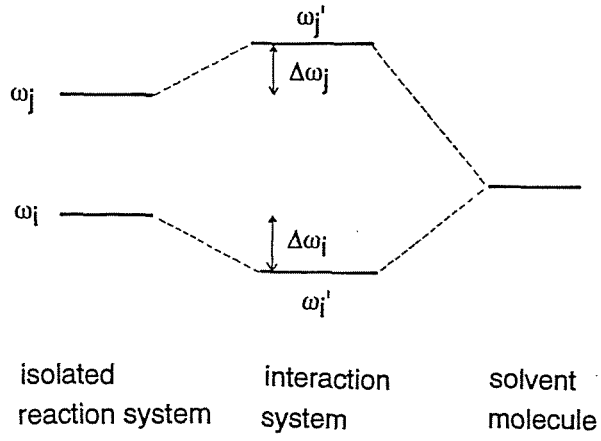

Figure VII-7. Schematic representation of the vibrational coupling between an isolated reaction molecule and a solvent molecule.

In the VC model, a Hessian matrix for the interaction system can be expressed by

$$K^S = (R_{ij},\ S_{rs},\ I_{rs}) \qquad (7.16)$$

where R_{ij} is the Hessian matrix element of the isolated reaction system (i.e., without any medium molecules) of dimension 3Nx3N (N is the number of atoms in a solute molecule), S_{ij} is the matrix of a solvent molecule (the dimension of the matrix is 18x18 in case of a methanol molecule), and I_{rs} is a matrix constructed of a cross term between the reaction system and the s-th solvent molecule. The Hessian matrix (7.16) is built from the matrices constructed for two-body system. By diagonalizing the Hessian matrix,

$$L = U^t M^{-1/2} K^S M^{-1/2} U \qquad (7.17)$$

the perturbed vibrational modes and frequencies can be obtained. The rate constant was calculated using Miller's theory (RRKM model including the tunnel effects)[13,46] on assuming one-dimensional symmetric Eckart potential.[16] The VC between the reaction molecule and

Table VII-10. Total energies(in a.u.) in vacuo and in the model cluster at the stationary points on the potential energy surface of CH_3O/CH_2OH rearrangement reaction. The basis set used is the Huzinaga-Dunning DZP ($D95V^{**}$) basis set.

	in vacuo[a]			in model cluster		
method	reactant	TS	product	reactant	TS	product
HF	-114.45252	-114.36803	-114.44716	-116.510304	-116.425323	-116.476985
MP2	-114.73021	-114.67668	-114.74719	-116.788404	-116.734234	-116.775368
MP3	-114.75467	-114.69240	-114.76331	-116.812560	-116.749550	-116.791798
MP4DQ	-114.75711	-114.69507	-114.76612	-116.815006	-116.752296	-116.794695
CCD	-114.75780	-114.69550	-114.76660	-116.815699	-116.752708	-116.795208
CCD+ST4	-114.76684	-114.70801	-114.77618	-116.824821	-116.764807	-116.804474

[a]From reference 4.

nearest four methanol molecules (three methanol molecules denoted by M_1, M_2 and M_3 on the first and second layers and a methanol molecule on the third layer) was included in the calculation. With this approximation, the dimension of the Hessian matrix to solve becomes 87x87 in this calculation.

d. Reaction in gas phase

Optimized geometrical parameters at the stationary points along the CH_3O/CH_2OH isomerization reaction coordinate are given in Table VII-9. Both levels of calculation gave a similar geometry

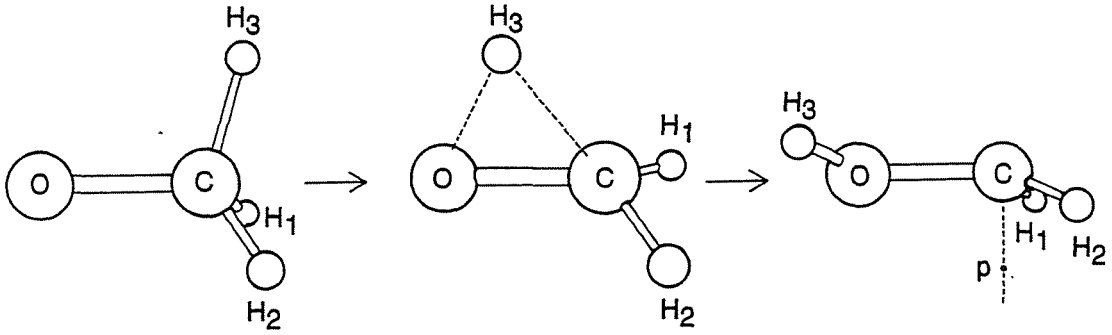

Reactant TS Product

The transition state structure has a triangular form (i.e., a hydrogen atom is located over the middle of the C-O bond). The reaction molecule keeps the *Cs* symmetry up to TS, whereas one changes to C1 symmetry in the product region. These features are essentially similar to that obtained by HF/D95V** and HF/6-31G** calculations.[25,39] Total energies calculated at several levels are summarized in Table VII-10. According to the most sophisticated calculation (CCDST4/D95V**), the activation energy including zero point vibrational contribution (E_{ZPE}=-4.04 kcal/mol) is calculated to be 32.88 kcal/mol. This activation energy is slightly lower than in the previous theoretical work (36 kcal/mol).[25]

e. Reaction in the model cluster

Total energies for the RC and TS in the model cluster are given in Table VII-10. The activation energies are listed in Table VII-11. The activation energy including the correction for zero point energy (E_{ZPE}=-4.77 kcal/mol) in the model cluster is calculated to be 32.91 kcal/mol, similar to that in vacuo (32.88 kcal/mol), indicating that the crystal field does not critically affect the activation energy.

Table VII-11. Barrier heights[a] (in kcal/mol) calculated with the D95V** basis set.

Method	In vacuo	in model cluster
HF	53.0	53.3
MP2	33.6	34.0
MP3	39.1	39.5
MP4DQ	38.1	39.4
CCD	39.1	39.5
CCD+ST4	36.92	37.66

[a]Values are not including zero point vibrational contributions.

f. Reaction in continuum medium

The solvation energies for the RC, TS and PD states in frozen methanol were calculated based on the continuum model. The results are shown in Table VII-12. Dipole moments of the reaction molecule at the RC and TS were calculated to be 2.06 and 2.13 Debye, respectively. The solvation energies of the TS estimated by eq.(7.15) was slightly larger than that of the RC (1.86 vs. 1.74 kcal/mol). Therefore, the activation energy perturbed by the continuum medium is corrected to be 32.76 kcal/mol.

Table VII-12. Dipole moments obtained at the HF/D95V** level (in Debye) and solvation energies E_{solv} in kcal/mol) calculated based on the continuum model.

	stationary point		
	RC	TS	PD
Dipole moment	2.06	2.13	1.66
E_{solv}	1.74	1.86	1.12

g. Vibrational frequencies

Harmonic vibrational frequencies at the stationary points of the reaction both in vacuo and in the model cluster were calculated at the HF/3-21G level, as summarized in Table VII-13. It should be noted that the low frequency modes shift to higher energy due to the medium effects. The motion of the low frequency modes, which mainly consist of the CH_3 rocking mode or the

C=O stretching mode, are restricted by the medium molecules, in the crystalline phase. This feature, obtained theoretically, is in good agreement with experimental results.[47] The negative frequency corresponding to the direction of the reaction coordinate at TS was hardly affected by the vibrational coupling with the medium molecules. The other frequencies of the reactant molecule in the model cluster have positive values as well as in vacuo. These results imply that the reaction coordinate is stabilized even in the model cluster.

Table VII-13. Theoretical vibrational frequencies(cm^{-1}) at the stationary points (reactant; RS and transition state; TS) of the $CH_3O\cdot/\cdot CH_2OH$ rearrangement reaction in vacuo and in the model cluster. Values are calculated at the HF/3-21G level. Zero point energies (ZPE) are in kcal/mol.

		in vacuo		in crystal phase	
sym.	assingment	RC	TS	RC	TS
a'	CH_3 str.	3248.1	3296.2	3249.7	3303.8
	CH_3 str.	3185.9	2506.4 **i**	3183.9	2506.1i
	CH_3 deform	1688.8	2141.4	1700.7	2177.8
	CH_3 deform	1585.8	1195.9	1581.2	1206.0
	CH_3 rock	1006.7	1011.7	1182.8	1036.1
	C=O str.	759.5	897.5	1015.0	944.8
a"	CH_3 str.	3268.5	3422.8	3292.6	3435.0
	CH_3 deform	1633.6	1616.7	1656.1	1609.6
	CH_3 rock	1137.1	1095.1	1276.0	1101.0
	ZPE	25.04	20.98	25.93	21.18

h. Reaction rates

Using these data obtained by MO calculations, we attempt to calculate the rate constants for the CH_3O/CH_2OH isomerization reaction in vacuo and in the model cluster. All parameters used in the rate constant calculation are listed in Table VII-14. The imaginary frequencies and the activation energies corrected with zero-point energies, listed in Table VII-14, are corresponding to the fitting parameters of the Eckart potential. The microcanonical rate constants calculated on the basis of the RRKM theory and VC-model are shown in Figure VII-8 as a function of total energy. The reaction in the model cluster (solid line A) is slightly faster in all energy regions than that in vacuo (solid line B). The difference between the reaction rates became larger in the higher energy region (> 33 kcal/mol).

Table VII-14. Parameters used in the RRKM rate calculations. A ; frequency factor in s^{-1}, ω; imaginary frequency at the TS in cm^{-1}, Ea; activation energy in kcal/mol, ZPE; zero-point energy in kcal/mol.

	in vacuo	in model cluster
A	1.32×10^{13}	2.15×10^{13}
ω	2506.4 i	2506.1 i
Ea (CCDST4/D95V**)	36.92	37.66
ΔZPE(HF/3-21G)	-4.04	-4.77
Ea + ΔZPE	32.88	32.89

In order to estimate the contribution of the tunnel effect in the reaction rate, the classical rate constant in the model cluster was calculated and compared with the rate including the tunnel effect (line A). The classical rate obtained are plotted in Figure VII-8 for line C. The difference between the rates (solid lines A and C) corresponds to the contribution of the quantum mechanical tunnel effect in the reaction. Although the difference is negligibly small in high energy region, one becomes significantly large below 34 kcal/mol. This result indicates that the tunnel effect dominates largely the reaction rate in the present system. The reaction rate calculated based on the continuum model are plotted by a dashed line in Figure VII-8. In this calculation, the activation energy corrected by the solvation energies in Table VII-12 was used together with the VC model. The reaction rate obtained by the VC model shifts to the faster rate region due to the continuum medium effect. This result implies that the continuum medium effect of the methanol matrix slightly promotes the reaction rate on the $CH_3O\cdot/\cdot CH_2OH$ isomerization.

Arrhenius plots for the reaction rates in the model cluster (line A) and in vacuo (dashed line B), shown in Figure VII-9, suggest that the reaction in the model cluster is slightly favored at all temperature range, although the difference is comparatively small. The temperature dependent reaction rate in a water cluster[39] is plotted in Figure VII-9 (line C) for comparison. It is clearly seen that the reaction rate in the water cluster is significantly faster than in the methanol cluster. This can be explained by the difference of the activation energies; these values are 26.82 kcal/mol in the water cluster and 32.89 kcal/mol in the methanol cluster, respectively. The former energy is lower by 6.06 kcal/mol than that in vacuo, which reflects the large electrostatic effects in the water cluster. These features are in good agreement with experimental one.[23]

i. Conclusion

In the present section, we have investigated the vibrational coupling effects on the CH_3O/CH_2OH isomerization reaction in a methanol polycrystalline phase. It is found that the effect slightly promotes the reaction rate in the solid phase and that the VC effect in the frozen methanol is significantly smaller than that in the water cluster.

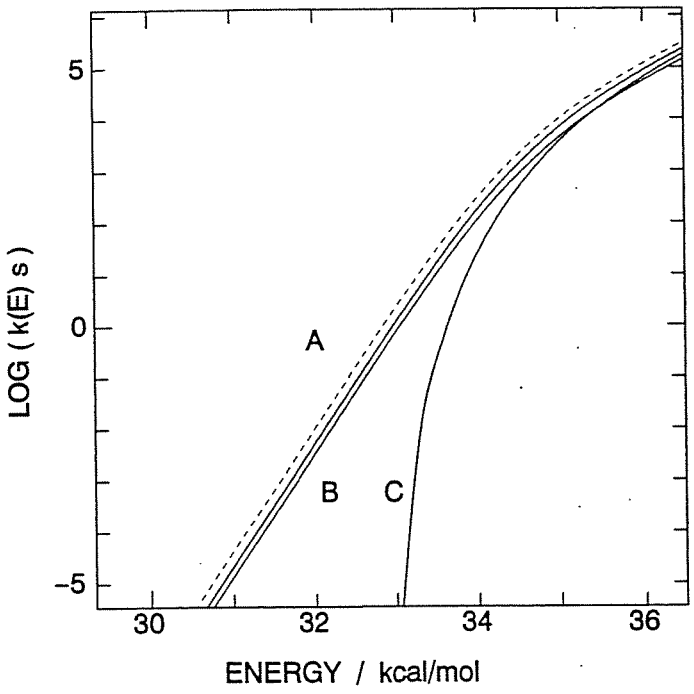

Figure VII-8. Microcanonical rate constants of the $CH_3O\cdot/\cdot CH_2OH$ isomerization reaction as a function of the total energy. (A) Rate constant in the methanol cluster calculated based on the VC model, (B) rate constant in vacuo, (C) Classical rate constant (i.e, the rate does not take into account the tunnel effect) in the model cluster calculated based on the VC effect. Dashed line indicates the reaction rate calculated based on the VC model plus the continuum model.

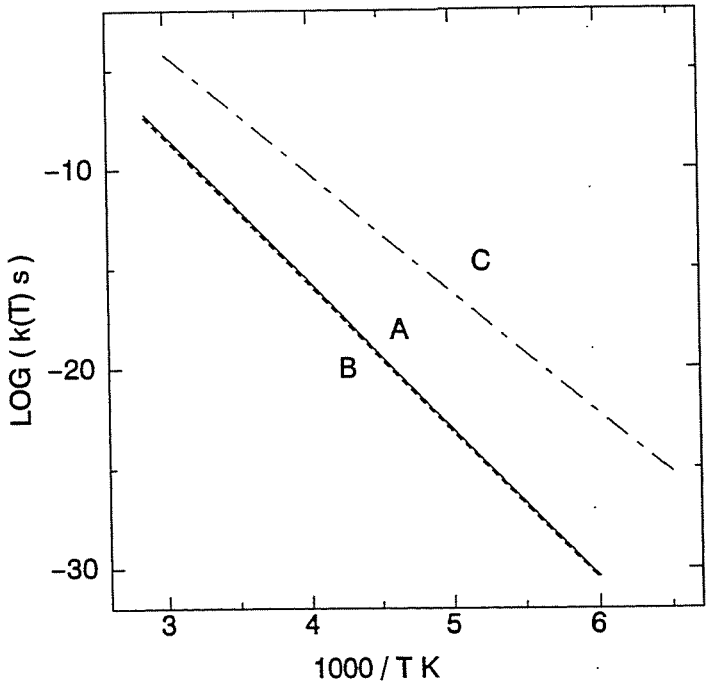

Figure VII-9. Arrhenius plots of the $CH_3O\cdot/\cdot CH_2OH$ isomerization reaction. (A) reaction rate constant in the methanol cluster, (B) in vacuo, (C) in a water cluster.

References

1. See, for instance: Reichardt, C. *Solvent effects in organic chemistry*; Verlag Chemie, Weinheim, NY, 1979.
   Ingold, C.K., Ed., *Structure and Mechanism in Organic Chemistry*, 2; Cornell University Press, Ithaca, NY, 1969.
2. Cukier, R. I.; Morillo, M. *J. Chem. Phys.* **1989**, *91,* 857.
3. Noell, J. O.; Morokuma, K. *Chem. Phys. Lett.* **1975**, *36*, 465.
   Noell, J. O.; Morokuma, K. *J. Phys. Chem.* **1977**, *81*, 2295.
4. Taurian, O. E.; Lunell, S. *J. Phys. Chem.* **1987**, *91*, 2249.
5. Newton, M. D. *J. Chem. Phys.* **1973**, *58*, 5833.
   Newton, M. D. *J. Phys. Chem.* **1975**, *79*, 2795.
6. Clark, T. *Faraday Discuss. Chem. Soc.* **1984**, *78*, 210.
7. Noell, J. O.; Morokuma, K. *J. Phys. Chem.* **1976**, *80*, 2675.
8. McCreery, J. H.; Christoffersen, R. E.; Hall, G. G. *J. Am. Chem. Soc.* **1976**, *98*, 7191.
   Rinaldi, D.; Ruiz-Lopez, M. F.; Rivail, J. L. *J. Chem. Phys.* **1983,** 78, 834.
   Pascual-Ahuir, J. L.; Tomasi, J.; Bonaccorsi, R. *J. Comput. Chem.* **1987**, *8*, 778.
9. Karelson,M. M.; Katritzky, A. R.; Zerner, M. C. *Int. J. Quantum. Chem. symp.* **1986**, *20*, 521.
10. Steinke, T.; Hänsele, E.; Clark, T. *J. Am. Chem. Soc.* **1989**, *111,* 9107.
11. See, for instance: Johnston, H. S. *Gas Phase Reaction Rate Theory*
    Ronald Press, NY, 1966, p 37; Miller, W. H. *Acc. Chem. Res.*, **1976**, *9*, 306.
    Forst, W. *Theory of Unimolecular Reactions*, Academic Press, NY, 1973.
12. Gray, S. K.; Miller, W. H.; Yamaguchi, Y.; Schaefer, H. F. *J. Am. Chem. Soc.* **1981**, *103*, 1900.
13. Miller, W. H. *J. Am. Chem. Soc.*, **1979**, *101,* 6810.
14. Robinson, P. J.; Holbrook, K.A. *Unimolecular Reactions*, Wiley, NY, 1972, p 131.
15. Miller, W. H. *J. Chem. Phys.* **1982**, *76*, 4904.
16. Eckart, C. *Phys. Rev.*, **1930**, *35*, 1303.
17. See, for instance: Pulay, P. *Modern Theoretical Chemistry*; Shaefer, H. F., Ed.; Plenum, NY, 1977, Vol. 4, pp 153-185.
18. See, for instance: Fish, A. *Oxidation of Organic Compounds,* Advances in Chemistry Series 76. Gould, R. F. Ed. American Chemical Soc., Washington, D. C., 1968, Vol. 1.
19. Pshezhetskii, S. Y.; Kotov, A. G.; Millinchuk, V. K.; Robinskii, V. A.; Tupikov, V.I. *EPR of Free Radicals in Radiation Chemistry*, Wiley, NY, 1974, pp 189-202.

20. Radford, H. E. *Chem. Phys. Lett.* **1980**, *71*, 195.
Batt, L.; Robinson, G. N. Intern. *J. Chem. Kinetics* **1979**, *11*, 1045.
21. Haney, M. A.; Franklin, J. L. *Trans. Faraday Soc.*, **1969**, *65* ,1794.
22. Batt, L.; Burrows, J. P.; Robinson, G. N. *Chem. Phys. Lett.* **1981**, *78*, 467.
23. Iwasaki, M.; Toriyama, K. *J. Am. Chem. Soc.* **1978**, *100*, 1964.
24. Iwasaki, M.; Toriyama, K. *J. Chem. Phys.* **1987**, *86*, 5970.
25. Saebo, S.; Radom, Leo; Shaefer, H. F. *J. Chem. Phys.* **1983**, *78*, 845.
26. Miller, W. H.; Handy, N. C.; Adams, J. E. *J. Chem. Phys.* **1980**, *72*, 99.
27. Colwell, S. M.; Handy, N. C. *J. Chem. Phys.* **1985**, *82*, 1281.
28. Dunning, T. H.; Hay, P. J. *Modern Theoretical Chemistry,* Plenum, NY, 1976.
Huzinaga, S. *J. Chem. Phys.* **1965**, *42*, 1293.
29. Schegel, H. B. *J. Comp. Chem.* **1982**, *3*, 214.
30. Bartlett, R. J. *J. Phys. Chem.* **1989**, *93*, 1697.
Lee, Y. S.; Kucharski, S. A.; Bartlett, R. J. *J. Chem. Phys.* **1984**, *81*, 5906.
Raghavachari, K. *J. Chem. Phys.* **1985**, *82*, 4607.
31. Krishman, R.; Frisch, M. J.; Pople, J. A. *J. Chem. Phys.* **1980**, *72*, 4244.
32. Weast, R. C. *Handbook of Physics and Chemistry* , 59th ed. Chemical Rubber, Cleveland, 1978, p. F245.
33. (a) Inoue, G.; Akimoto, H.; and Okuda, M. *Chem. Phys. Lett.* **1979**, *63*, 213.
and *J. Chem. Phys.* **1980**, *72*, 1769.
34. Jacox, M.E. *Chem. Phys.* **1981**, *59*, 213.
35. Engelking, P. C.; Ellison, B. G. and Lineberger, W. C., *J. Chem. Phys.* **1978**, *69*, 1826.
36. (a) Karlström, G., *J. Phys. Chem.*, **1988**, *92*, 1318.
(b) Alimi, R.; Gerber, R. B., *Phys. Rev. Lett.* **1990**, *64*, 1453.
37. Tachibana, A.; Koizumi, M.; Murashima, M.; Yamabe, T., *Theor. Chim. Acta.* **1989**, *75*, 401.
38. Tachibana, A.; Fueno, H.; Tanaka, E.; Murashima, M.; Koizumi, K.; Yamabe, T., *Int. J. Quantum. Chem.* **1991**, *39*, 561.
39. Tachikawa, H.;. Lunell, S.; Törnkvist, C.; Lund, A.,. Int. J. Quantum. Chem. **1992**, *43*, 449.
40. Tauer, K.J.; Lipscomb, W.N., Acta Crystallogr. **1952**, *5*, 606., (C-O bond distance 1.44 A, O··O hydrogen bond 2.68 A, C-O··O angle 108°, CH_3··CH_3 3.64 A, CH_3··O 4.1 A, O··O 4.0 A).
41. (a) Tachikawa, H.; Shiotani, M.; Ohta, K., *J. Phys. Chem.*, **1992** *96*, 165.
(b) Tachikawa, H.; Ogasawara, M., *J. Phys. Chem.* **1990**, *94*, 1746.

(c) Tachikawa, H.; Ichikawa, T.;. Yoshida, Y., *J. Am. Chem. Soc.*, **1990**, *112*, 982.

(d) Tachikawa, H.; Murai, H.; Yoshida, H., *J. Chem. Soc. Faraday Trans.* **1993**, *89*, 2369.

(e) Tachikawa, H.; Lund, A.; Ogasawara, M., *Can. J. Chem.* **1993**, *71*, 118.

42. Frish, M.J; Binkley, J.S; Schlegel, H.B; Raghavachari, K; Melius, C.F; Martin, R.L; Stewart, J.J.P; Bobrowicz, F.W; Rohlfing, C.M; Kahn, L.R; DeFrees, D.J; Seeger, R; Whiteside, R.A; Fox, D.J; Fleuder, E.M; Topiol, S; Pople, J.A., Ab-initio molecular orbital calculation program GAUSSIAN86, Carnegie-Mellon Quantum Chemistry Publishing Unit; Pittsburgh, PA.

43. (a) Pople, J. A.; Krishnan, R.; Schlegel, H. B.; Binkley, J.S., *Int. J. Quantum. Chem.*, **1978**, *14*, 545.

(b) Chiles, R. A.; Dykstra, C.E., *Chem. Phys. Lett.* **1981**, *80*, 69.

(c) Raghavachari, K., *J. Chem. Phys.* **1985**, *82,* 4607.

(d) Hariharan, P. C.; Pople, J. A., *Theor. Chim. Acta.*, **1973**, *28*, 213.

(e) Dunning, T. H.; Hay, P. J., *Modern Theoretical Chemistry*, Plenum, New York, 1976.

(f) Huzinaga, S., *J. Chem. Phys.* **1965**, *42*, 1293.

(g) Huzinaga, S., Physical science data, Gaussian basis sets., Huzinaga, S., (Ed) Elsevier: Amsterdam, **1984,** Vol. 16.

(h) Tatewaki, H.; Huzinaga, S., *J. Comput. Chem.* **1980**, *1*, 205.

(i) Pulay, P., in *Modern Theoretical Chemistry,* H.F.Schaefer III, Ed. (Plenum, New York) 1977, vol.4, Chap 4.

44. (a) van der Zwan, G.; Hynes, J. T., *J. Chem. Phys.* **1983**, *78*, 4174.

(b) Lee, M.S.; Gippert, G.P., Soman, K.V.; Case, D.A.; Wright,, P.E., *Science* , **1989**, *245*, 635.

45. Salem, L.; Electron in Chemical Reactions: First Principles, John Wiley, New York, 1982, Chap. 8.

46. (a) Miller, W.H., *J. Am. Chem. Soc.* **1979**, *101*, 6810.

(b) Miller, W.H., *J. Chem. Phys.* **1982**, *76*, 4904.

(c) Miller, W.H., *Tunneling,* J.Jortner and B.Pullman (Eds), D.Reidel, Boston, 1986, p91.

47. Falk, M.; Whalley, E., *J. Chem. Phys.* **1961**, *34*, 1554.

CHAPTER VIII

INTERMOLECULAR HYDROGEN ATOM TRANSFER REACTION IN CONDENSED PHASE: $CH_3O + CH_3OH \rightarrow CH_3OH + CH_2OH$ REACTION

1. Introduction

Unimolecular isomerization of radical produced at low temperatures in the solid phase has been topical in radiation chemistry.[1] Iwasaki and Toriyama found, by using ESR spectroscopy, that methoxy radical ($CH_3O\cdot$), produced by γ-irradiation of frozen methanol at 4.2 K, converts to the hydroxymethyl radical ($\cdot CH_2OH$) by thermal annealing from 4.2 K to 77 K.[2,3] Two reaction channels,

$$CH_3O\cdot \rightarrow \cdot CH_2OH \qquad \text{(I)}$$

and

$$CH_3O\cdot + CH_3OH \rightarrow \cdot CH_2OH + CH_3OH \qquad \text{(II)},$$

have been considered as the conversion pathway of the CH_3O radical in frozen methanol. The reaction channels, I and II, are the intra- and inter-molecular hydrogen atom transfer reactions, respectively. Both channels lead to a same product ($\cdot CH_2OH$), so that it is difficult to determine experimentally the predominant reaction channel. Hence the reaction mechanism of the isomerization of $CH_3O\cdot$ in frozen methanol has been controversial.[1-3]

In this chapter, we investigated theoretically channels I and II by using the *ab-initio* MO method and the RRKM theory. The purposes of the present study are: *i)* to determine a dominant reaction channel of $CH_3O\cdot$ at low temperature and *ii)* to provide theoretical information on the above radical isomerization mechanism.

2. Method

The *Ab-initio* MO method and the RRKM rate theory have provided valuable information on the reaction mechanism of unstable radicals in matrices.[4] Hence we have used the *ab-initio* MO method together with the RRKM theory in the present study.

The *ab-initio* MO calculations were performed at the Hartree-Fock (HF) and post-HF (MP2) levels of theory.[5] Geometries at the stationary points along the reaction coordinate; reactant (RC), product molecules (PD) and the structure at the transition state (TS) were fully optimized at the HF/STO-3G, HF/3-21G and HF/6-31G* levels[5] using the UHF energy gradient method.[6] For channel I, previously reported geometries were also employed.[7] By

using the optimized geometries, single-point calculations were performed at the MP2/6-31G* level. As open-shell doublets, the expectation value of the spin operator $<S^2>$ should be 0.75; in the UHF calculations presented here this value did not exceed 0.7739.

The rate constant was calculated based on the RRKM theory including the tunnel effects[7,8] on assuming one-dimensional Eckart potential.[9] Frequency factors and imaginary frequencies for both channels were calculated at the HF/STO-3G level.

The medium effect on the activation energy of the reactions was estimated from the continuum model.[10] According to the continuum model, the solvation energy of a dipole moment in a cavity is expressed by

$$E_{solv} = \frac{\varepsilon - 1}{2\varepsilon + 1} \cdot \frac{\mu^2}{r^3} \qquad (8.1)$$

where ε is dielectric constant (approximately 2.0 in case of a methanol matrix), μ is dipole moment of the molecule and r is cavity radius. The cavity radiuses for the channels I and II, estimated from van der Waals radii, are 4 a.u and 8 a.u., respectively. Activation energy corrected by the solvation energy is expressed by

$$(E_a)_{solv} = (E_a)_{vacuo} + (E_{solv})_{TS} - (E_{solv})_{RC} \qquad (8.2)$$

where $(E_{solv})_{TS}$ and $(E_{solv})_{RC}$ are solvation energies of the reaction molecule at TS and RC states, respectively, and $(E_a)_{vacuo}$ is an activation energy without solvent.

3. Results

A. Energy diagrams of the reaction

The optimized geometrical parameters for the reactants, products, and stable intermediate are given in Tables VIII-1 for channel I and VIII-2 for channel II, respectively. The geometrical parameters defined are shown below.

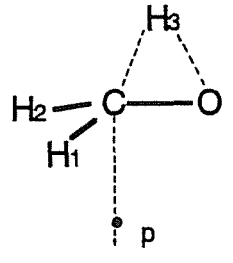

Reaction Channel I

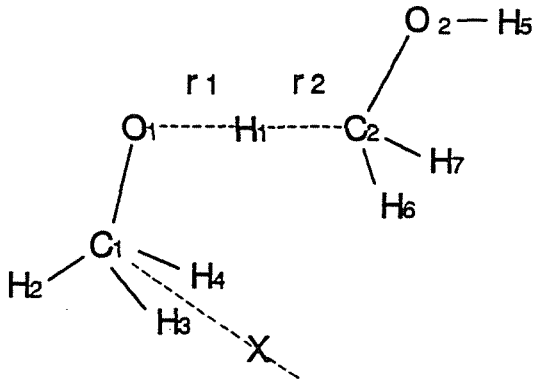

Reaction Channel II

Table VIII-1. Optimized geometries for the reaction channel I calculated at the HF/6-31G* level. Values are in A and degrees.

	RC	TS	PD
r(C-O)	1.3824	1.3673	1.3586
r(C-H_1)	1.0855	1.0781	1.0781
r(C-H_2)	1.0855	1.0781	1.0730
r(C-H_3)	1.0878	1.2777	
r(O-H)			0.9464
∠OCH_1	111.60	117.21	117.68
∠OCH_2	111.60	117.21	112.72
∠OCH_3	106.11	53.17	110.24
∠$PCOH_1$	62.08	74.99	64.24
∠$PCOH_3$	180.0	180.0	102.2

Table VIII-2. Optimized geometries for the complex and the TS-II. Values are in A and degrees.

	HF/STO-3G		HF/3-21G		HF/6-31G*	
	complex	TS-II	complex	TS-II	complex	TS-II
r(H_1-O_1)	2.4834	1.1047	2.3986	1.1659	2.8722	1.1845
r(H_1-C_2)	1.0917	1.4334	1.0768	1.3662	1.0801	1.3254
r(C_1-O_1)	1.4405	1.4361	1.4451	1.4490	1.3826	1.3956
r(C_1-H_2)	1.0927	1.0922	1.0847	1.0817	1.0877	1.0844
r(C_1-H_3)	1.0936	1.0945	1.0809	1.0837	1.0854	1.0870
∠$O_1C_1H_2$	107.6	107.3	105.9	105.5	106.0	106.2
∠$O_1C_1H_3$	111.5	112.5	111.0	112.3	111.5	112.4
∠$H_2C_1O_1H_3$	118.9	118.7	118.2	118.1	117.9	118.2
∠$H_1O_1C_1$	180.0	103.7	180.0	106.8	180.0	106.7
r(C_2-O_2)	1.4333	1.4139	1.4439	1.4127	1.4014	1.3748
r(O_2-H_5)	0.9913	0.9933	0.9658	0.9683	0.9462	0.9487
r(C_2-H_6)	1.0950	1.0944	1.0860	1.0806	1.0879	1.0836
∠$H_1C_2O_2$	107.8	104.4	106.7	103.3	107.5	104.6
∠$C_2O_2H_5$	103.8	104.5	110.1	111.6	109.3	110.2
∠$O_2C_2H_6$	112.2	115.4	111.9	115.3	111.9	114.7
∠$H_6C_2O_2H_1$	119.0	112.9	119.0	112.0	119.0	113.2

The geometries for channel I, calculated at the HF/6-31G* level are in good agreement with previously reported values.[7,11] Three independent calculations for channel II gave a similar geometry. Total energies for both channels are listed in Table VIII-3. Based on the results derived from the most sophisticated calculation (MP2/631G*//HF/6-31G*), the energy diagrams of the reactions are illustrated in Fugure VIII-1. The activation energy obtained for channel I is 34.8 kcal/mol and is three times larger than that for channel II (12.6 kcal/mol). This result indicates that reaction channel II is energetically favored over channel I. The reactions are exothermic by 8.8 kcal/mol.

In the initial step for channel II, it is found that a weakly bound complex of $CH_3O\cdot$ radical with CH_3OH molecule is formed. The stabilization energy of the complex is 2.1 kcal/mol with respect to the isolated molecules. The intermolecular distance in the complex, r_1, is calculated to be 2.8722 A. The distance r_1 becomes shorter by 1.1845 A at the TS. The value of r_1/r_2 obtained as 0.893 at the TS implies that the reaction has a late barrier.

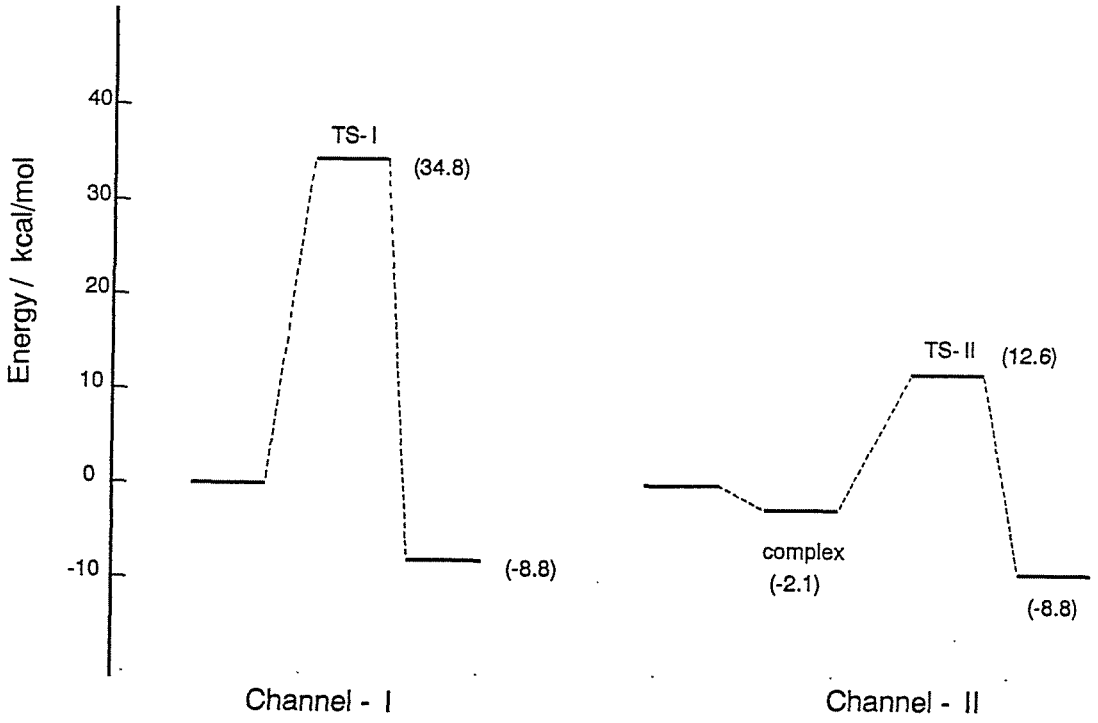

Figure VIII-1. Energy diagrams for the radical isomerization $CH_3O\cdot/\cdot CH_2OH$ calculated at the MP2/6-31G*//HF/6-31G* level. Channels I and II are the intra- and intermolecular hydrogen transfer reactions, respectively.

Table VIII-3. Total energies (au) and relative energies (in parentheses, kcal/mol)

channel	species	HF/3-21G //HF/3-21G	HF/6-31G* //HF/6-31G*	MP2/6-31G* //HF/6-31G*	$< S^2 >^a$
I	CH_3O	-113.79195(0.0)	-114.42075(0.0)	-114.70967(0.0)	0.7513
	TS-I	-113.69365(61.7)	-114.33059(56.6)	-114.65421(34.8)	0.7739
	CH_2OH	-113.76950(14.1)	-114.40876(7.5)	-114.72369(-8.8)	0.7531
II	CH_3O+CH_3OH	-228.18979(0.0)	-229.45617(0.0)	-230.03063(0.0)	0.7513
	complex	-228.19324(-2.2)	-229.45682(-0.4)	-230.03390(-2.1)	0.7514
	TS-II	-228.13495(34.4)	-229.39616(37.7)	-230.01055(12.6)	0.7664
	CH_2OH+CH_3OH	-228.16736(14.1)	-229.44417(7.5)	-230.06862(-8.8)	0.7513

[a]MP2/6-31G*//HF/6-31G* value

Table VIII-4. Parameters used for the RRKM rate calculations for the reaction channels I and II. V_0 is classical barrier hight, ω_i is imaginary frequency, A frequency factor, ΔZPE the difference of zero-point energies beteween the RC and TS states and s is number of degree of freedom.

	I	II
V_0(MP2/6-31G*), kcal/mol	34.8	12.6
ω_i (HF/STO-3G), cm^{-1}	2979.4	2765.5
A (HF/STO-3G), s^{-1}	1.53×10^{13}	8.12×10^{9}
ΔZPE(HF/STO-3G), kcal/mol	-4.68	-3.59
$V_0+\Delta$ZPE,kcal/mol	30.07	10.73
s	9	27

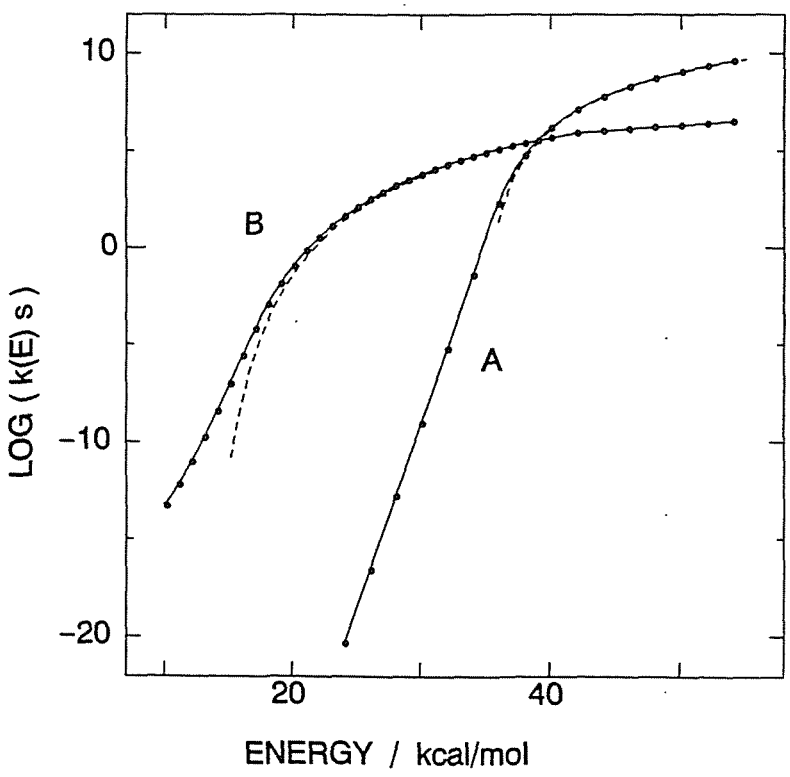

Figure VIII-2. RRKM reaction rate constants for channel I (line A) and for channel II (line B). Dashed line indicates the classical reaction rate for reaction channel II.

B. Rate constant calculations

The RRKM parameters used for the rate constant calculations are listed in Table VIII-4. Frequency factors and imaginary frequencies are obtained at the HF/STO-3G level. The imaginary frequency for channel-II (2765.5*i*) is slightly smaller than that for channel I (2979.4*i*). This means that the tunneling probability for channel I is larger than that for channel II if two channels have a same barrier height.

Figure VIII-2 shows the RRKM reaction rates for both channels calculated as a function of energy. The reaction rate for channel II is significantly faster at low energy region than that for channel I due to the lower barrier-height of channel II. At high energy region above 1.7 eV, reaction channel I becomes faster than channel II due to the large frequency factor of channel I.

The classical rate constant (i.e. without tunneling) for channel II is given by a dashed line in Figure VIII-2. The difference between the quantum and the classical values is quite large at low energy region (E<15 kcal/mol). This result indicates that the tunnel effect on the reaction rate plays an important role in reaction channel II at low temperatures.

C. Continuum medium effect on the reaction rate

In order to estimate solvent effects on the reaction rate, the solvation energies for the RC and the TS are calculated by using eqs.(8.1) and (8.2). Dipole moments and solvation energies obtained at the HF/6-31G* level are listed in Table VIII-5. The calculated dipole moments for channel I gave a similar value at the TS and the RC (2.0003 vs. 2.0602 Debye), whereas the one for channel II at the TS (3.6005 Debye) was remarkably larger than that for the RC (1.6981 Debye). The estimated solvation energies for channel II are, however, negligibly small due to a large cavity radius (8 a.u).

Table VIII-5. Dipole moments (in Debye) and solvation energies (E_{solv}, in kcal/mol) calculated at the HF/6-31G* level.

	I		II	
	RC	TS	RC	TS
Dipole moment	2.0003	2.0602	1.6981	3.6005
r, a.u.	4.00			8.00
E_{solv}	1.25	1.288	0.109	0.492

The corrected activation energies are estimated to be 30.07 kcal/mol for channel I and 10.73 kcal/mol for channel II. By using these activation energies, the reaction rates for both channels are calculated. As shown in Table VIII-6, the reaction rates for both channels shift slightly to faster rates region due to solvation effects. These results indicate that the solvation effect slightly accelerates the reaction rates in frozen methanol.

Table VIII-6. Solvation effects on the reaction rates.

	log (k(E) s)			
	I		II	
energy kcal/mol	in vacuo	in cavity	in vacuo	in cavity
10	-48.99	-48.79	-12.15	-11.12
15	-33.97	-33.79	-3.97	-3.16
20	-21.22	-21.05	0.99	1.44
25	-9.94	-9.78	3.37	3.67
30	0.30	0.44	4.74	4.96
35	6.40	6.45	5.63	5.81
40	8.34	8.36	6.26	6.40

4. Discussion

In the present work, the isomerization reactions, $CH_3O\cdot \rightarrow \cdot CH_2OH$ in frozen methanol, have been investigated by the *ab-initio* MO method and the RRKM theory. As the isomerization pathways, two reaction channels are considered: one is the intramolecular hydrogen transfer reaction, $CH_3O \rightarrow CH_2OH$ (channel I), the other is the hydrogen abstraction from a matrix methanol molecule by $CH_3O\cdot$ radical, $CH_3O + CH_3OH \rightarrow CH_3OH + CH_2OH$ (channel II).

The present calculations showed that reaction channel II is dominant at low energy region, whereas reaction channel II is favored at high energy region. This result suggests that reaction channel II is a dominant pathway for the low temperature thermal reaction below 77 K.

The present calculation, however, does not completely exclude the possibility for channel I. The RRKM rates suggest that channel II proceeds preferentially if an energy above 1.7 eV is given in the reaction system. In such case, the electron-cation recombination reaction

$$CH_3OH_2^+ + e^- \rightarrow CH_3 + H_2O$$

may be a candidate of the energy supply.

References

1. (a) Lund, A.; Shiotani, M., eds. *Radical ionic systems* (Kluwe, Dordrecht, 1991).
2. (a) Iwasaki, M.; Toriyama, K., *J. Am. Chem. Soc.*, **1987**, *100*, 1964.
   (b) Toriyama,K.; Iwasaki, M., *J. Am. Chem. Soc.*,**1979**, *101*, 2516.
3. Toriyama, K.; Iwasaki, M., *J. Chem. Phys.*, **1987**, *86*, 5970.
4. (a) Tachikawa, H; Ohtake, A.; Yoshida, H., *J. Phys. Chem.* **1993**, *97*, 11944.
   (b) Tachikawa, H; Hokari, N.; Yoshida, H., *J. Phys. Chem.* **1993**, *97*, 10035.
   (c) Tachikawa, H; Murai, H; Yoshida, H, *J. Chem. Soc. Faraday Trans.* **1993**, *89*, 2369.
   (d) Tachikwa, H., *Chem. Phys. Lett.*, **1993**, *212*, 27.
   (e) Tachikawa, H; Lunnel, S; Tornkvist, C; Lund, A, *Int. J. Quantum. Chem.* **1992**, *43*, 449, and *J. Mol. Struct (THEOCHEM)*, (in press).
5. Frish, M. J; Binkley, J. S; Schlegel, H. B; Raghavachari, K; Melius, C. F; Martin, R. L; Stewart, J. J. P; Bobrowicz, F. W; Rohlfing, C. M; Kahn, L. R; DeFrees, D. J; Seeger, R; Whiteside, R. A; Fox, D. J; Fleuder, E. M; Topiol, S; Pople, J. A., *Ab-initio* molecular orbital calculation program GAUSSIAN86, Carnegie-Mellon Quantum Chemistry Publishing Unit; Pittsburgh, PA.
6. Schaefer III, H. F., Ed. Applications in Electronic Structure Theory; Plenum: New York, **1977**; Vol. 4, p153.
7. Tachikawa, H.; Lunell, S.; Tornkvist, C.; Lund, A.,, *Int. J. Quntum. Chem.*, **1992**, *43*, 449.
8. (a) Miller, W.H., *J. Am. Chem. Soc.*, **1979**, *101*, 6810.
   (b) Miller, W. H., Tunneling, J. Jortner and B.Pullman, eds. (D.Reidel, Boston, 1986), pp.91-101.
9. Eckart, C., *Phys. Rev.* **1930**, *35*, 1303.
10. Karlstrom, G., *J. Phys. Chem.*, **1988**, *92*, 1318.
11. Saebo, S.; Radom, L.; Schaefer III, H. F., *J. Chem. Phys.*, **1983**, *78*, 845.

CONCLUDING REMARKS

Dynamics of charge, proton and hydrogen-atom transfers are the most fundamental and important processes in chemical reaction. However, there is a few theoretical study on these transfer reactions by means of the *a ppriori* dynamical method, because it is difficult to obtain the realistic *ab-initio* potential energy surface (PES) of these transfer reactions. In addition, in order to elucidate these reaction mechanisms, one needs to calculate the PES in wide region, to treat the non-adiabatic transition and to estimate quantum mechanical tunnel effect on the reaction rate.

In the present thesis work, PESs for the transfer reactions were calculated by means of *ab-initio* MO method including electron correlation, and the reaction dynamics on the *ab-initio* fitted PES was studied by both statistic theory and *quasi*-classical trajectory calculation. As a statistic theory to calculate the reaction rate, transition state theory, actually Rice-Ramsperger-Kussel-Murcus (RRKM) theory, was used. Primary aims of this thesis work are to provide theoretical information on the relevant PESs of these reactions, and to elucidate the reaction mechanism for them.

The main achievements in this thesis work are followings; (1) the new model for the charge-transfer reaction $N^+ + CO \rightarrow N + CO^+$ at low collision energy was proposed on the basis of both the PES characteristics and the dynamical calculation, and the vibrational-rotational state specificity of the product was reasonably explained by the proposed reaction model, (2) for the proton transfer reaction $O^- + HF \rightarrow OH(v,J) + F^-$, it was suggested that lifetime of the intermediate complex $[OHF]^-$ formed in collision region determines the product vibrational and rotational states, and (3) the new model for the hydrogen atom transfer reaction $NH_3(v)^+ + NH_3 \rightarrow NH_4^+ + NH_2$ and the charge transfer reaction $NH_3^+(v) + NH_3 \rightarrow NH_3 + NH_3^+$ was proposed, and (4) the reaction rates for the hydrogen atom transfer reactions were calculated by means of both RRKM theory and short-cut tunneling paths on 2-dimensional PES, and the quantum mechanical tunneling effect was shown to be important in hydrogen atom transfer reactions in condensed phase.

The present thesis work would provide considerable information on the mechanism of the light-particle transfer reactions in both gas- and condensed-phases and would encourage the further application of *ab-initio* MO and *quasi*-classical trajectory methods to studies of more complicated reaction systems.

LIST OF PUBLICATIONS

This thesis work is presented following papers.

1) Hiroto Tachikawa, Nobuyuki Hokari, and Hiroshi Yoshida

"An ab-initio MO Study on Hydrogen Abstraction from Methanol by Methyl Radical"

J. Phys. Chem., **1993**, 97, 10035-10041.

Abstract: The H-atom abstraction from methanol by methyl radical has been studied theoretically based on ab-initio MO calculations of the reaction system at the HF/3-21G and MP4SDQ/6-31G**//MP2 /6-31G levels. The rate constant was estimated for two reaction channels,

$CH_3 + CH_3OH \rightarrow CH_4 + CH_2OH$ (I)

and $CH_3 + CH_3OH \rightarrow CH_4 + CH_3O$, (II)

though the intrinsic reaction coordinate by the RRKM theory including the tunneling effect and through the short cut paths on the two-dimensional potential energy surface. The Arrhenius plot of the rate constant for both the reaction channels starts to deviate from a straight line at about 100 K and approaches to a limitting value, showing the importance of the quantum tunneling effect at low temperature. The H-abstraction from the hydroxyl group is theoretically predicted to dominate over that from the methyl group at low temperature, in contradiction with the previous results of ESR experiments on the methyl radical in solid methanol. This contradiction is possibly explained by taking into account the hydrogen-bonding in condensed phases which effectively blocks the reaction site for the H-abstraction from the hydroxyl group.

2) Hiroto Tachikawa, Atsushi Ohtake and Hiroshi Yoshida

"A Theoretical Study of Charge Transfer Reactions: Potential Surface and Classical Trajectory Study of $N^+ + CO \rightarrow N + CO^+$"

J. Phys. Chem. **1993**, *97*, 11944-11949.

Abstract : Potential energy surfaces (PESs) of the charge transfer reaction, $N^+ + CO \rightarrow N + CO^+$, have been calculated by *ab-initio* MO methods in order to shed light on the detailed

reaction mechanism. This reaction is a mode specific one in which the vibrational modes of the product CO^+ cation are populated in a non-Boltzmann distri-bution. The *ab-initio* MO calculation including electron correlat-ion gives a strongly bound [NCO^+] complex ($1^3\Sigma^-$) on the ground state PES, and a weakly bound [NCO^+]* complex ($2^3A''$) on the first excited state PES. Based on the ab-initio MO calculations, we propose a reaction model composed of dual reaction channels in the charge transfer process; one is an intermediate channel model in which the reaction proceeds via an intermediate complex (the ground state NCO^+ complex); the other is a direct channel model in which the reaction proceeds directly without the ground state intermediate. The mechanism of the charge transfer is discussed based on the PES characteristics. Furthermore, using LEPS-PESs fitted to the *ab-initio* PESs, classical trajectory calculations were performed. We find that the intermediate channel gives vibrationally excited CO^+ cations, whereas the CO^+ cation formed via the direct channel is in the vibrational ground state.

3) Hiroto Tachikawa

"Reaction mechanism of the radical isomerization from $CH_3O\cdot$ to $\cdot CH_2OH$ in frozen methanol: An ab-initio MO and RRKM study"

Chem. Phys. Lett.., **1993**, *212*, 27-31.

Abstract: The reaction mechanism of the radical isomerizations of $CH_3O\cdot/\cdot CH_2OH$ in frozen methanol has been investigated by ab-initio MO method and the RRKM theory. We consider two reaction channels as the conversion pathway; one is an intramolecular hydrogen rearrangement in $CH_3O\cdot$ radical (channel I) and the other is a hydrogen abstraction from a matrix methanol molecule by the $CH_3O\cdot$ radical (channel-II). Activation energies for the channels I and II are 34.8 and 14.7 kcal/mol at the MP2/6-31G* level, respectively, indicating that the latter channel is energetically favored. The RRKM calculations show that the reaction rate for channel II is significantly faster than that for channel I at low energy region, whereas reaction channel I is a dominant reaction pathway at high energy region above 1.7 eV. Furthermore, it was found that the quantum mechanical tunnel effect on the reaction rate plays an important role in the present isomerization reaction. Solvation effects on the reaction rate was also discussed based on the continuum model.

4) Hiroto Tachikawa, Sten Lunell, Christer Törnkvist, and Anders Lund,.

"Theoretical Study on Solvation Effects in Chemical Reactions:
A Vibrational Coupling Model"

Int. J. Quantum Chem. **1992**, 43, 449-461.

Abstract: A vibrational coupling model to treat the solvation effect in chemical reaction rate calculations is proposed and applied to the intramolecular hydrogen transfer reaction, $CH_3O\cdot \rightarrow \cdot CH_2OH$ in the condensed phase. In this simple model, the effect of solvation is considered as the vibrational couplings between the molecules constructing the reaction system and the solvent molecules. We considered ten water molecules, which are surrounding the reaction system in the first solvation shell, in the vibrational coupling calculation. The effect of solvation causes a significant change in the chemical reaction rate. This change is mainly caused by a lowering of the activation energy. The effect of the vibrational coupling also causes slightly a increase of the rate constant in the tunneling region. On the basis of those calculations, we also discuss the possibility that the present reaction might occur in the condensed phase at low temperature.

5) Hiroto Tachikawa, Christer Törnkvist, Anders Lund, and Sten Lunell

"Theoretical Study on Vibrational Coupling Effects in the Isomerization Reactions
in frozen methanol"

J. Mol. Struct. (THEOCHEM). **1994**, *304*, 25-33.

A vibrational coupling (VC) model previously introduced by us (H. Tachikawa, S. Lunell, C. Törnkvist, and A. Lund, *Int. J. Quantum Chem.* **1992**, *43*, 449) to estimate reaction rates including solvent effects has been applied to a reaction in the crystalline phase, namely the intramolecular hydrogen transfer reaction $CH_3O\cdot \rightarrow \cdot CH_2OH$ in the methanol polycrystalline phase. The calculations were carried out at the ab-initio HF and CCD-ST4 (double substituted coupled cluster theory) levels with 3-21G and D95V** basis sets. The VC between the reaction system and the surrounding four methanol molecules was considered in the present calculation. The VC effect slightly increased the reaction rate in all energy regions. The reaction mechanism in the methanol polycrystalline phase is discussed.

6) Hiroto Tachikawa and Shinji Tomoda

"A Theoretical Study on the vibrationally state-selected hydrogen transfer reaction: $NH_3^+(v) + NH_3 \rightarrow NH_4^+ + NH_2$: An *Ab-initio* MR-SD-CI and Classical Trajectory Approach

Chem. Phys., **1994**, *182*, 185-194.

Abstract: *Ab-initio* MR-SD-CI and classical trajectory calculations have been performed to elucidate the vibrational mode specificity of the title reaction, whose reactive cross section is enhanced by vibrational excitation of the ν_2 umbrella-bending mode of NH_3^+. Potential energy surfaces (PESs) of the reaction have been obtained for vibrationally ground and excited states (vibrational quantum numbers, v=0 and 2, respectively) by assuming a hydrogen bonded structure with fixed bending angles. The MO calculations show that a hydrogen transfer is composed of two elementary steps: 1) an electron transfer from NH_3 to NH_3^+ at avoided crossing region on the entrance PES, and 2) a proton transfer in the $(NH_3.NH_3)^+$ intermediate complex region. The PESs show that the avoided crossing point shifts to larger inter-molecular separation due to vibrational excitation. Using the *ab-initio* fitted PESs, the classical trajectory calculations elucidate the reaction dynamics. The maximum value of the impact parameter (b_{max}) for the reaction is increased by the vibrational excitation. Based on these theoretical results, a simple reaction model has been proposed, in which the electron capturing volume of NH_3^+ increases with increasing vibrational quantum number v.

7) Hiroto Tachikawa, Hiroshi Takamura and Hiroshi Yoshida

"Potential Energy Surfaces and Dynamics of Proton Transfer Reaction $O^- + HF \rightarrow OH(v) + F^-$ ".

J. Phys. Chem., **1994**, *98*, 5298.

Abstract: The gas phase proton transfer reaction, $O^- + HF \rightarrow OH(v=0,1) + F^-$, has been studied with *ab-initio* MO method and *quasi*-classical trajectory calculations. A strongly bound intermediate complex $[OHF]^-$ is found on the ground state potential energy surface (PES) obtained by the *ab-initio* MO method. The intermediate complex is most stable at the collinear form. Three dimensional *quasi*-classical trajectory calculations are performed with *ab-initio* fitted PESs. The results show that the enhanced collision energy from 1.198 to 4.10 kcal/mol

increases the product OH(v=1) fractional population, P(v=1) = {OH(v=1) / [OH(v=0) + OH(v=1)]}. Theoretical result suggests that this increase is due to the energy transfer from the translational mode to the vibrational mode of O-H in the deeper intermediate complex region. The trajectory calculations show that P(v=1) at a collision energy of 5.31 kcal/mol is slightly smaller than that of 4.10 kcal/mol. These results are in reasonably agreement with experimental features derived by Leone and co-workers [*J. Chem. Phys.*, **1992**, *96*, 298]. On the basis of the theoretical calculations, we propose a reaction model composed of two reaction channels: one is an intermediate complex channel model in which the reaction proceeds via a long-lived intermediate complex $[OHF]^*$, and the other is a direct channel model in which the reaction proceeds directly without the long-lived complex. The direct channel gives vibrationally excited OH(v=1, J =0) radical, whereas the complex channel leads to vibrationally ground and rotationally excited OH(v=0, J=J') radical.

In order to keekp the volume of the thesis within reasonable limits the following articles have been omitted.

8) Hiroto Tachikawa, Hiroyuki Murai and Hiroshi Yoshida

"Structure and electronic state of ion-pair complexes formed between C=O carbonyl compounds and sodium atom.: An ab-initio MO and MR-SD-CI study "

J. Chem. Soc. Faraday Trans. **1993**, *89*, 2369-2373.

Abstract: Geometric structure and electronic state of ion-pairs, formed by an electron transfer from alkali-metal to C=O carbonyl compounds, have been determined by using the ab-initio MO and MR-SD-CI methods. As model systems of the ion-pair, acetone-Na (AT-Na) and formaldehyde-Na (FA-Na) systems were chosen. The geometry optimizations of FA-Na ion-pair gave two structures as the stable form. One is a linear form with the $C=O^-Na$ angle of 168.7° and the other one is the p-form with the angle of 87.6°. The total energies of both ion-pairs are the similar to each other, although the energy calculation shows that the p-form is slightly more stable than the linear form. On the other hand, the geometry optimization of the AT-Na ion-pair gave only a linear form for the stable structure. The MR-SD-CI wave-functions of the ion-pairs indicate that the interaction between the alkali-metal and the C=O carbonyl group is composed of the atractive coulomb force $[C=O^-\cdots Na^+]$ at the ground state, whereas

the bonding nature varries the weakly attractive Van der Waals force [C=O··Na] at the first excited state. From an analysis of the excited state wave functions, the first absorption band of the ionpairs is assigned to the charge transfer (CT) transition expressed by $\pi^* \rightarrow$ Na(3s). The solvent effects on the spin density of the carbonyl oxygen in 2-methyltetrahydrofuran (MTHF) matrix were also discussed on the basis of the fractional charge model.

9) Hiroto Tachikawa, Anders Lund and Masaaki Ogasawara

"A Model Calculation on Structures and Excitation Energies of Hydrated Electron"

Can. J. Chem. **1993**, *71*, 118-124.

Abstract: Model calculations were made on the hydrated electron by using the *abinitio* MO method combined with the MR-SD-CI method and the coupled cluster theory. The models used in the calculations were water clusters denoted by $[e^-(H_2O)_n (H_2O)_m]$, where n=2,3,4 and 6 for the first solvation shell and m=0-28 for the second and third solvation shells. In these model calculations, the interactions between the excess electron and the water molecules in the first solvation shell are explicitly calculated by ab-initio MO methods and the water molecules in the second and third solvation shells were represented by the fractional charges obtained at the MP2/D95V** level. The stabilization energies and the solvation radius $r(e^-\text{-}O)$, in terms of the distance between the center of the cavity and an oxygen atom of the surrounding water molecules, increased monotonically with the number of water molecules in the first shell. On the other hand, the first excitation energy was not dependent on the number of water molecules in solvation shells, but constant with the value of ca. 2.0 eV. On the basis of the present calculations, we suggest that (1) the energetic stability of excess electrons depends on both short-range interaction and long-range interaction, (2) the first excitation energy is critically affected by only the short-range interactions, and the excitation is theoretically attributed to the *1s* $\rightarrow$*2p* transition of the excess electron.

10) Hiroto Tachikawa, Masaru Shiotani and Katsuhisa Ohta

"Structure and Formation Mechanisms od Methyl- and Dimethylacetylene Dimer Cations: ESR and *Ab-initio* MO Studies.

J. Phys. Chem., **1992**, *96*, 165-171.

11) Hiroto Tachikawa, Masaaki Ogasawara and Hiroshi Yoshida
"Structure and Reactivity of PMMA Ion Radicals: Ab-initio approach."
Radiat. Phys. Chem. **1991**, *37*, 107-110.

12) Hiroto Tachikawa, Tsuneki Ichikawa and Hiroshi Yoshida
"Geometrical Structure and Electronic States of the Hydrated Titanium (III) Ion. An Ab-initio CI study"
J. Am. Chem. Soc., **1990**, *112*, 982-987

13) Hiroto Tachikawa, Tsuneki Ichikawa and Hiroshi Yoshida
"Hydration Structure of Ti(III) Ion. ESR and Electron Spin Echo Study."
J. Am. Chem. Soc., **1990**, *112*, 977-982.

14) Hiroto Tachikawa and Masaaki Ogasawara
"Ab-initio MO study on the water dimer anion"
J. Phys. Chem., **1990**, 94, 1746-1750.

15) Hiroto Tachikawa, Masaaki Ogasawara, Mikael Lindgren and Anders Lund
"Ab-initio Calculation on Localized Electron in Alcoholic Matrix: Hydrogen Bond Defect Model"
J. Phys. Chem. **1988**, *92*, 1712-1725.

16) Hiroto Tachikawa and Nobuhiro Ohta
"Photodissociation mechanism of acetaldehyde: RRK and RRKM study"
Chem. Phys. Lett., **1994**, *224*, 465-469.

Acknowledgements

The present investigation has been carried out under the direction of Professor Hiroshi Yoshida for the period 1987 - 1993 and is presented as a thesis to Faculty of Engineering, Hokkaido University. A short, but very fruitful time was spend at Linköping University, Sweden, during the period October 1989 to February 1990.

The author wishes to express his profound gratitude to Professor Hiroshi Yoshida for his variable advises and continuous encouragement through the work. He wished to extend his appreciation to Prof. Masaaki Ogasawara, Prof. Anders Lund in Linköping University, Prof. Sten Lunnel in Uppsala University and Dr. Tsuneki Ichikawa for their helpful advice and discussion. The thanks are also expressed to Dr. Hitoshi Koizumi and to all the members for their encouragement's. The author directs his special thanks to Miss Ako Kotsugai for helping of bookbinding.

Last but far from least, appreciation must be expressed to the author's family for their continual encouragement without which the present study could not have been done.

January 1994

Hiroto Tachikawa